UNIVERSITY OF OKLAHOMA

GRADUATE COLLEGE

EVALUATION OF HUFF-N-PUFF EOR IN VARIOUS LIQUID RICH SHALES

A THESIS

SUBMITTED TO THE GRADUATE FACULTY

in partial fulfillment of the requirements for the

Degree of

MASTER OF SCIENCE

By

SIDI MAMOUDOU
Norman, Oklahoma
2020

Downloaded from SHAREOK. Persistent Handle URL: https://hdl.handle.net/11244/326661

EVALUATION OF HUFF-N-PUFF EOR IN VARIOUS LIQUID RICH SHALES

A THESIS APPROVED FOR THE
MEWBOURNE SCHOOL OF PETROLEUM AND GEOLOGICAL ENGINEERING

BY THE COMMITTEE CONSISTING OF

Dr. Carl Sondergeld, Chair

Dr. Chandra Rai

Dr. Ali Ousseini Tinni

© Copyright by SIDI MAMOUDOU 2020
All Rights Reserved.

Dedicated to

My advisors, friends, and family

ACKNOWLEDGMENTS

I would like to thank my family for their support during this master's degree. Particularly my aunt Rahama Beida for her moral support.

My deepest gratitude goes to Dr. Sondergeld and Dr. Rai for their guidance throughout this entire master's program. They have tested my knowledge and pushed my critical thinking ability up to a new frontier.

I would also like to thank Dr. Tinni, Dr. Dang and Dr. Curtis for their constant mentorship.

I am also thankful to Micaela Langevin and Gary Stowe for their help and daily assistance.

I would like to thank my IC^3 colleges for making these few years an enjoyable journey, especially Abhinav Mittal and Chris Ratzlaff.

I would like to thank OVINTIV for providing rock and oil samples to carry out this study. I am immensely grateful to Rich Newhart, Tom Smagala and Chris Bement for their guidance, expertise and insight on this EOR initiative.

Finally, I would like to thank the members of the Unconventional Shale Gas Consortium for their continuous support.

Table of Contents

ACKNOWLEDGMENTS ..... **V**

LIST OF TABLES ..... **IX**

LIST OF FIGURES ..... **X**

ABSTRACT ..... **XXIV**

CHAPTER 1: INTRODUCTION **1**

1.1 Motivation and problem statement **1**

1.2 Scope of the thesis **4**

1.3 Organization of the thesis **5**

CHAPTER 2: BACKGROUND RESEARCH AND LITERATURE REVIEW **6**

2.1 What is a shale? **6**

2.2 What is EOR Huff-n-Puff? **8**

2.3 Review IC^3 crushed huff-n-puff gas injection in unconventional reservoirs **12**

2.3.1 Sample size/surface area 12

2.3.2 Injection pressure 16

2.3.3 Soaking time/ residence time 19

2.3.4 Solvent composition 25

2.3.4 Lean vs rich solvent EOR 27

2.4 Discussion **28**

2.5 Conclusions: **30**

CHAPTER 3: METHODOLOGY **31**

3.1 General experimental workflow **31**

3.2 Experimental procedures **32**

3.3 Instrument and Theory Review **35**

3.3.1 Minimum Miscibility Pressure (MMP) 35

3.3.2 Nuclear Magnetic Resonance (NMR) 36

3.3.3 Source Rock Analysis / HAWK 40

3.3.4 Mercury Injection Capillary Pressure 42

3.3.5 Isothermal Adsorption and Pore Size Distribution 43

3.3.6 Scanning Electron Microscope (SEM) 44

3.3.7 Total Organic Carbon 45

3.3.8 Helium Pycnometry 45

3.3.9 Fourier Transform Infrared Spectroscopy (FTIR) 46

CHAPTER 4: RESULTS AND DISCUSSION **47**

4.1 Sample Description **47**

4.1.1 Pre-HnF pore throat and pore body size 48

4.1.2 As received fluid saturation 50

4.1.3 Water signal identification 51

4.2 Case study **55**

4.2.1 Eagle Ford (Preserved) 55

4.2.2 Duvernay (Preserved) 60

4.2.3 Uinta Basin 1 (Non-Preserved) 65
4.2.4 Uinta Basin 2 (Non-Preserved) 71
4.2.5 Montney 1 (Non-Preserved) 75
4.2.6 Montney 2 (Non-Preserved) 79
4.2.7 Meramec (Non-Preserved) 83

4.3 Performance evaluation 87

4.4 Performance control 88

CHAPTER 5: CONCLUSIONS 93

5.1 Summary 93

REFERENCES 94

APPENDIX 98

Appendix A: List of Acronyms 98

Appendix B: EOR HnP methodology 99

Appendix C: NMR sensitivity analysis 101

LIST OF TABLES

Table 1 - Recent experimental EOR studies showing various EOR scheme on major unconventional plays. All studies display optimistic recovery after EOR. However, it is essential to mention that these studied were carried by saturating rock sample with produced oil (Du et al., 2019). 10

Table 2 - Recent simulation studies showing the potential of huff-n-puff EOR. However, most studies have focused on CO_2 EOR. CO_2 has been shown to be a very efficient solvent but its availability on field location becomes an issue (Du et al., 2019). 11

Table 3 - Eagle Ford description with FTIR mineralogy, TOC and total porosity..... 12

Table 4 - 12Mhz Oxford Geospec2 NMR T_2 and T_1-T_2 measurement parameters. 33

Table 5 - Correspondence between modified Rock Pyrolysis and HCs fraction (Abrams et al., 2017) 42

Table 6 - Petrophysical properties of the 7 samples presented in this study. 47

LIST OF FIGURES

Figure 1 - Average 4-week US domestic field production of crude oil since 2001 (EIA 2019). ... 1

Figure 2 - Map of major shale gas and oil plays in the US Lower 48 states (EIA 2016). 2

Figure 3 - Average oil production per well in the Eagle Ford (EIA 2016) showing steep decline after few months of production. 3

Figure 4 - Additional 30-70% recovery from huff-n-puff gas in the Eagle Ford compared to primary depletion, reported by EOG Resources (Thomas et al., 2016). 3

Figure 5 - Mineralogy of several shale reservoirs based on average clay content, carbonate (calcite+dolomite), quartz and feldspar (Boak et al., 2011). Not all shales are truly shales, for example, Eagle Ford, Niobrara or Meramec. 6

Figure 6 - Backscattered electron (BSE) image of FIB milled shales from Barnett, Horn river, Marcellus and Haynesville showing the presence of organic and inorganic pores (Curtis et al., 2013). 7

Figure 7 - General distribution of different fluids and pore system in shale. Complication arises by the coexistence of inorganic pores which can be oil, water, or mixed wet; and organic pores which are assumed to be oil wet (Dang et al., 2018). 8

Figure 8 - Eagle Ford EOR pilot test showing incremental and cumulative production rate after Huff-n-Puff. 30% additional oil recovery is achieved after EOR compared to primary depletion. (Hoffman et al., 2018) 12

Figure 9 - Core plug dimensions with associated external surface area to volume ratios (S/V). These twin plug samples were cored parallel to bedding. 13

Figure 10 - NMR T_2 relaxation response during HnP experiment with C_1:C_2(72:28) at 4500 psi and 150 ºF for a) plug S/V=4.6 in^{-1} b) plug S/V=6.6 in^{-1} c) S/V=10.6 in^{-1}. The soaking

time was 24-hours and the production time 24-hours, which represent one cycle in our experiment..... 15

Figure 11 – HnP recovery as a function of S/V. Overall the higher the S/V the greater the recovery. The sample with larger S/V plateaued earlier than the other samples. This observation underscores the importance of S/V during EOR..... 15

Figure 12 - Summary of S/V study on various play, using different injectate and particle sizes. Only the crushed HnP shows recovery greater that 60%, which means that irrespective to the HnP scheme S/V plays a critical role in HC mobilization..... 16

Figure 13 - Comparison between fast and slow injection rates during HnP, on Eagle Ford crushed sample (7-8mm) at 150 ºF using a mixture of C_1:C_2(72:28) at 4500 psi (Minh 2018). Higher injection rate shows 10% greater recovery after 6 cycles..... 17

Figure 14 - Impact of injection pressure relative to MMP on crushed Eagle Ford with mixture C_1:C_2(72:28) using similar operating conditions at 150 ºF. Huff-n-puff should be conducted at pressure above MMP. (Modified after Minh 2018) 18

Figure 15 - GC-MS analysis on fluid pre and post huff-n-puff a) above MMP and b) below MMP. The experiment was carried on preserved Eagle Ford crushed sample (7-8 mm) at 150 ºF and 1000 psi above MMP (4500 psi) using the mixture C_1:C_2 (72:28). At injection pressure above MMP greater HCs fraction are mobilized up to C_{25} against C_{19} below MMP. (Dang 2019)..... 19

Figure 16 - a) Impact of soaking time of crushed Eagle Ford recovery. The longer the soaking time the greater the incremental recovery on a cycle basis. However, b) when the number of cycles is converted to residence time the cumulative recovery becomes similar. For

field application residence time becomes more meaningful as a possible upscaling/optimization parameter. (Minh 2018; Dang 2019)..... 20

Figure 17 - Impact of residence time on 8 saturated Wolfcamp samples (Modified after Yu 2016). Residence time can be used to determine optimal contact time between a solvent and a reservoir for optimization and upscaling purpose. The optimal residence for N_2 to deplete the Wolfcamp reservoir is around 20-hours, beyond this time, there is no additional recovery..... 21

Figure 18 - Pressure profile comparison during HnP for three Eagle Ford plugs with different soak and production time at 150°F. Sample 1 (blue) correspond to 1-hour soak and 1-hour production for a single cycle. Sample 2 (red) shows the effect of longer production time with 1-hour soak and 4.75-hours production. Sample 3 (green) shows the injection profile for longer soak and longer production 3-hours and 4.75 hours. 22

Figure 19 - NMR T_2 relaxation response during HnP experiment with C_1:C_2(72:28) at 4200 psi and 150 ºF for three dodecane saturated Eagle Ford plugs for various soak and production periods. a) 1 cycle represents 1-hour soak and 1-hour production. b) 1 cycle represents 1-hour soak and 4.75-hours soak. c) 1 cycle represents 3-hours soak and 4.75-hours. 24

Figure 20 - Effect of soaking time and production time on recovery. Increase soak and production time does not increase dodecane recovery 25

Figure 21 - Effect of injection gases composition on huff-n-puff recovery on Eagle Ford sample at 150 °F, using various gases. For each gas the injection pressure was 1000 psi above relative oil/gas MMP. Pure ethane shows the greatest recovery in the fewest cycles followed by CO_2, C_1:C_2 (72:28) and the field gas (C_1:C_2:C_3+/76:14:10). (Dang 2019) .. 26

Figure 22 - HAWK pyrolysis results after HnP using various gases. Ethane is found to be more efficient in removing heavier HCs (up to C_{27}), compared to other gases. (Dang 2019)... 26

Figure 23 - Impact of ethane enrichment during HnP, crushed Eagle Ford are contacted with a lean solvent C_1:C_2 (95:5) mixture and then a richer mixture C_1:C_2 (78:28). The dashed line represents the cycle after which the new solvent was introduced. 10% additional recovery is unlocked when the solvent is enrichment from 5 to 28% ethane after 24-hours..... 27

Figure 24 - Single well simulation comparison between a lean gas injection C_1:C_2 (93:7) vs rich gas injection C_1:C_2 (68:32). Like experimental work, rich gas injection yield 12.5% additional oil recovery (Courtesy of Ovintiv)..... 28

Figure 25 - Experimental apparatus/techniques used to measure EOR HnP performance. The green color represents measurements carried before and after EOR, and the grey color represents measurements used for initial petrophysical characterization. 31

Figure 26 - HnP experimental schematic. The crushed sample is placed inside a high-pressure cell, located within an oven. A mixture of methane: ethane (72:28 ±2%) is injected into high pressure cell via a pump station with precise pressure control; the pressure vessel outlet has a peioduction choke to control production rate and production time..... 32

Figure 27 – a) Example of NMR T_2 relaxation pre- and post- HnP for the same crushed sample. The graph shows incremental distribution of the left axis and cumulative distribution on the right axis. The difference between the two spectra represents the total fluid produced. b) Associated T_1-T_2 maps for the same crushed samples pre- and post- EOR. In both maps HC and water can be discriminated by separating signal clusters. 1:1 line is

traditionally associated with low viscosity fluid such as brine. While, HCs tends to have larger T_1:T_2 ratio. (Dang 2019) 34

Figure 28 - Example of FC-MMP between a mixture of C_1:C_2 (72:28 mol%) and a crude oil from Meramec (3.5±0.03 cP at 150 ºF). Above MMP capillary height is visible however at or below MMP (3500 psi) the capillary height vanishes (Mukherjee 2020). The measurement is carried in a high-pressure and high-temperature cell (Pmax=10,000 psi and Tmax=350ºF). 35

Figure 29 - FC MMP between several produced oil and a mixture of C_1:C_2 (72:28 mol%) measurement at 150 ºF (black) and 185 ºF (red). At 150 ºF Uinta basin oil 2 and 3 were below pour point, hence MMP was determined at 185ºF. The MMP values are used to determine injection pressure during HnP. In this study the injection pressure was kept at 1000 psi above MMP. 36

Figure 30 - Incremental (a) and (b) cumulative NMR T_2 relaxation spectrum (NSA=16) for various dodecane oil volume. The glass vial signal was also measured and labelled “blank”. Its value was removed during calculation. 39

Figure 31 - T_2 NMR relaxation volume as function of gravimetric volume using dodecane oil (0.75g/cc). The red line represents the 1:1 line. NMR is sensitive enough to measure bulk volume up to 0.1cc. Note there is a slight deviation as volume increases. 39

Figure 32 - Traditional source rock analysis pyrogram. S1 represent the volume of free HC that is producible up to 300 ºC. S2 represents the amount of HC generated by thermal cracking, its temperature Tmax is a thermal maturity indicator, from 300-550 ºC. The S3 peak is the amount of CO_2 by kerogen, up to 600 ºC (Boyer et al., 2006) 40

Figure 33 - HAWK pyrograms of a shale using traditional pyrolysis (a) and the modified 4-steps procedure (b). The traditional source Rock Eval pyrolysis program is modified yielding a finer resolution of the S1 peak into: S_{11}, S_{12}, S_{13} and S_{14}. 41

Figure 34 - HAWK sensitivity analysis, where the same shale sample was 5 runs using 4 heating steps. The plot shows a decreased in oil FID standard deviation as the HC becomes heavier. Overall HAWK measurement displays excellent accuracy (±2%) in hydrocarbon characterization on shale samples. 42

Figure 35 - Example of pore throat size alteration after 10 HnP cycles on a Duvernay shale at 150 ºF. The experiment was carried at 1000 psi above MMP by cyclically injecting a mixture of C_1:C_2 (72:28). Large increase in pore throat sizes < 10nm after EOR shows that the solvent could open smaller pore throats which could provide access to larger pore bodies. (Dang 2019) 43

Figure 36 - Pore size distribution alteration after HnP using DFT slit pore inversion on a Duvernay shale. Huff-n-puff was carried at 150 ºF using a C_1:C_2(72:28) as injectate at 1000 psi above MMP. The BET surface area is increased by almost a factor of two after EOR from 1.4 to 2.7±0.2 m^2/g showing that the solvent was capable to open larger or more pore bodies after EOR. 44

Figure 37 - Mercury injection capillary pressure measurements of the samples used in this study. Eagle Ford, Duvernay, Uinta 1 and 2 appear tighter with pore throats <20nm compared to the Montney 2 and Meramec formations, which have larger pore throats. 48

Figure 38 - SEM images showing pore body size contrasts between Montney 2 (Left) and Eagle Ford (Right) on the same scale. Large μm size pores are visible inside the OM of the Montney 2 sample (white arrows). 49

Figure 39 - Porous region in the Eagle Ford sample to the left. Magnified in image of the same sample showing pore bodies ranging from 5-20nm inside the organic material. 49
Figure 40 - HAWK analysis using the 4-step heating protocol on the as received samples. Notice that preserved sample (Eagle Ford and Duvernay) have the highest HC saturation, mostly made of lighter HC, S_{11}. The HC concentration of others sample is lower but more homogeneous. 50
Figure 41 - As received T_1-T_2 maps of crushed samples on the same scale. Notice Eagle Ford, Duvernay and Montney 2 have the highest oil saturation. Low residual oil saturation is observed in Uinta 2, Montney 1 and Meramec with high water saturation. 51
Figure 42 - Water and oil volume after 96-hours imbibition in 70% $MnCl_2$ solution based on T_1-T_2 maps. The water signal initially increases as water is entering the rock with no $MnCl_2$ ions, after 24-hours $MnCl_2$ ions are mixing with the water inside the sample resulting in a decrease in NMR volume. After 96-hours the water volume drops below its initial value. However, the oil volume remains constant as the $MnCl_2$ does not mix with the oil inside the sample. 52
Figure 43 - T_1-T_2 of preserved Eagle Ford before and after 96-hours imbibition in 70% Manganese chloride solution. The maps show a general decrease in the intensity of the T_1-T_2~1-10 peak, confirming that this signal is water. 53
Figure 44 - MMP at 150 ºF with mixture of C_1:C_2 (72:28). No oil was available for Montney so the MMP was calculated using molecular simulation of Montney 1 oil composition(red). These MMP values will be used as injection pressure reference during HnP performance evaluation. 54

Figure 45 - Positive relationship between MMP and a) produced oil viscosity at 150 ºF and b) residual rock heaviness fraction from HAWK. Overall, the heavier the oil the higher the MMP. Hence the higher the compression pressure required to achieve efficient HC mobilization HnP 55

Figure 46 - SARA analysis of Eagle Ford produced oils from the same well pad in red and core plug extract from 200 ft core sampled from the same well. Note both produced oils and residual extract oil have a composition rich in saturated alkanes with limited resins and asphaltenes. (Courtesy of Ovintiv) 56

Figure 47 - NMR T_2 spectra for 12 cycles of HnP for the Eagle Ford sample. Hydrocarbon recovered are preferentially from the larger pore bodies (1-10ms). HnP cycles were conducted using a rich gas mixture of C_1:C_2 (72:28) at 4500 psi (1000 psi above MMP) and 150ºF. One cycle corresponds to 1-hour soak and 1-hour production (Minh 2019). 57

Figure 48 - 2D T_1-T_2 maps of the Eagle Ford sample pre- and post- EOR. Comparison of fluids signal shows that 73% of the fluid production is oil and 27% is water. For this sample the solvent C_1:C_2 (72:28) can mobilize both oil and water. 57

Figure 49 - HAWK pyrolysis pre- and post- HnP on Eagle Ford crushed sample using the same conditions. Note only light HC fractions S11 and S12 are mobilized after 12 cycles of HnP. 58

Figure 50 - Cumulative recovery as function of residence time for Eagle Ford crushed sample. Note the solvent was able to mobilize 45% of the *in-situ* fluid (Minh 2019)..... 58

Figure 51 - a) Isothermal nitrogen BET adsorption measurement pre- and post- EOR for an Eagle Ford sample. Nano-pores around 2nm were opened after HnP. BET shows cleaning of

smaller pores <200nm and an increase in surface area from 0.8 to 2.8m^2/g. b) MICP does not show significant change in pore throat size (Dang 2019)..... 59
Figure 52 - SEM image pre- (left) and post- (right) HnP. No significant microstructural alteration was observed in the OM. However, we observe porosity generation between organic and inorganic interfaces, which might alter the rock wettability and fluid recovery (oil/brine) during HnP. 60
Figure 53 - NMR T_2 spectra during HnP for Duvernay crushed sample. 10 cycles were conducted using a rich gas mixture of C_1:C_2 (72:28) at 3900 psi (1000 psi above MMP) and 150°F. One cycle corresponds to 1-hour soak and 1-hour production (Dang 2019). 61
Figure 54 - Cumulative recovery as function of residence time for Duvernay sample crushed sample. Note the solvent was able to mobilize 43% of the *in-situ* fluid. 62
Figure 55 - HAWK pyrolysis pre- and post- HnP on a Duvernay crushed sample. Note the solvent was able to mobilize HC fraction up to C_{27} 62
Figure 56 - 2D T1-T2 maps of the Duvernay sample pre- (left) and post- (right) EOR. Mostly oil is produced during this test (83%) with some water (17%). 63
Figure 57 - a) Isothermal nitrogen adsorption before and after EOR showing opening of smaller pores and surface area increases from 1.4 m^2/g to 2.7 m^2/g. b) MICP shows increase in pore throat size by almost 4 times after EOR. 64
Figure 58 – Pre- (left) and post- (right) EOR SEM images taken on the same scale, showing dissolution of the organic matter resulting in an increase by 50 % of the organic pore size after solvent injection. 64
Figure 59 – Subtracted incremental T_2 spectrum from Figure 48 of Duvernay shale showing produced volume during each cycle of HnP. This figure shows that HC production is not

bias toward fast or slow relaxation times, HC comes out of both fast and slow relaxation times (i.e. small and large pores) with progressive HnP cycles..... 65
Figure 60 - Regional stratigraphy of the Uinta basin. The Uteland Butte is the basal green carbonates of the Green River formation (Ramakrishna et al., 2012) 66
Figure 61 - Images of brown and yellow wax received from the Uinta basin at room temperature. 67
Figure 62 - T_2 relaxation spectra of Uinta 1 and Uinta 2 produced HC. The main peak of Uinta 1 is 220 ms, while Uinta 2 is 400 ms. 67
Figure 63 - NMR T_2 spectra during HnP for Uinta 1 crushed sample. Small depletion is observed after EOR. Note that T_2 peaks shifts to the left during HnP signifying that the left-over oil is getting heavier. 68
Figure 64 - Cumulative recovery as function of residence time for Uinta 1 sample crushed sample. Note the solvent performance is very poor, only around 10% 68
Figure 65 - 2D T_1-T_2 maps of Uinta 1 sample pre- (left) and post- (right) HnF. After EOR only HC is produced. 69
Figure 66 - HAWK pyrolysis pre- and post- HnP on Uinta 1 crushed sample. Note mostly S_{11} and S_{12} are produced but there is a large volume of S_{13} and S_{14} left behind. 69
Figure 67 - a) Isothermal nitrogen adsorption before and after EOR showing modest increase in surface area (<10%) from 2.5 m^2/g to 2.8 m^2/g. b) MICP shows modest increase in pore throat radius as well. 70
Figure 68 - SEM image pre- (left) and post- (right) HnP show no significant microstructural alteration was observed in the OM. 71

Figure 69: 2D T_1-T_2 maps of Uinta 2 sample pre- (left) and post- (right) HnP. Very low HC present in the sample pre- EOR. Note after EOR mostly water is produced..... 72
Figure 70 - Cumulative recovery as function of residence time for Uinta 2 crushed sample. Note the cumulative production is around 28 % but most of the fluid produced is water. 72
Figure 71 - NMR T_2 spectra during huff-n-puff for Uinta 2 crushed sample. Relatively smaller pore bodies (<1ms) are depleted during EOR. 73
Figure 72 - HAWK pyrolysis pre- and post- HnP on Uinta 2 crushed sample. After EOR HC fractions up to C_{27} are produced. Note the overall oil FID is substantially lower than the other formations. 73
Figure 73 - a) Isothermal nitrogen adsorption before and after EOR showing 30% increase in surface area from very small pores (<10nm). b) However, MICP shows no major change in pore throat radii. 74
Figure 74 - SEM image pre- (left) and post- (right) HnP. No significant microstructural alteration was observed in the OM. Note Uinta 2 has significantly more clay than Uinta 1. 75
Figure 75 - 2D T_1-T_2 maps of Montney 1 sample pre- (left) and post- (right) HnP. After HnP 46% of oil and 54% of water was produced. 76
Figure 76 - NMR T_2 spectra during HnP for Montney 1 crushed sample. Most of the production happens during cycle 1. Note based on T_2 alone no clear distinction can be made to discriminate fluid type. 76
Figure 77 - Cumulative recovery as function of residence time for Montney 1 crushed sample. Note cycle 1 is the most efficient with almost 20% recovery. The ultimate recovery ~24% is achieved after 12-hours. 77

Figure 78 - HAWK pyrolysis pre- and post- HnP on Montney 1 crushed samples. After EOR HC fraction up to C_{24} are produced, but most of the oil mobilized are lighter HC ($<C_{17}$) 77

Figure 79 - Isothermal nitrogen adsorption before and after EOR showing increase surface area from 0.4 m^2/g to 1.6 m^2/g coming from very small pores (4-5 nm). b) However, MICP shows no major change in pore throat radii. 78

Figure 80 - SEM image pre- (left) and post- (right) HnP. No microstructural alteration is observed after EOR. Note the extensive amount of debris after EOR, which plug pores and reduces recovery..... 79

Figure 81 - 2D T_1-T_2 maps of Montney 2 sample pre- (left) and post- (right) HnP. The sample has high initial oil saturation with no residual water. During EOR substantial volume of HC is produced. 80

Figure 82 - NMR T_2 spectra during HnP for Montney 2 crushed sample. The depletion in this sample is gradual and well behaved. Note that the main T_2 peaks shift to the left suggesting that the left-over HC is getting heavier..... 80

Figure 83 - Cumulative recovery as a function of residence time for Montney 2 crushed sample. Note that after 20-hours, 50% of HC is recovered with a gradual production rate. 81

Figure 84 - HAWK pyrolysis pre- and post- HnP on Montney 2 crushed sample. After EOR HC fractions up to C_{24} are produced, but most of the oil mobilized is lighter HC ($<C_{17}$). 81

Figure 85 - Isothermal nitrogen adsorption before and after EOR showing small change in surface area; from 0.0018 m^2/g to 0.0075 m^2/g from small pores. b) However, MICP shows large increase in pore throats from 800nm to 1000nm. 82

Figure 86 - SEM image pre- (left) and post- (right) HnP showing dissolution of the OM microstructure on Montney 2 after HnP. The increase in pore size agrees well with BET

and MICP interpretation. The new dimensions after EOR in the OM are greater by a factor of 2. 83
Figure 87 - 2D T_1-T_2 maps of Meramec sample pre- (left) and post- (right) HnP. The sample has very low initial oil and water content. Note the clear separation between the two oil and HC clusters. In this case water in present in relatively smaller pores while the residual oil is in larger pores. 84
Figure 88 - NMR T_2 spectra during huff-n-puff for Meramec crushed sample. Larger oil wet pores are depleted first (1-10ms) in the first 2 cycles and water pores are depleted in smaller pores (T_2<1ms) 84
Figure 89 - Cumulative recovery as function of residence time for Meramec crushed sample. A total recovery of 44% is observed after 12-hours. Note that the error bars are large due low initial residual saturation. 85
Figure 90 - HAWK pyrolysis pre- and post- HnP on Meramec crushed sample. After EOR HC fractions up to C_{24} are produced, but most of the oil mobilized is lighter HC (<C_{17}). 85
Figure 91 - Isothermal nitrogen adsorption before and after EOR showing little increase in surface area from 0.6 m^2/g to 0.8 m^2/g coming from very small pores (<200nm.) b) MICP shows large pores compared to other tight formation in this study but a slight change in pore throat size distribution from 50 to 40nm is observed after EOR. Note after EOR there no pore throat below 20nm, which could attribute to some pore blockage. 86
Figure 92 - SEM image pre- (left) and post- (right) HnP showing no microstructural alteration of Meramec. Mostly clay minerals and inorganic material are visible 87
Figure 93 - Summary of cumulative oil recovery after HnP. Montney appears to be the best candidate followed by Duvernay and Eagle Ford. 88

Figure 94 - Relationships between NMR oil recovery with HAWK heaviness fraction, oil viscosity, total porosity and average MICP pore throat size. A strong dependence is observed between the recovery factor and the oil composition (produced oil viscosity and residual oil composition)..... 90
Figure 95 - Relationships between NMR oil with TOC and mineralogy. A weak dependence is observed between the organic content and mineralogy. 91
Figure 96 - Oil recovery as function of HAWK heaviness fraction with (a) and without Montney 2 (b). Improved correlation is observed when Montney 2 is removed from the analysis. Oil recovery seems to be controlled by the oil composition and pore throat size. 92

ABSTRACT

Cyclical gas injection Enhanced Oil Recovery (EOR) known as “Huff-n-Puff” (HnP) has experienced renewed interest since the EOG success in the Eagle Ford shale play. HnP consists of injecting CO_2 or a hydrocarbon solvent at a pressure above Minimum Miscibility Pressure (MMP) to maximize oil mobility. Re-pressurizing previously hydraulically fractured reservoir can yield an additional 30-70% more oil (Thomas et al., 2016). Traditional laboratory EOR studies usually focus on recovery evaluation on saturated plug samples and neglect microstructural alteration of the rock.

Our study consists of evaluation of cyclical gas injection performance on crushed samples with a rich mixture of methane and ethane (72:28mol%) on “preserved” or “as received” rock samples from; the Eagle Ford, Duvernay, Uinta basin, Montney and Meramec. A case by case evaluation of these formations is presented to capture the dynamic changes behind HnP by focusing on three major elements, the oil (viscosity and composition), the rock (porosity, pore throat size, pore body size, internal surface area and microstructural changes), and the solvent (MMP). This workflow integrates several petrophysical tools such as NMR, HAWK pyrolysis, MICP, BET, TOC, Helium Pycnometry SEM imaging to measure recovery and characterize rock-fluid interactions. A sensitivity analysis on NMR fluid recovery is performed to determine the major control parameters on EOR.

The results show that EOR HnP recovery is controlled mostly by the reservoir oil composition and pore throat size distribution. Rock properties such as mineralogy, TOC and total porosity are secondary controls on recovery. Pore throat size distribution is found to control production rate during EOR. The tighter the rock (pore throats size distribution <20nm) the more gradual the HC production. However, when the pore throats are large (>20nm) faster depletion is observed.

In addition, a newly define HAWK heaviness fraction, which is the ratio of the heavy components S_{14} to the total HAWK HC production can be used as a proxy to quickly screen cyclical gas candidates. Sample with HAWK heaviness fraction > 0.20% are found to be poor candidates for EOR using the rich gas.

Finally, SEM observations after EOR shows alteration of the organic matter but also alteration between organic and inorganic minerals.

CHAPTER 1: INTRODUCTION

1.1 Motivation and problem statement

In the last 20 years, organic rich shale plays have emerged as a major source of hydrocarbon production in the Unites States. The U.S oil and gas production has seen an increase in production since 2010 due to the combination of hydraulic fracturing and horizontal drilling technology. These technologies are responsible for the "shale revolution". According to the EIA **(Fig.1**) additional wells produced from tight reservoirs led to an increase of crude oil production from an average of 5.5 MMbbl/day to more than 12 MMbbl/day from 2010 to 2019. **Fig.2** shows the location of the major shale plays in the lower 48 such as the Eagle Ford, Bakken and the Permian Basin.

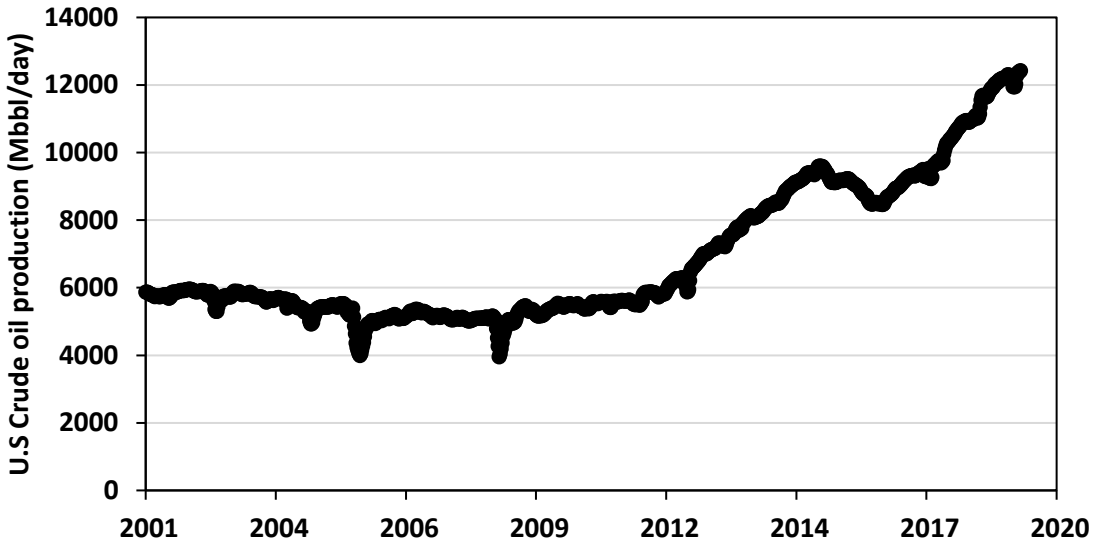

Figure 1 - Average 4-week US domestic field production of crude oil since 2001 (EIA 2019).

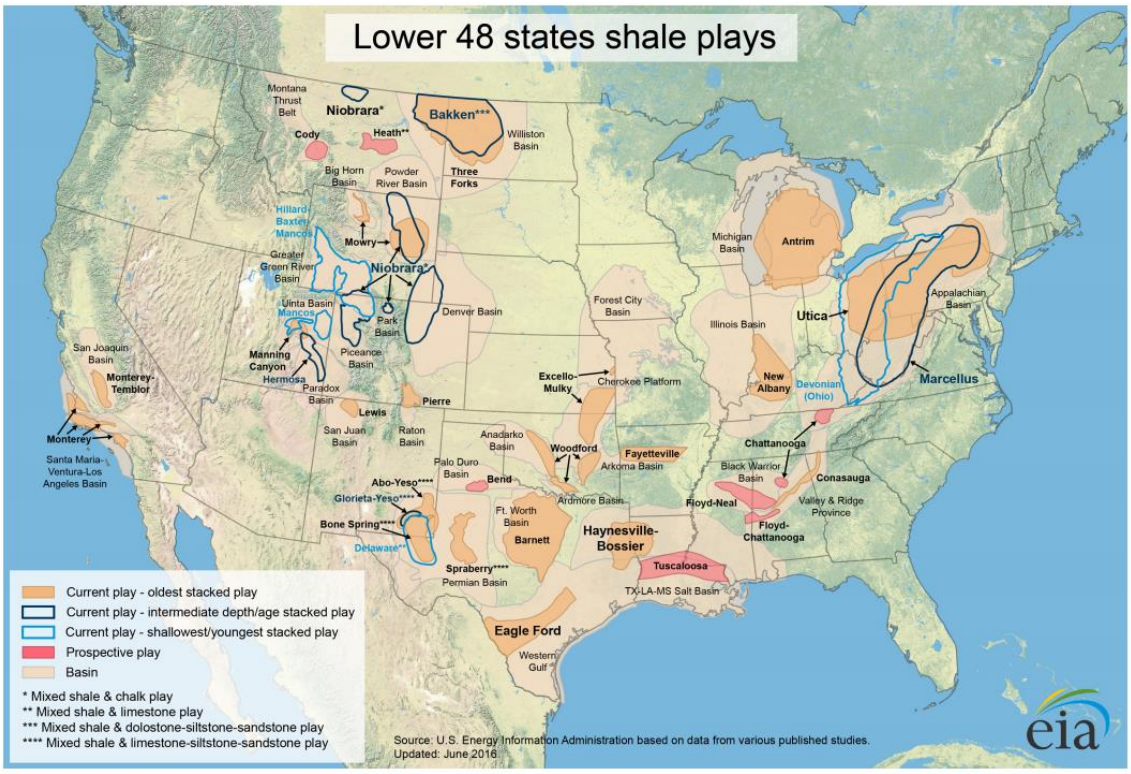

Figure 2 - Map of major shale gas and oil plays in the US Lower 48 states (EIA 2016).

The shale revolution has unlocked additional oil and gas from tight rocks; however, the initial production is high during the first few months but declines steeply, often by half or more of initial production rate within the first 6 to 12 months (King 2014). **Fig.3** is an example of average oil production per well in the Eagle Ford play. Primary recovery in tight formations is usually low, for example, in the Bakken, the oil recovery factor is approximately 4-6% (Hawthorne et al., 2013). It becomes essential to evaluate more sustainable production methods in order to recover additional oil and gas locked in the subsurface. One method of EOR that has attracted attention in the last few years is the cyclical gas injection also known as HnP. In 2016, EOG Resources announced successful gas injection EOR in the Eagle Ford resulting in the additional recovery of 30-70% (Hoffman 2018). They set the standard for both the industry and academia looking for a low-cost method to add reserves by injecting natural gas (Rassenfoss 2017).

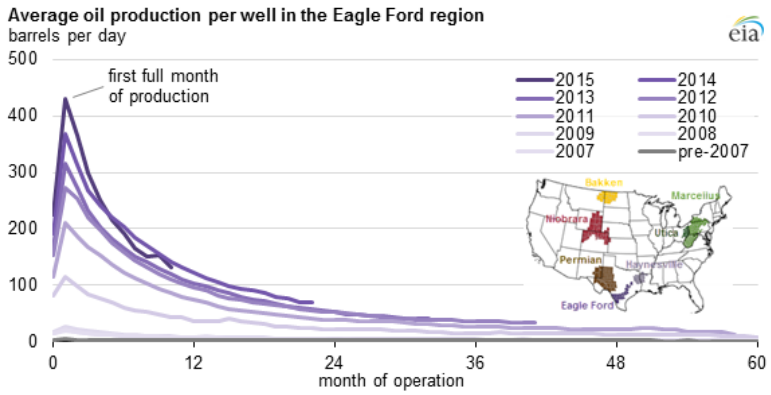

Figure 3 - Average oil production per well in the Eagle Ford (EIA 2016) showing steep decline after few months of production.

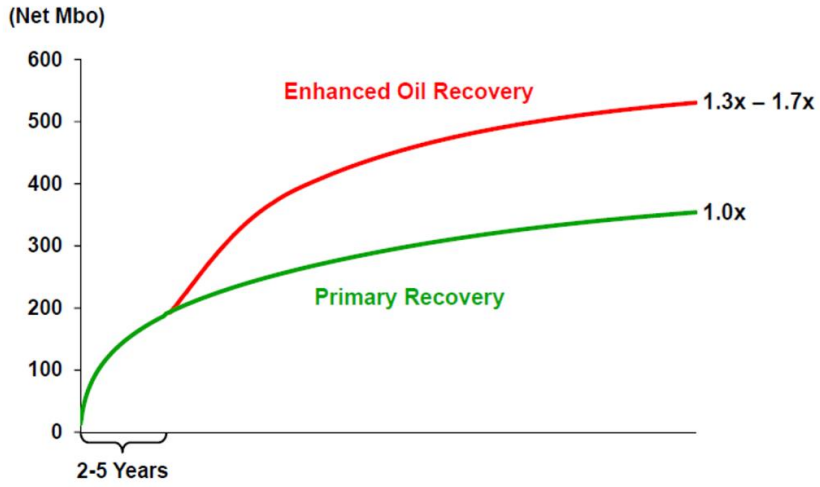

Figure 4 - Additional 30-70% recovery from huff-n-puff gas in the Eagle Ford compared to primary depletion, reported by EOG Resources (Thomas et al., 2016).

Numerous experimental and simulation studies have focused on EOR injection on recombined oil saturated rock samples. They generally overlook structural changes in the rock after gas injection. In this study we propose to evaluate EOR performance in different shales in "preserved" or "as received" states with a rich mixture of C_1:C_2 (72:28), then investigate the major oil and rock properties controlling hydrocarbon recovery in these plays with an "in-house workflow".

1.2 Scope of the thesis

The focus of this work is to experimentally evaluate huff-n-puff recovery and microstructural alterations on various liquid rich shales from Eagle Ford, Duvernay, Uinta basin, Montney and Meramec. A case by case performance evaluation is made to determine the significant control parameters from each play. Those parameters are typically the oil composition, pore size distribution, pore throat size, porosity, organic content, internal surface area, and mineralogy. The objective of this study is to fundamentally understand the major controls on recovery of miscible gas injection EOR and ultimately suggest a screening workflow to help companies assess potential EOR candidates.

1.3 Organization of the thesis

This thesis is divided into five chapters and is presented as follows:

- Chapter 1; introduces the motivation, problem statement and describe the scope of this study.
- Chapter 2; includes a literature review on gas injection EOR and the field study in unconventional reservoirs.
- Chapter 3; describes the details of the equipment, methodologies, and experimental procedures for huff-n-puff tests.
- Chapter 4; discusses the result and analyses of the study.
- Chapter 5; presents the conclusion and the most significant findings.

CHAPTER 2: BACKGROUND RESEARCH AND LITERATURE REVIEW

2.1 What is a shale?

Shales are laminated fine grained (particles size < 4 μm) sedimentary rock made of quartz, carbonates and clays minerals. Shale mineralogy is dominated by clays. However, it is important to mention that not all unconventional reservoirs are dominated by clays **(Fig.5).**

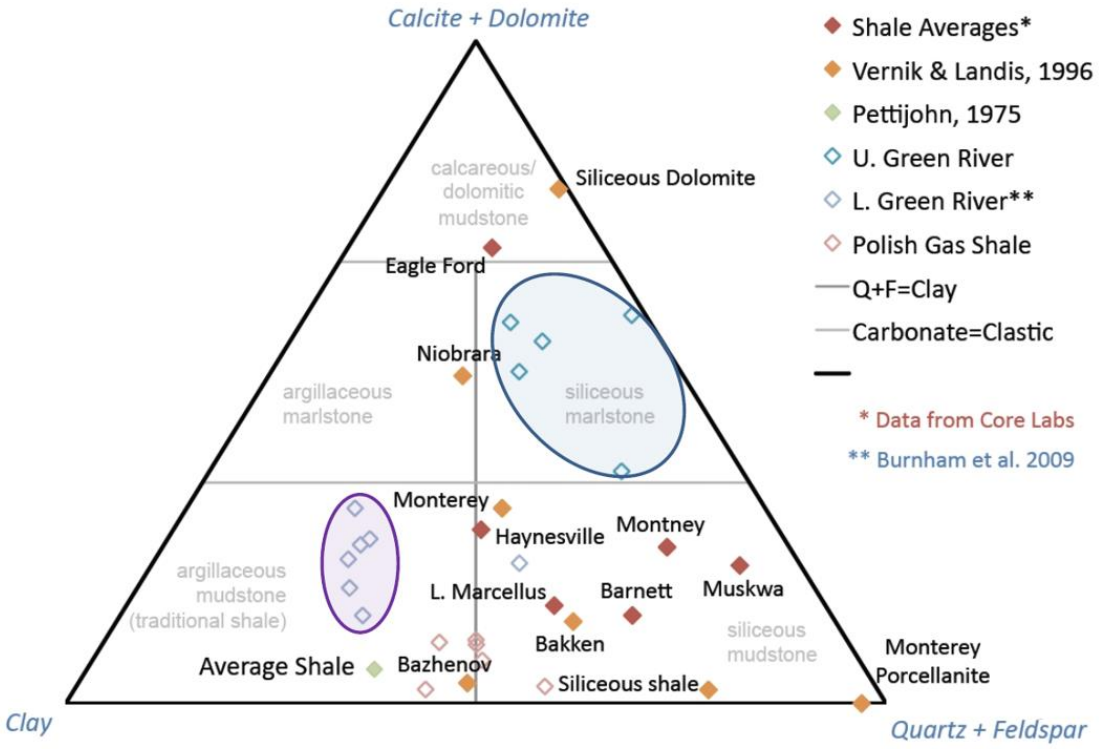

Figure 5 - Mineralogy of several shale reservoirs based on average clay content, carbonate (calcite+dolomite), quartz and feldspar (Boak et al., 2011). Not all shales are truly shales, for example, Eagle Ford, Niobrara or Meramec.

The main commonality between shale reservoirs is the presence of organic matter. The main two components of these reservoirs are organic matter and inorganic minerals **(Fig.6).** These two components directly control the quality and properties of these reservoirs.

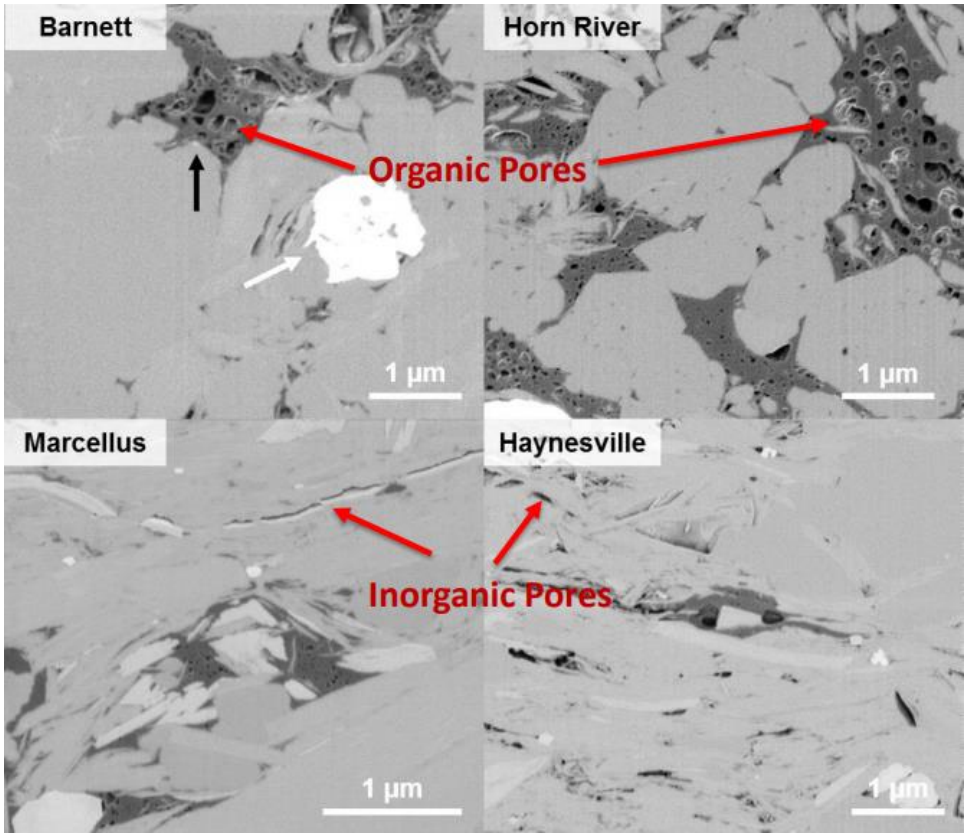

Figure 6 - Backscattered electron (BSE) image of FIB milled shales from Barnett, Horn river, Marcellus and Haynesville showing the presence of organic and inorganic pores (Curtis et al., 2013).

In addition to the mineralogy, fluid partitioning inside shales pore system add another layer of complexity to their flow properties. **Fig.7** shows the components of shale rock and co-existence of different pore fluid and pore fluid system. Inorganic pores can be oil wet, water wet or both, while organic pores are assumed to be oil wet (Dang et al., 2018). The presence of mixed wettability system adds another layer of complexity in storage and transport for these unconventional reservoirs. As opposed to conventional petroleum system, which consists of source rock, reservoir rock, and a seal. A shale was the traditional seal for conventional reservoirs, due to their low porosity and permeability. Today's growing energy demands and technology advances such as horizontal drilling and hydraulic fracturing have allowed economical production of these hydrocarbon rich reservoirs.

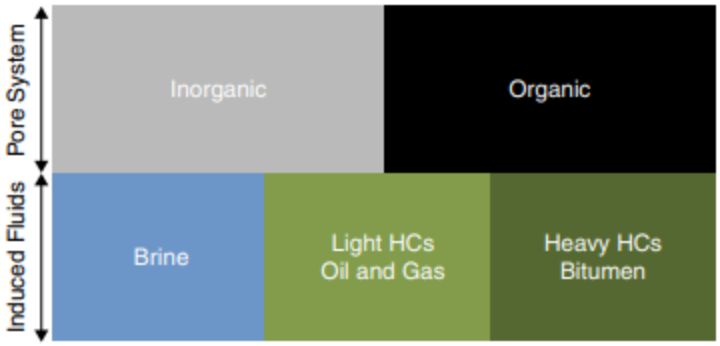

Figure 7 - General distribution of different fluids and pore system in shale. Complication arises by the coexistence of inorganic pores which can be oil, water, or mixed wet; and organic pores which are assumed to be oil wet (Dang et al., 2018).

2.2 What is EOR Huff-n-Puff?

Traditional EOR (Enhanced Oil Recovery) consists of injecting a fluid into the reservoir to improve sweep efficiency, either water or gas (usually CO_2 or hydrocarbon-based solvents), but due to ultra-low permeability water injection becomes impossible in unconventional reservoirs. Only gas injection represents a viable solution. HnP consists of injecting a solvent gas at pressure above MMP. The gas is allowed to soak into the rock for a period of time and then the well is put back on production. During the soaking period the gas will move from the fractures into the liquid hydrocarbons in the matrix through advection and diffusion. The gas will dissolve into the oil causing it to expand and be expelled into the fractures. Other mechanisms, such as viscosity reduction and vaporization may also be active, but they are expected to be less important for the liquid rich windows of unconventional reservoirs (Hoffman et al., 2019). Simulation and experimental work have shown very promising results, **Table 1** and **Table 2** summarize recent simulation and experimental studies in EOR. The results are very optimistic with oil recoveries greater than 90% from laboratory experiments and 50% from simulation.

The authors of these studies have focused on various parameters controlling recoveries. Gamadi et al. (2013, 2014) investigated the performance of HnP using N_2 and CO_2 as injectant on Barnett,

Mancos, and Eagle Ford rock samples saturated with mineral oil (Soltrol 130). They found that N_2 could increase the recovery from 10-50% depending on the injection pressure and shale core type. Yu and Sheng (2016) studied the impact of soaking and production times on N_2 huff-n-puff performance. They found that HnP could enhance recovery up to 45%. The same authors concluded that a major factor controlling recovery in tight rock is re-pressurization. However, most of these studies are based on re-saturated rock samples. The novelty of this thesis is the use of "preserved" or "as received" samples with fluid composition much closer to the original reservoir composition to capture more accurately HnP EOR responses.

Table 1 - Recent experimental EOR studies showing various EOR scheme on major unconventional plays. All studies display optimistic recovery after EOR. However, it is essential to mention that these studied were carried by saturating rock sample with produced oil (Du et al., 2019).

Experimental Study									
Oil Sample	Rock Sample	K (μd)	Porosity (%)	Injection Gas	Method	Pinj (psi)	T (°F)	Production	Oil RF (%)
Mineral oil (Soltrol-130)	Barnett	-	-	N_2	cyclic gas injection	1000	95	1 d (soaking)	6.5
						2000			11.23
						3000			14.91
						3500			17.79
	Marcos	-	-			3000		1 d (soaking)	13.5
								2 d (soaking)	16.96
								3 d (soaking)	19.59
Bakken oil	Bakken	270–830	18.6–23.1	CO_2	near-miscible huff-n-puff	1349	140	40 h	63
					miscible huff-n-puff	2031		60 h	61
					waterflodding	1668		-	51.5
					immiscible huff-n-puff	1015		60 h	42.8
Bakken oil	Bakken	290–440	18.9–23.6	water+CO_2	water-alternating-CO_2		145.4	-	80.1–88.1
Wolfcamp	Eagle Ford	0.24	7.28	CO_2	huff-n-puff	1600	72	7 h (soaking)	56.8 (7 circles)

Experimental Study									
Oil Sample	Rock Sample	K (μd)	Porosity (%)	Injection Gas	Method	Pinj (psi)	T (°F)	Production	Oil RF (%)
Dead oil from Wolfcamp shale	Eagle Ford	0.085	4.4	N_2	flooding	1000	72	48 h	17.94
					huff-n-puff				22.52
		0.4	13.1		flooding				19.88
					huff-n-puff				24.13
Mineral oil (Soltrol-130)	Eagle Ford	0.5	5	N_2	cyclic gas injection	1000	95	-	14.23–45.45
									11.41–39.66
C_{10}-C_{13} Isoalkanes	Eagle Ford	-	7.7	CO_2	cyclic gas injection	850–3500	95	-	20-71
	Mancos	-	5			850–500			10–31
						3500			43–63
Bakken oil	Middle Bakken	8.1–103.5	4.4–5.4	C_1	oil extraction	5000	230	24 h	>90
				C_2					nearly 100
				C_1/C_2 (85/15)					>90
				CO_2					>90
				N_2					26
	Lower Bakken	5.25	3.8	C_1					≈18
				C_1/C_2 (85/15)					≈27
				CO_2					≈32
				N_2					<10
Bakken oil	Upper Bakken	-	-	SC CO_2	oil extraction	5000	230	7 h	≈10–43
	Lower Bakken	-	-						≈8–48

Table 2 - Recent simulation studies showing the potential of huff-n-puff EOR. However, most studies have focused on CO_2 EOR. CO_2 has been shown to be a very efficient solvent but its availability on field location becomes an issue (Du et al., 2019).

				Simulation Study						
Formation	K (μD)	ϕ (%)	Injection	Method	Natural Fracture	Model	Diffusion	Confiment Effect	Production	Increased Oil RF (%)
Field-scale	0.1	6	CO_2	huff-n-puff	30 mD	DFN	Yes	Yes	5000 d	10 (0.1 uD) 131.8 (1 uD) 11.5 (inject for 60 d) 13.3 (inject for 200 d)
Bakken	1 10 100	7	CO_2	huff-n-puff	NA	Single porosity	Yes	No	30 y	2.35 1.4 −0.7
Bakken	10, 0.001	8	CO_2	huff-n-puff	NA	Single porosity	No	No	60 d	≈−0.6–0.01
Bakken	10 (homo01) 10 (hete04)	8	CO_2	huff-n-puff	NA	Single porosity	No	No	700 d	−0.13 (10 d soaking) −0.23 (20 d soaking) −0.24 (10 d soaking) −0.33 (20 d soaking)
Bakken	10	8	CO_2	huff-n-puff	NA	Single porosity	Yes	No	5500 d	10.9 (Ppro = 1000 psia, 3 circles) 22.8 (Ppro = 2900 psia, 3 circles) 16.5 (Ppro = 3500 psia, 3 circles) ≈0 (inject after 30 d, 1 circle) 0.6 (inject after 200 d, 1 circle) 0.9 (inject after 500 d, 1 circle)
Eagle Ford	0.1	6	CO_2	gas flooding cyclic gas injection waterflooding cyclic waterflooding	NA	Single porosity	No	No	70 y	15.12 14.42 11.9 11.03
Middle Bakken	50	10	produced gas	huff-n-puff	NA	Single porosity	No	Yes	800 d	15.4 (Pinj = 1000 psi)
Middle Bakken	1 100	7	CO_2	huff-n-puff gas flooding huff-n-puff gas flooding	Conductivity 30 mD-ft	EDFM	Yes	No	18 y	2.56 −1.79 14.34 30.06
Middle Bakken	20	5.6	CO2	huff-n-puff	NA	EDFM	Yes	No	7000 d	5.9 (3 cycles)
Bakken	1	8	CO2	huff-n-puff	1.2 mD 4 mD	Dual permeability	Yes	No	>7000 d	55.1 49.8
Eagle Ford	0.9	12	CO2	huff-n-puff	Conductivity 10 mD-ft	EDFM	Yes	Yes	7300 d	9.1 (D = 0.01 cm^2/s) 3.8 (D = 0.001 cm^2/s) −5.1 (D = 0.0001 cm^2/s) −6.9 (D = 0.00001 cm^2/s)

In addition to simulation and experimental tests, field EOR test pilots have been implemented since 2008 in the Bakken and Eagle Ford (Hoffman 2016, 2018). The Bakken EOR pilot did not yield additional recovery after HnP mainly because of containment issue. Injected gas was observed at offset wells during soaking periods. However, the Eagle Ford pilot displayed oil rate increases after gas injection as can be seen in **Fig.8.** These two pilots clearly indicate that EOR huff-n-puff works but additional research and pilots planning is needed to make these operations economical. Additional information such as cost of compressors, solvent cost and availability, soaking time and their associated production loss must also be considered by operators in order to strategically implement EOR field HnP.

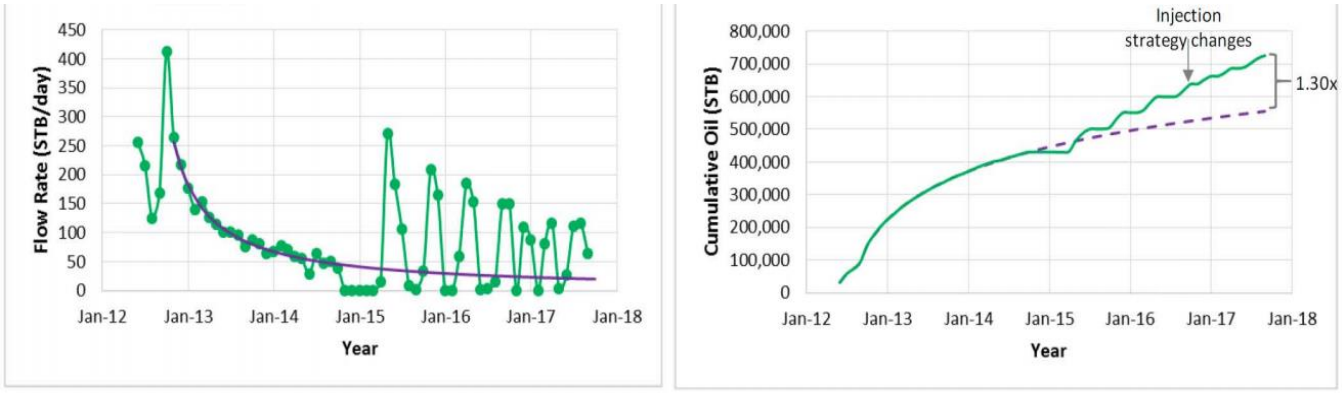

Figure 8 - Eagle Ford EOR pilot test showing incremental and cumulative production rate after Huff-n-Puff. 30% additional oil recovery is achieved after EOR compared to primary depletion. (Hoffman et al., 2018)

2.3 Review IC^3 crushed huff-n-puff gas injection in unconventional reservoirs

This section reviews various EOR key operational parameters for HnP field application, such as sample size, injection pressure relative to MMP, injection rates, soaking time/ residence time, solvent composition, production rates and lean versus rich gas EOR. These experiments were carried using an Eagle Ford sample. Table 3 shows sample properties.

Table 3 - Eagle Ford description with FTIR mineralogy, TOC and total porosity.

Sample	State	Total Porosity (%)	TOC (wt%)	Total Clays (wt%)	Total Carbonates (wt%)	Quartz+Feldspar (wt%)	Others
Eagle Ford	Preserved	5.1	5.0	16	62	13	8

2.3.1 Sample size/surface area

The impact of sample size on EOR was first investigated by Sheng and Li (2016), on saturated Wolfcamp shale with various lengths and diameters. They found that diameter has more impact on oil recovery than length. They concluded that the two main parameters controlling recovery are the apparent surface to volume ratio and the pressure gradient along the radial axis of the core.

Later Minh (2018) investigated the impact of surface area on crushed Eagle Ford at 150 °F with CO_2 as an injectate using different particle sizes (6.7-8mm, 4.76-.6.7mm, 2-4.7mm, 0.9-2mm). He found that smaller the particle size (i.e. the larger the external surface area) the larger the cumulative recovery. Similar experiment was carried out on a preserved Eagle Ford plug of similar 1.5in radius but various length (1in, 0.5in and 0.25in). The geometry of these samples along with their associated external surface area to volume ratio (S/V) is presented in **Fig.9**. **Fig.10** shows the NMR T_2 relaxation responses of these three plugs during HnP, where large pores (T_2>1ms) are depleted first then followed by smaller pore bodies (T_2<1ms). Like crushed HnP results, as S/V increases recovery also increases. **Fig.11** shows that the sample with high S/V of 10.6 in^{-1} recovery plateaued faster at 60% after 4 cycles only, while the sample with S/V of 6.6 in^{-1} and 4.6 in^{-1} recovery plateaued after subsequent cycles. Observations that underscore the importance of S/V for EOR performance.

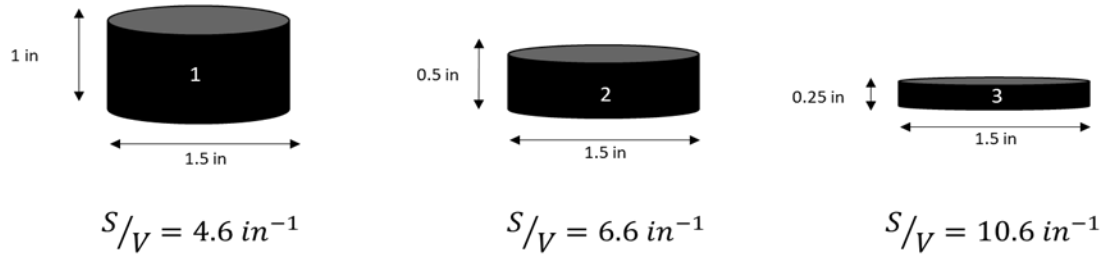

Figure 9 - Core plug dimensions with associated external surface area to volume ratios (S/V). These twin plug samples were cored parallel to bedding.

a)

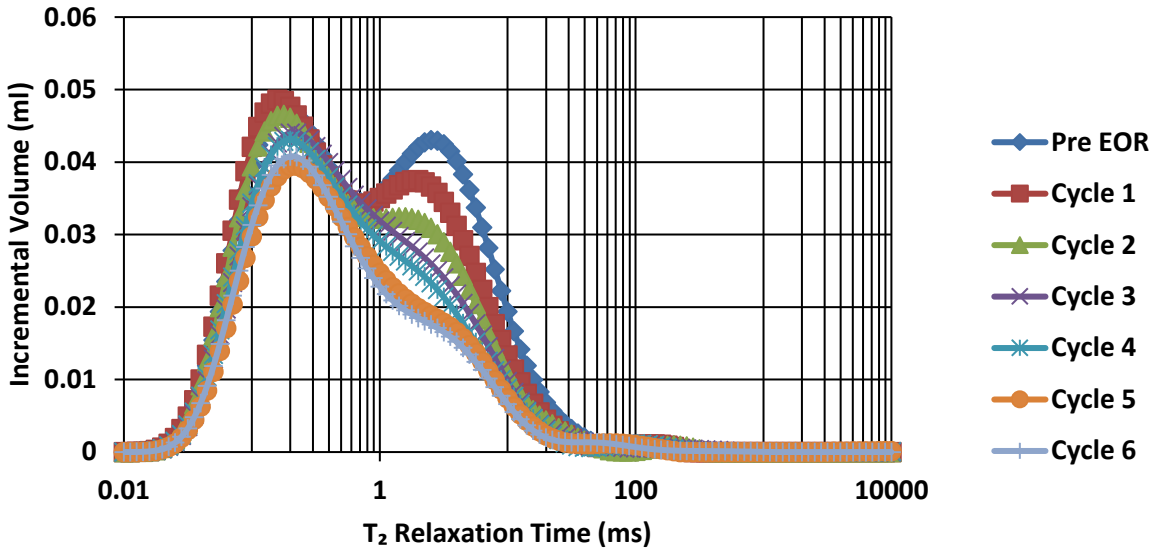
0.06
0.05
0.04
0.03
0.02
0.01
0
Incremental Volume (ml)
0.01
1
100
10000
T₂ Relaxation Time (ms)
Pre EOR
Cycle 1
Cycle 2
Cycle 3
Cycle 4
Cycle 5
Cycle 6

b)

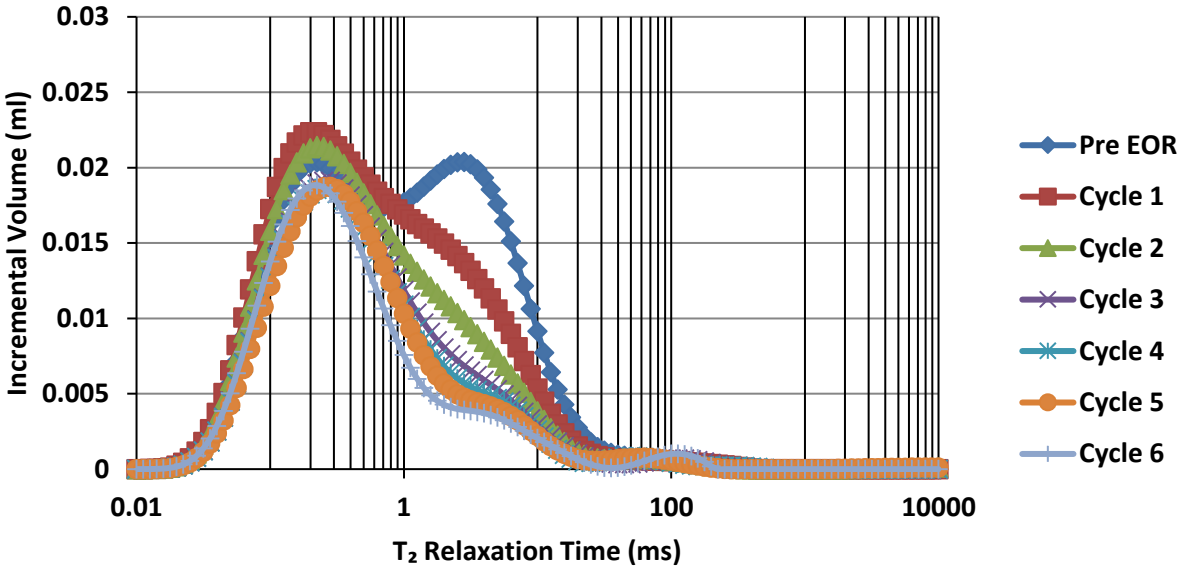
0.03
0.025
0.02
0.015
0.01
0.005
0
Incremental Volume (ml)
0.01
1
100
10000
T₂ Relaxation Time (ms)
Pre EOR
Cycle 1
Cycle 2
Cycle 3
Cycle 4
Cycle 5
Cycle 6

c)

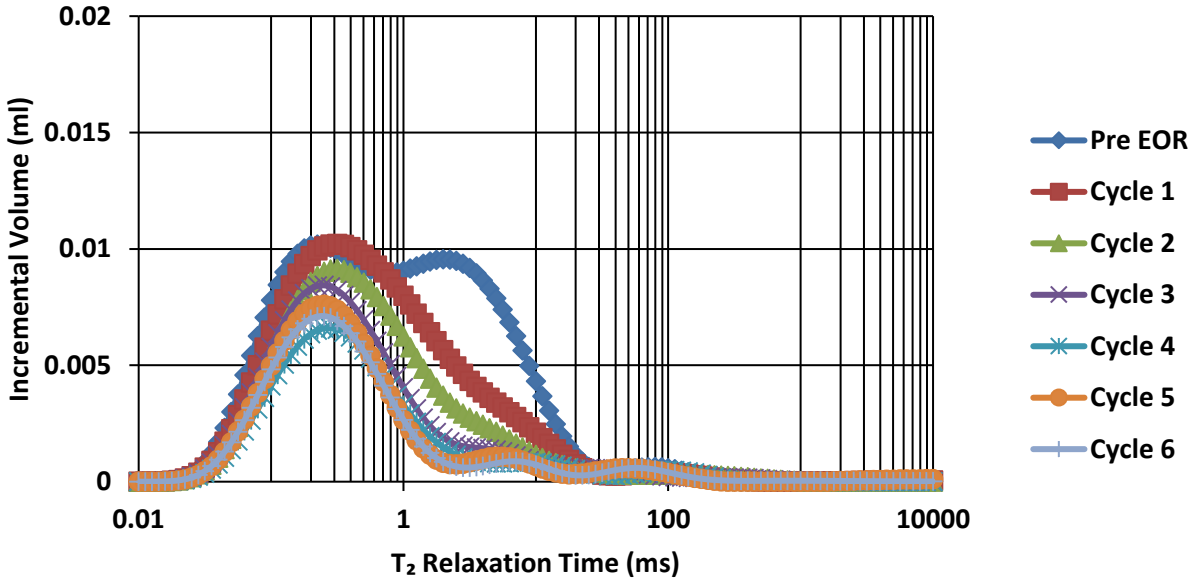

Figure 10 - NMR T_2 relaxation response during HnP experiment with C_1:C_2(72:28) at 4500 psi and 150 ºF for a) plug S/V=4.6 in^{-1} b) plug S/V=6.6 in^{-1} c) S/V=10.6 in^{-1}. The soaking time was 24-hours and the production time 24-hours, which represent one cycle in our experiment.

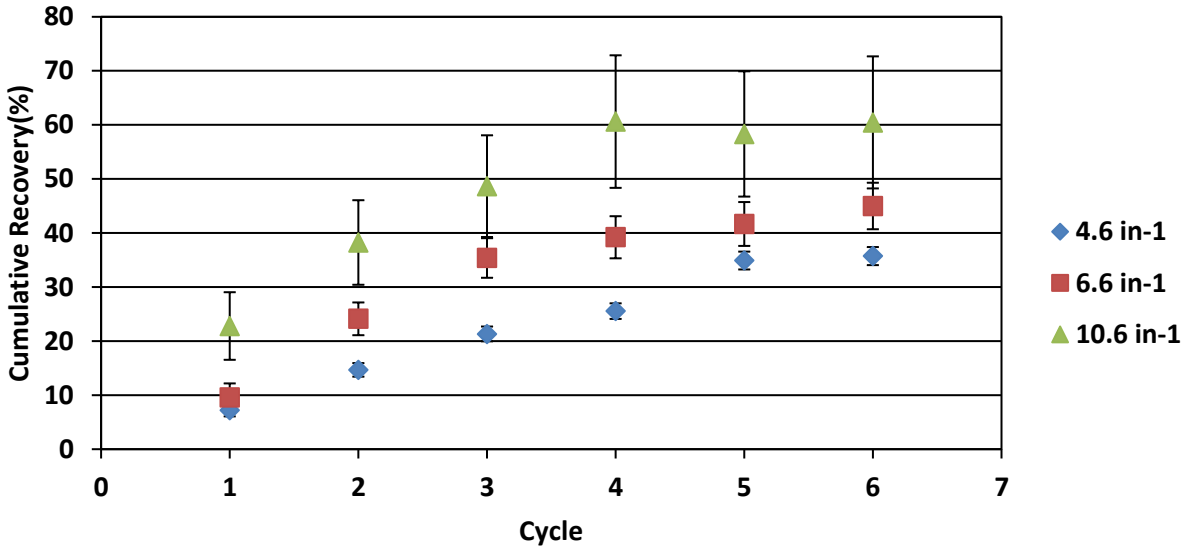

Figure 11 – HnP recovery as a function of S/V. Overall the higher the S/V the greater the recovery. The sample with larger S/V plateaued earlier than the other samples. This observation underscores the importance of S/V during EOR

Fig.12 summarizes literature data and additional S/V experiments on Eagle Ford and Wolfcamp shale using different injectate and particles sizes. It is clearly visible that irrespective of the operating conditions and solvent used, the recovery is the highest for crushed samples, which, emphasizes the importance of hydraulic fracture job quality pre-cyclical gas injection. Fracture geometry and stimulated reservoir volume must be optimal before injection.

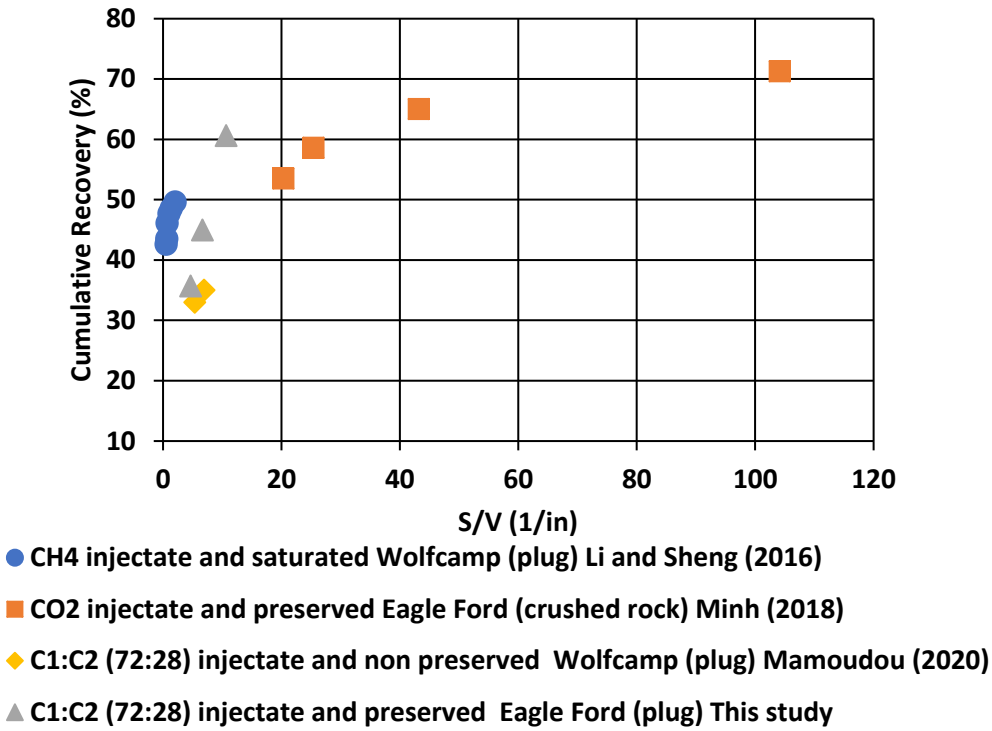

Figure 12 - Summary of S/V study on various play, using different injectate and particle sizes. Only the crushed HnP shows recovery greater that 60%, which means that irrespective to the HnP scheme S/V plays a critical role in HC mobilization.

2.3.2 Injection pressure

Another operational parameter of interest for HnP operation is the injection pressure relative to MMP. These parameters are strongly tied to field compressor use. Typical compressor system cost $4-4.5millions with injection pressures between 7000-9000 psi (JPT 2019). **Fig.13** shows the effect of fast injection rates (1.5cc/min) versus low injection rates (30cc/min). In this experiment

the soak time and production time was kept to 1-hour. The data shows that HC is mobilized even during the injection phase. Moreover, comparing the two injection rates, fast injection yields 10% more recovery after 6 cycles. In other words, fast injection period tends to be more beneficial. **Fig.14** summarizes the effect of injection pressure relative to MMP using the mixture of C_1:C_2(72:28) on crushed Eagle Ford samples. The results show that there are no substantial additional benefits associated with injecting at high pressure above MMP (2000 psi vs 1000 psi above MMP). The injection pressure should always be kept above MMP to maximize recovery. Subsequent gas chromatography analysis on the rock residual fluid shows that injection above MMP can vaporize heavier HC fraction up to C_{25}, while below MMP HC mobilization is limited to C_{19} **(Fig.15)**

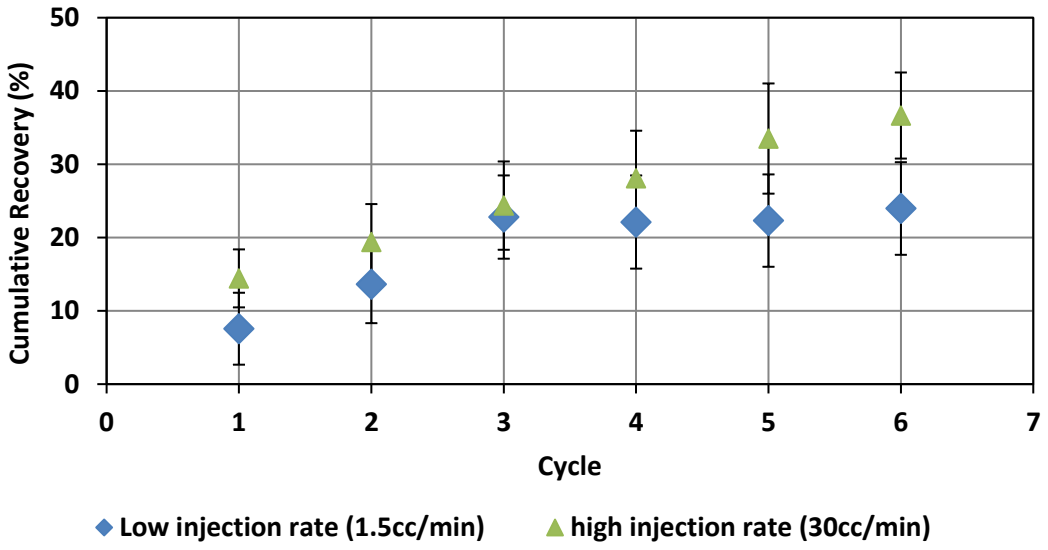

Figure 13 - Comparison between fast and slow injection rates during HnP, on Eagle Ford crushed sample (7-8mm) at 150 ºF using a mixture of C_1:C_2(72:28) at 4500 psi (Minh 2018). Higher injection rate shows 10% greater recovery after 6 cycles.

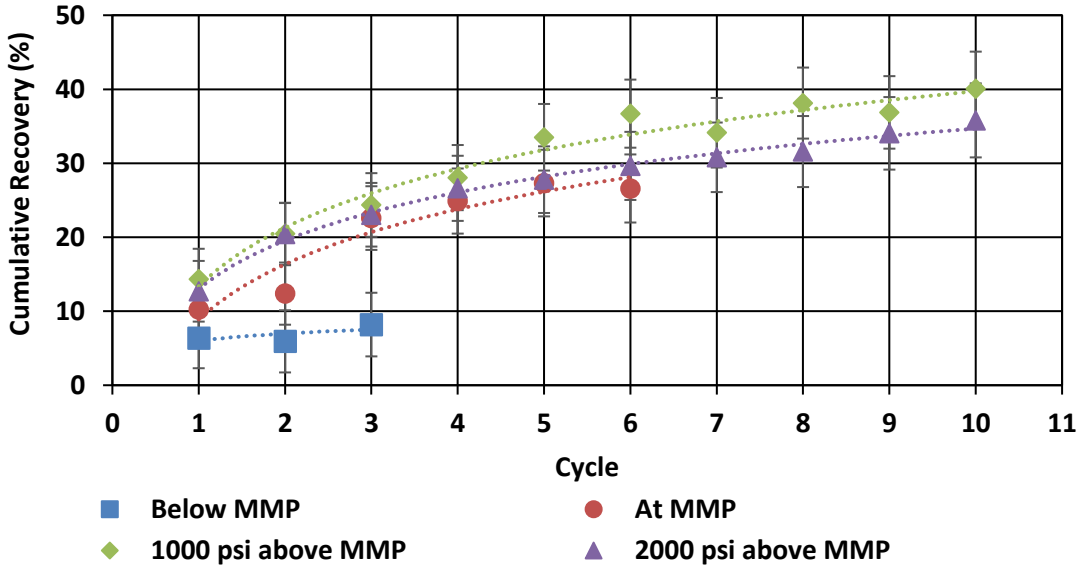

Figure 14 - Impact of injection pressure relative to MMP on crushed Eagle Ford with mixture C_1:C_2(72:28) using similar operating conditions at 150 ºF. Huff-n-puff should be conducted at pressure above MMP. (Modified after Minh 2018)

a)

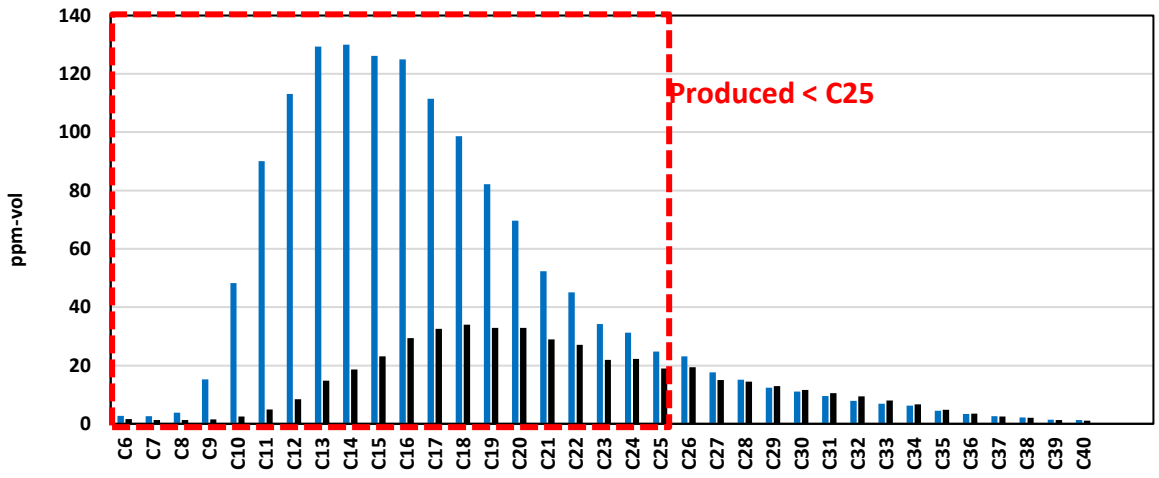

b)

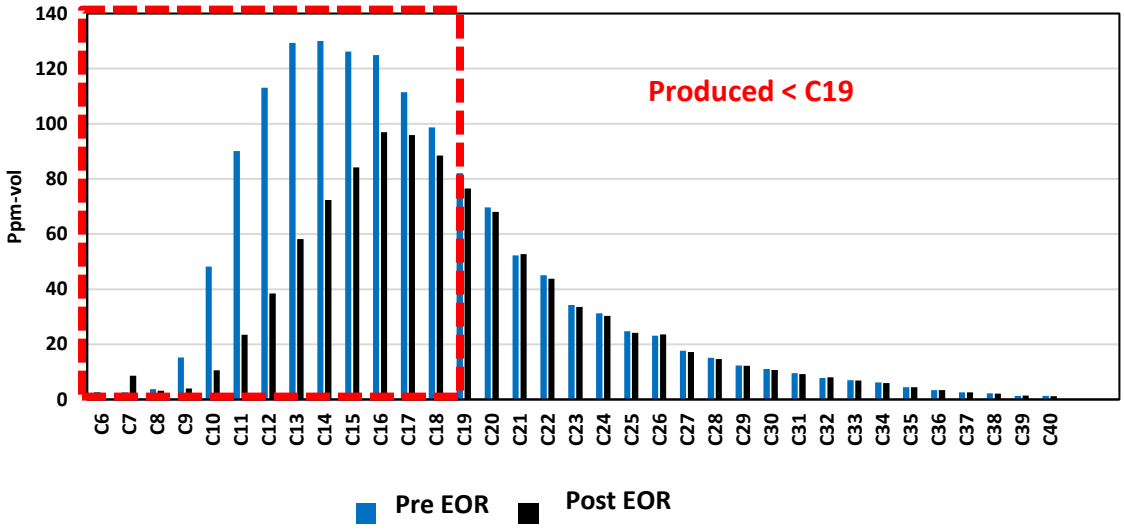

Figure 15 - GC-MS analysis on fluid pre and post huff-n-puff a) above MMP and b) below MMP. The experiment was carried on preserved Eagle Ford crushed sample (7-8 mm) at 150 ºF and 1000 psi above MMP (4500 psi) using the mixture C_1:C_2 (72:28). At injection pressure above MMP greater HCs fraction are mobilized up to C_{25} against C_{19} below MMP. (Dang 2019)

2.3.3 Soaking time/ residence time

Another important big question for HnP field implementation is the shut-in time also known as soak time. Several experimental and simulation studies (Li et al., 2016; Yu et al., 2016) have shown the importance of soak period on recovery efficiency and highlighted the fact that above a certain range, longer soak has no improvement on oil recovery. Minh (2018) observed similar recoveries (**Fig.16**) on crushed preserved Eagle Ford samples after 1-hour, 3-hours and 6-hours, when the responses are analyzed as function the cumulative residence time. It was defined "residence time" as the sum of soak and production times or the total amount of time the solvent is in contact with the formation and highlights its importance as an optimization parameter for field application. For instance, Yu et al (2016) conducted a series of cyclical gas injection with N_2 at 104 ºF and 1000 psi on saturated Wolfcamp samples. When the data is converted into residence time instead of

cycles, optimal timing to deplete these plugs can be found to be around 20-hours; going above 20-hours does not yield additional recovery and a residence less than that value might not be enough to economically mobilize HC **(Fig.17).**

a)

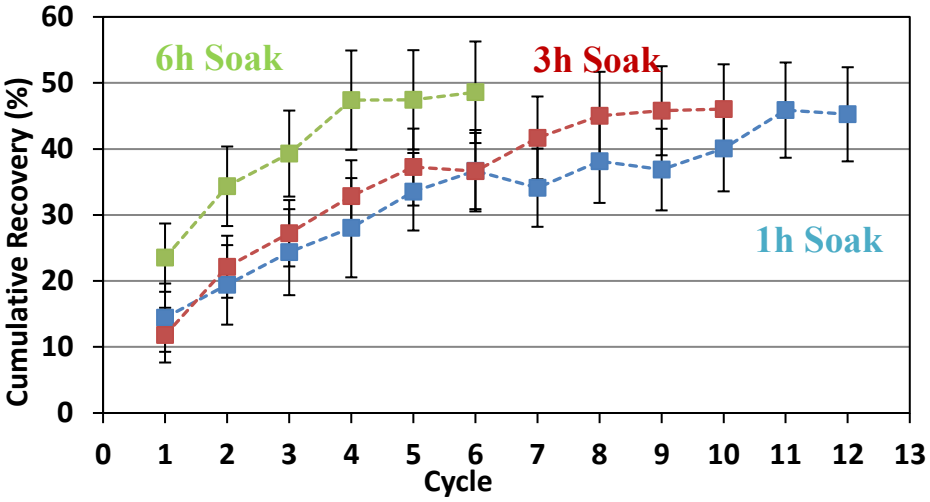

b)

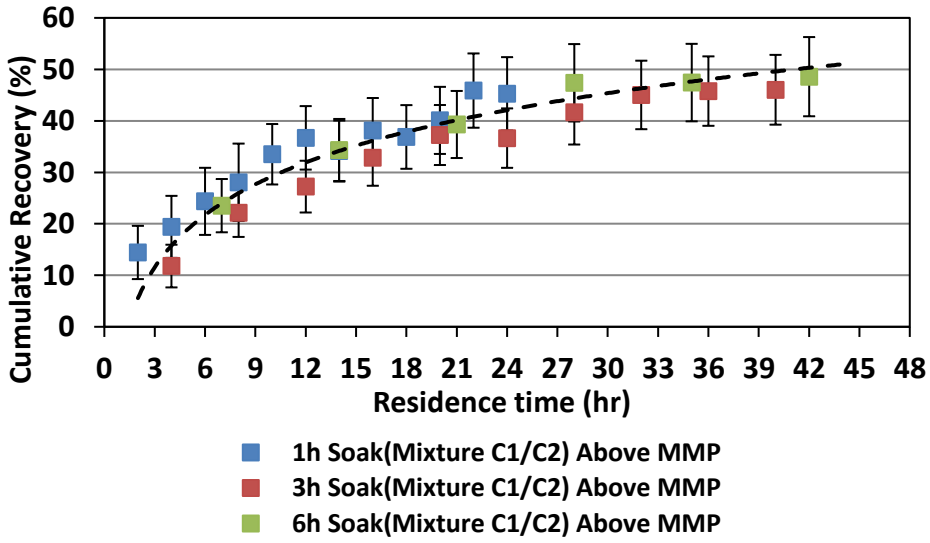

Figure 16 - a) Impact of soaking time of crushed Eagle Ford recovery. The longer the soaking time the greater the incremental recovery on a cycle basis. However, b) when the number of cycles is converted to residence time the cumulative recovery becomes similar. For field application residence time becomes more meaningful as a possible upscaling/optimization parameter. (Minh 2018; Dang 2019)

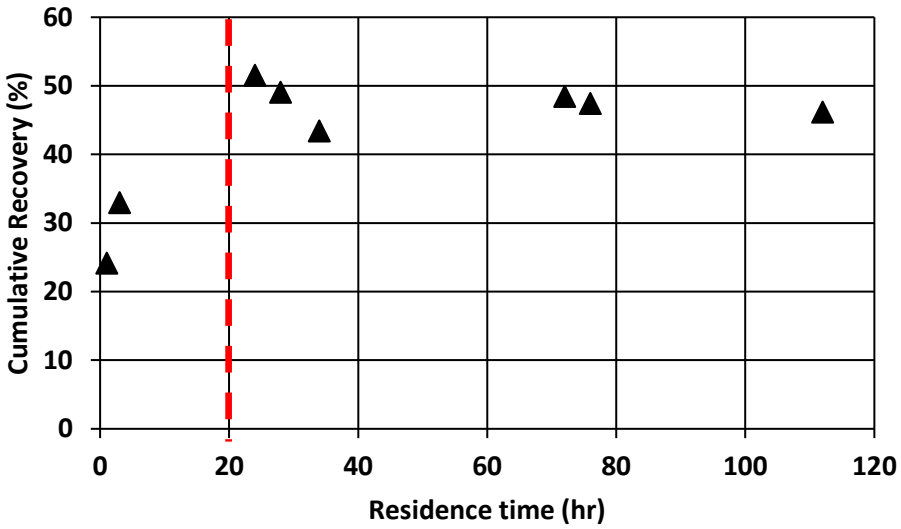

Figure 17 - Impact of residence time on 8 saturated Wolfcamp samples (Modified after Yu 2016). Residence time can be used to determine optimal contact time between a solvent and a reservoir for optimization and upscaling purpose. The optimal residence for N_2 to deplete the Wolfcamp reservoir is around 20-hours, beyond this time, there is no additional recovery.

Residence time was defined earlier by Minh (2018) and Dang (2019) as the sum of soak and production time; but their work only focused on the soak period. The next set of HnP propose to verify the concept of residence time as an EOR controlling factor by varying soak time (1-hour vs 3-hours) but also production time (1-hour vs 4.75-hours) on cleaned and dodecane saturated Eagle Ford plugs. The main two questions this subsections addresses: (1) What parameter controls the residence time, soak or production time, or a combination of both? (2) What would be the optimal HnP schedule to mobilize efficiently HC? To address these questions three samples were cleaned with a mixture of toluene- methanol (80%-20% by vol) for 24-hours by Soxhlet extraction to remove the original fluids, then saturated for 24-hours at 5000 psi with dodecane. **Fig.18** shows the pressure profiles during the experiments for the three samples, with 1-hour soak and 1-hour production (1h+1hr), 1-hour soak and 4.75-hours production (1h+4.75h) and 3-hours soak and

4.75-hours production (3+4.75h). All three tests were carried at 150°F and 1000 psi above MMP during the soak phase. **Fig.20 (a,b and c))** show the associated T_2 responses during HnP.

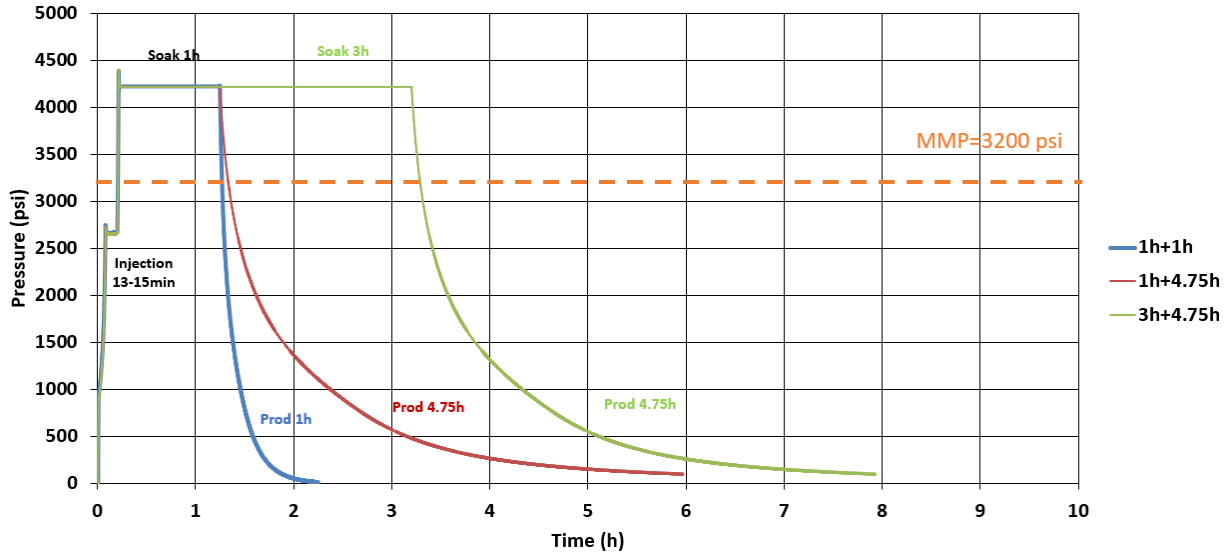

Figure 18 - Pressure profile comparison during HnP for three Eagle Ford plugs with different soak and production time at 150°F. Sample 1 (blue) correspond to 1-hour soak and 1-hour production for a single cycle. Sample 2 (red) shows the effect of longer production time with 1-hour soak and 4.75-hours production. Sample 3 (green) shows the injection profile for longer soak and longer production 3-hours and 4.75 hours.

a)

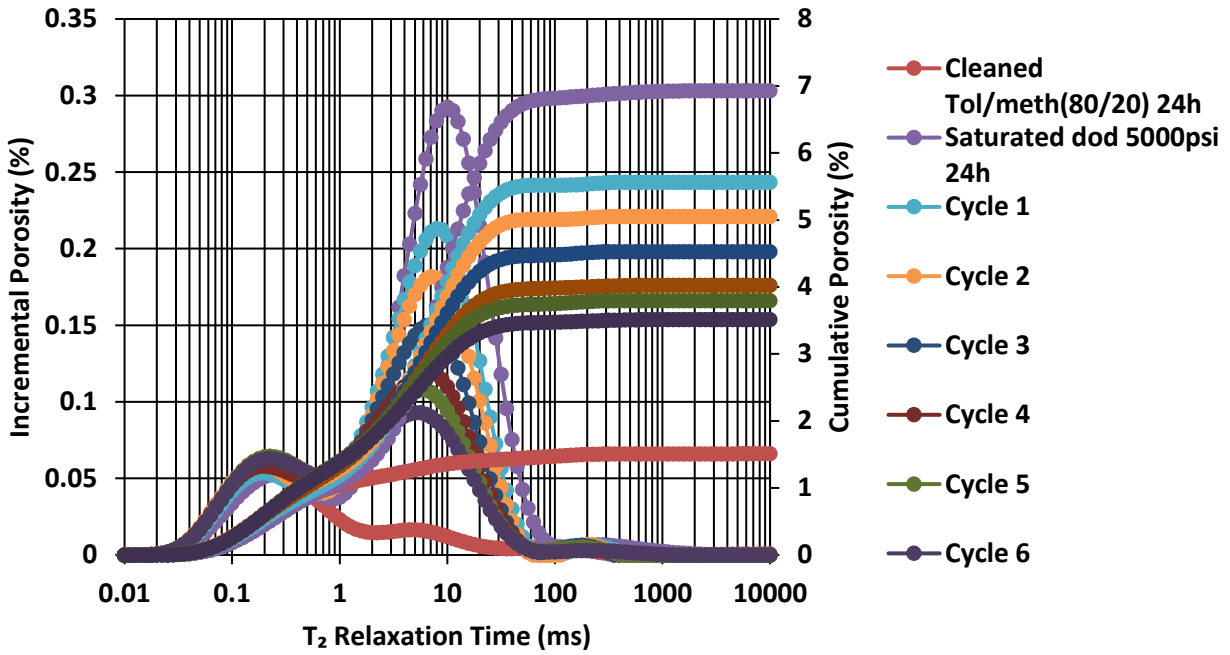
Incremental Porosity (%)
Cumulative Porosity (%)
T₂ Relaxation Time (ms)
0.35
0.3
0.25
0.2
0.15
0.1
0.05
0
8
7
6
5
4
3
2
1
0
0.01
0.1
1
10
100
1000
10000
Cleaned Tol/meth(80/20) 24h
Saturated dod 5000psi 24h
Cycle 1
Cycle 2
Cycle 3
Cycle 4
Cycle 5
Cycle 6

b)

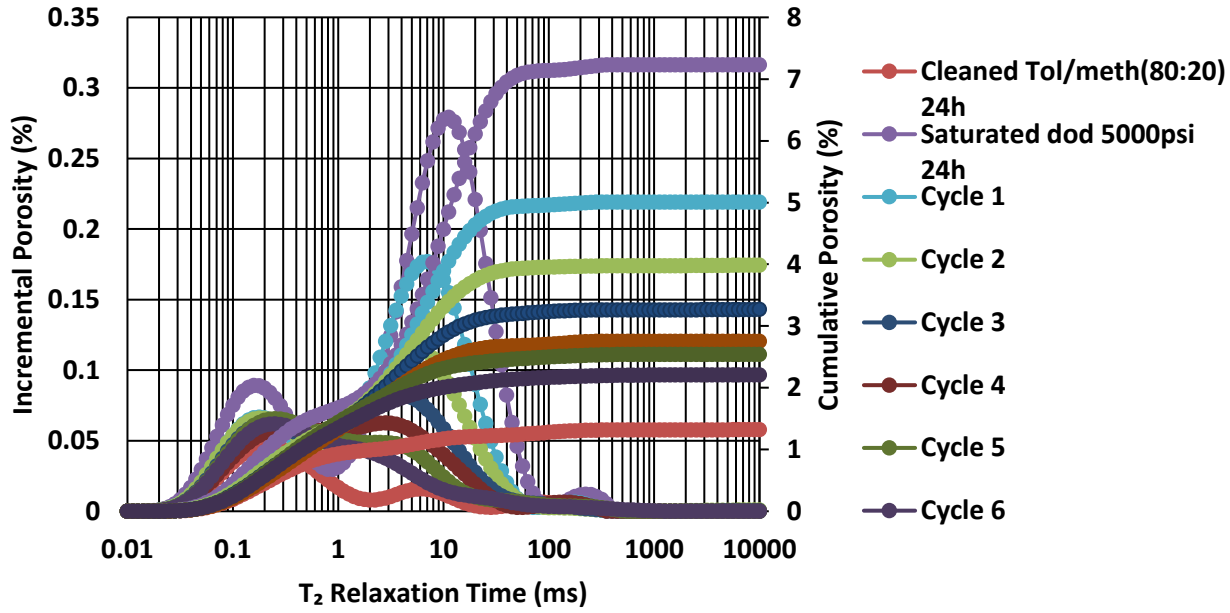
Incremental Porosity (%)
Cumulative Porosity (%)
T₂ Relaxation Time (ms)
0.35
0.3
0.25
0.2
0.15
0.1
0.05
0
8
7
6
5
4
3
2
1
0
0.01
0.1
1
10
100
1000
10000
Cleaned Tol/meth(80:20) 24h
Saturated dod 5000psi 24h
Cycle 1
Cycle 2
Cycle 3
Cycle 4
Cycle 5
Cycle 6

c)

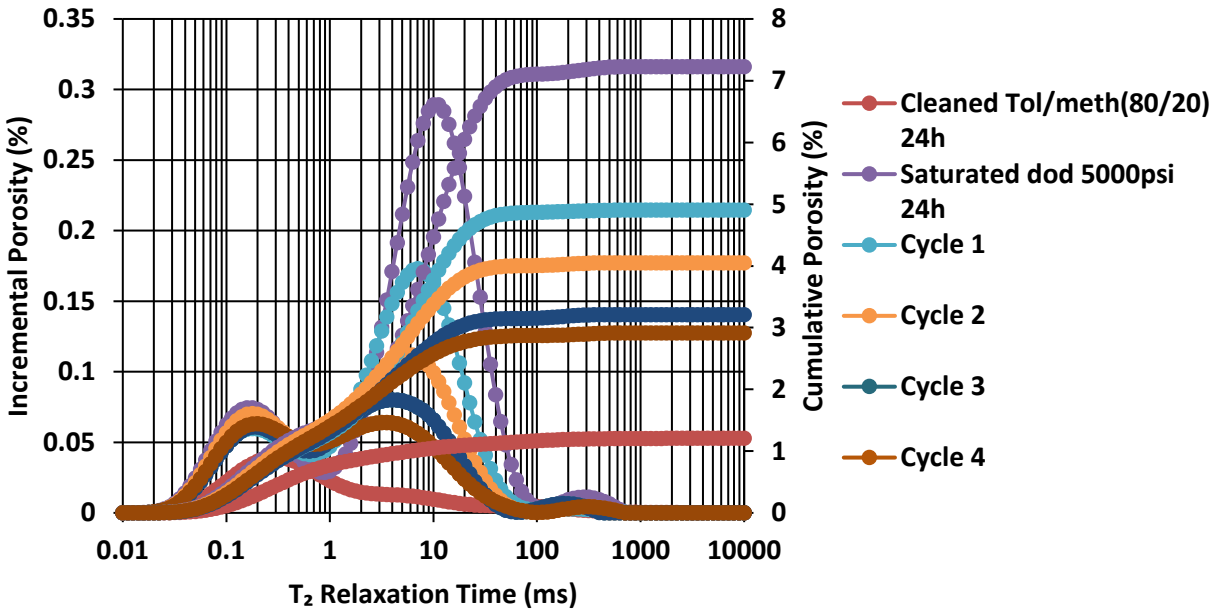

Figure 19 - NMR T_2 relaxation response during HnP experiment with C_1:C_2(72:28) at 4200 psi and 150 ºF for three dodecane saturated Eagle Ford plugs for various soak and production periods. a) 1 cycle represents 1-hour soak and 1-hour production. b) 1 cycle represents 1-hour soak and 4.75-hours soak. c) 1 cycle represents 3-hours soak and 4.75-hours.

Fig.20 shows that irrespective of the soaking or production time the recovery is the same and the values are withing instrument error. When we increase the production time from 1-hour to 4.75-hours, while keeping the soaking constant to 1-hour there is no additional recovery. Also, increasing the soak from 1-hour to 3-hours, while keeping the production to 4.75-hours also does not promote significant HC mobilization. The same volume of dodecane is produced whether we increase the soaking or the production for these plugs.

Similar observations were also made by Perez (2020) regarding soak and production using molecular simulation on saturated kerogen model with a black oil. The sample size is different but some of the observations between plug measurements and molecular simulation agrees well. The study found that increase soak time does not provide deeper penetration of the solvent gas into the

rock matrix. The soaking phase provides limited solvent penetration restricted to 3nm beyond fracture face. When scaling the simulation model to an actual reservoir the solvent penetration is no more than 2 feet (Perez and Devegowda 2020a). Which means that soaking might not be a critical factor during HnP. In our experiment the longer soak was found to be even slightly detrimental, which suggest that longer soak might even alter solvent efficiency.

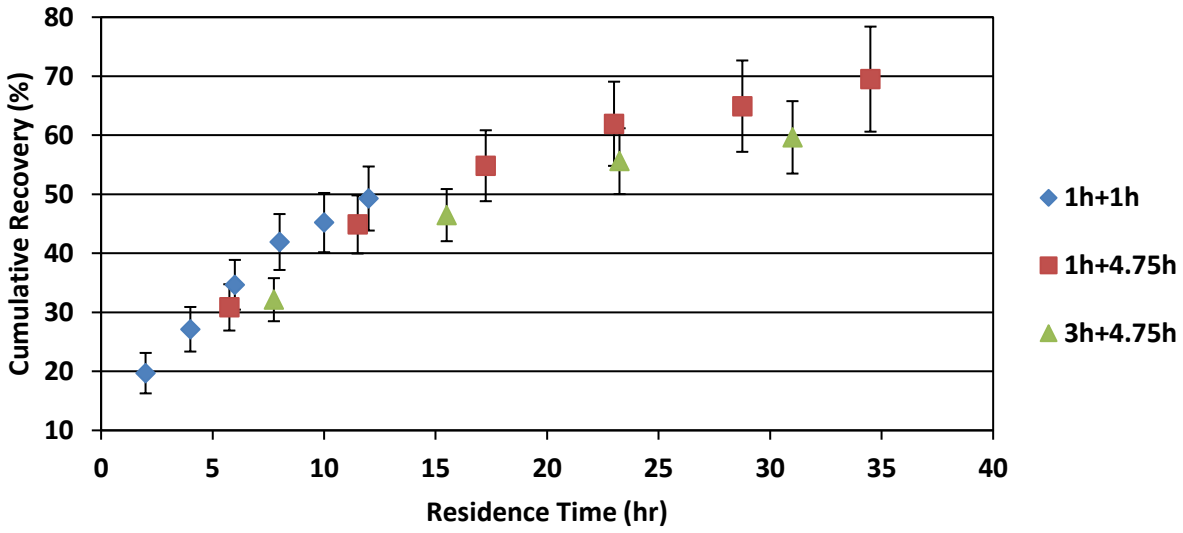

Figure 20 - Effect of soaking time and production time on recovery. Increase soak and production time does not increase dodecane recovery

2.3.4 Solvent composition

Fig.21 shows the effect of different gas compositions on recovery from Eagle Ford shale samples under the same experimental conditions (1-hour soak and 1-hour production at 1000 psi above MMP). The results demonstrate that ethane performance is the best when compared to the other gases tested in terms of number of cycles needed for maximum recovery. A recovery of 40% was achieved in 6 hours for ethane, 4 hours for CO_2 and around 16 hours of residence time for C_1:C_2 (72:28) mixture and the field gas (C_1:C_2:C_3+/76:14:10).

In terms of produced HCs, at 150 °F, ethane was the only solvent capable of mobilizing heavier hydrocarbon fractions up to C_{27}; while CO_2 and the mixture of C_1:C_2 (72:28) and field gas were only able to efficiently mobilize HCs up to C_{24} (**Fig.22**).

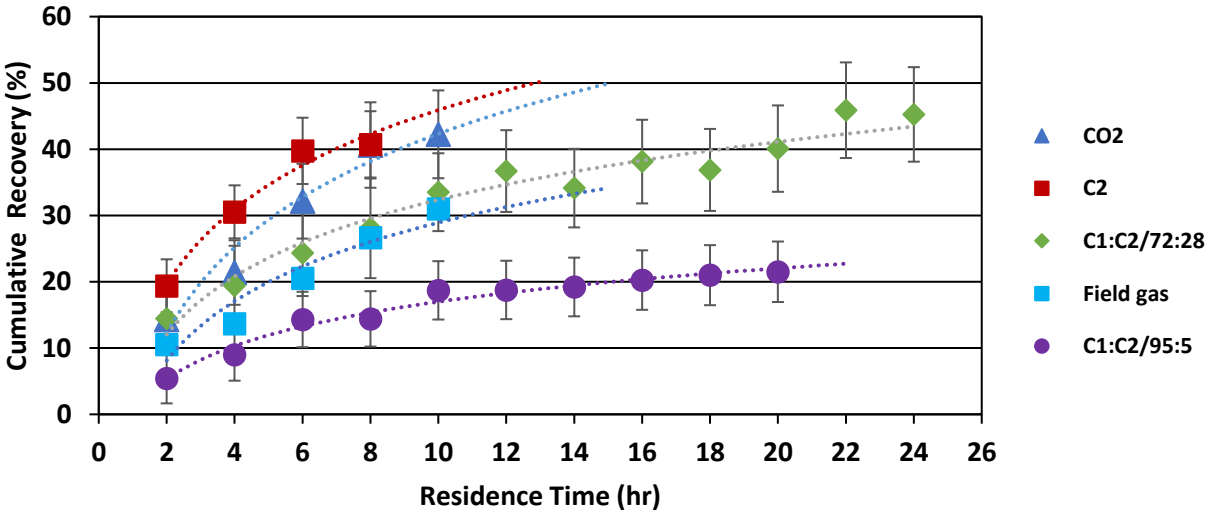

Figure 21 - Effect of injection gases composition on huff-n-puff recovery on Eagle Ford sample at 150 °F, using various gases. For each gas the injection pressure was 1000 psi above relative oil/gas MMP. Pure ethane shows the greatest recovery in the fewest cycles followed by CO_2, C_1:C_2 (72:28) and the field gas (C_1:C_2:C_3+/76:14:10). (Dang 2019)

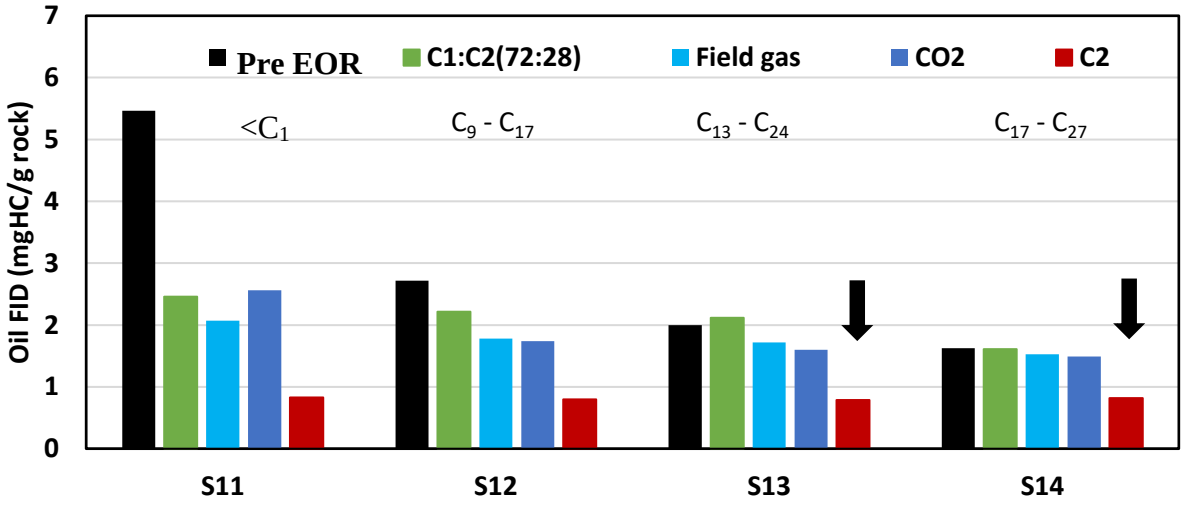

Figure 22 - HAWK pyrolysis results after HnP using various gases. Ethane is found to be more efficient in removing heavier HCs (up to C_{27}), compared to other gases. (Dang 2019)

2.3.4 Lean vs rich solvent EOR

Another optimization parameter is the injection gas composition. EOR was initially performed with a lean mixture of methane and ethane C_1:C_2 (95:5), then switched to a mixture richer in ethane, C_1:C_2 (72:28) to determine additional recovery. The same experimental conditions were kept (1-hour soak and 1-hour production at 150°F). MMP was not measured using the mixture C_1:C_2 (95:5), but since the solvent was mostly methane, its MMP was based on pure methane MMP value around 5732±300 psi. Injection pressure of 6000 psi for C_1:C_2 (95:5) and 4500 psi for C_1:C_2 (72:28) were used for this experiment.

Fig.23 shows that enriching the gas from 5 to 28 % yields an additional 10% recovery. This observation is also verified by simulation work on an offset single well from the same Eagle Ford reservoir (Nitec model courtesy of Ovintiv). Based on their simulation study, enriching the solvent from 7 to 32 % yields an additional 12.5% (see **Fig.24**).

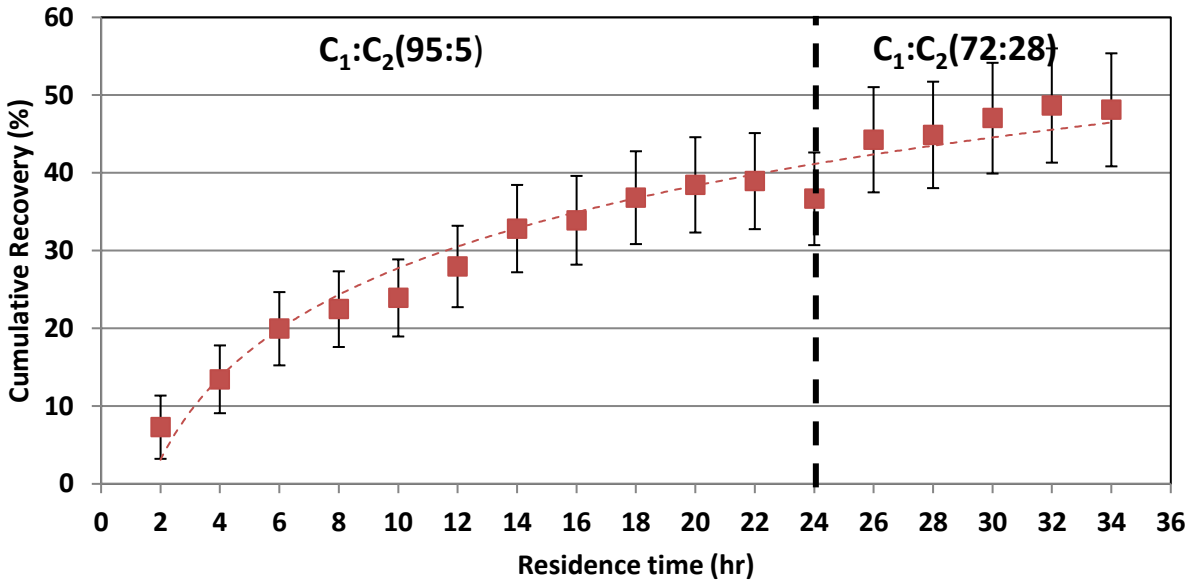

Figure 23 - Impact of ethane enrichment during HnP, crushed Eagle Ford are contacted with a lean solvent C_1:C_2 (95:5) mixture and then a richer mixture C_1:C_2 (78:28). The dashed line represents the cycle after which the new solvent was introduced. 10% additional recovery is unlocked when the solvent is enrichment from 5 to 28% ethane after 24-hours.

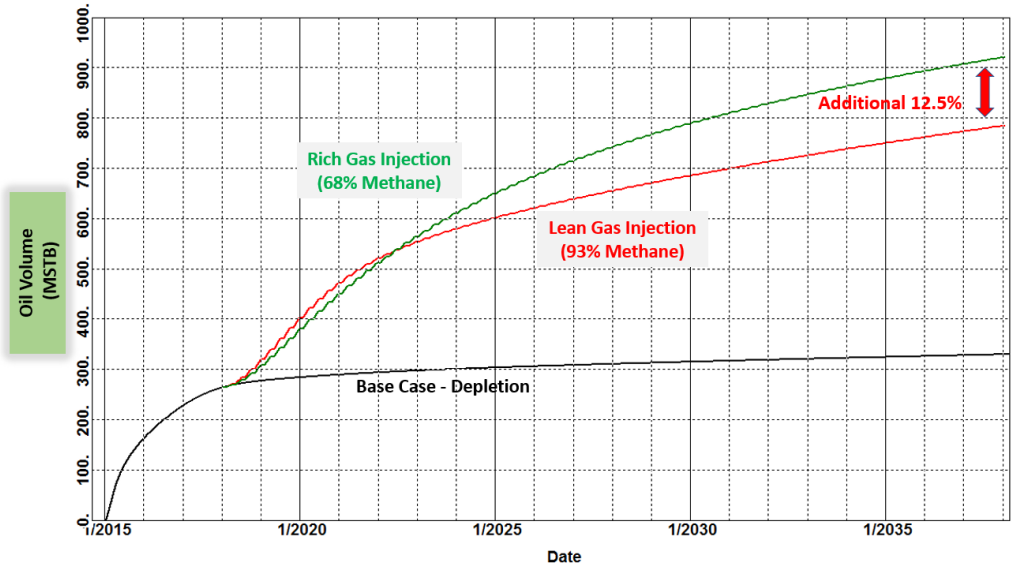

Figure 24 - Single well simulation comparison between a lean gas injection C_1:C_2 (93:7) vs rich gas injection C_1:C_2 (68:32). Like experimental work, rich gas injection yield 12.5% additional oil recovery (Courtesy of Ovintiv).

2.4 Discussion

Chapter 2 reviews several critical parameters that the operator can optimize during HnP. The above results on preserved Eagle Ford shows that not all parameters improve oil recovery. The most two important parameters that yield additional recovery are the surface area and the solvent composition. The soaking and production time were found to have minimal to no impact on recovery for the sample studied.

Increasing the surface S/V ratio for a plug from 4.6in^{-1} to 10.6in^{-1} increased the recovery from 35% to 60%. When the S/V ratio is large the solvent contact with the rock increases, which yield higher recovery. The rationale behind this observation is that for tight formation such as the Eagle Ford, diffusion coefficient is small, Dang (2019) reported values ranging 1-2×10^{-8} m^2/s. Therefore, the solvent penetration in rock is limited to near fracture zones. Perez (2020) also shows that for a single fracture using a molecular simulation on a kerogen saturated black oil and a rich solvent in

ethane, penetration depth of the solvent is limited to 3-4nm away from the microfractures. These conclusions also explain the low impact of soaking time on oil recovery. In other words, longer soak does not favor deeper solvent penetration. This underscore the importance of knowing the size of the stimulated reservoir volume after hydraulic fracturing in order to increase contact with the reservoir prior HnP.

The solvent composition is also another major component of an HnP success. For hydrocarbon-based solvent, richer solvent will tend to have higher recovery. Pure ethane is capable to efficiently mobilize heavier HC fraction S_{14} (up to C_{27}) compared to other solvents, its recovery is the highest with 45%, followed by the rich mixture C_1:C_2 (72:28) with 35% and C_1:C_2 (95:5) with 19% after 12-hours residence time for crushed rocks.

2.5 Conclusions:

Crushed rock (7-8mm) can be used for rapid screening for potential candidates for EOR. From the experimental data the following conclusion can be drawn:

- Specific surface area S/V is a major controlling factor for EOR performance, the greater the S/V the greater the recovery, whether it is a crushed or plug test. EOR candidates must have a larger S/V to allows greater contact between solvent and the rock.
- Injection pressure above MMP results in mobilization of heavier hydrocarbons (up to C_{25}) and higher recovery.
- Residence time (soaking +production time) controls the recovery factor and can be used as an upscaling parameter for field application.
- For the same experimental conditions, ethane was found to be the best solvent because of its lower MMP and its capability to remove heavier HC (up to C_{27}). Enriching the solvent during HnP on Eagle Ford samples yielded an additional 10%. Simulation studies between rich vs lean gas shows similar recovery factor of 12.5%.

CHAPTER 3: METHODOLOGY

Chapter 3 describes the details of the experimental equipment and procedures used in this study.

3.1 General experimental workflow

Most of the available HnP experiments in the literature focused on injection at reservoir condition; however, due to instrument limitation this study will be conducted at temperature of 150 °F (65°C) inside a Despach LEB2-18-1 oven. This project consists of a series of experiments to investigate the effect of various parameters on EOR on crushed samples. **Fig.25** shows the different apparatus/techniques used to measure EOR efficiency.

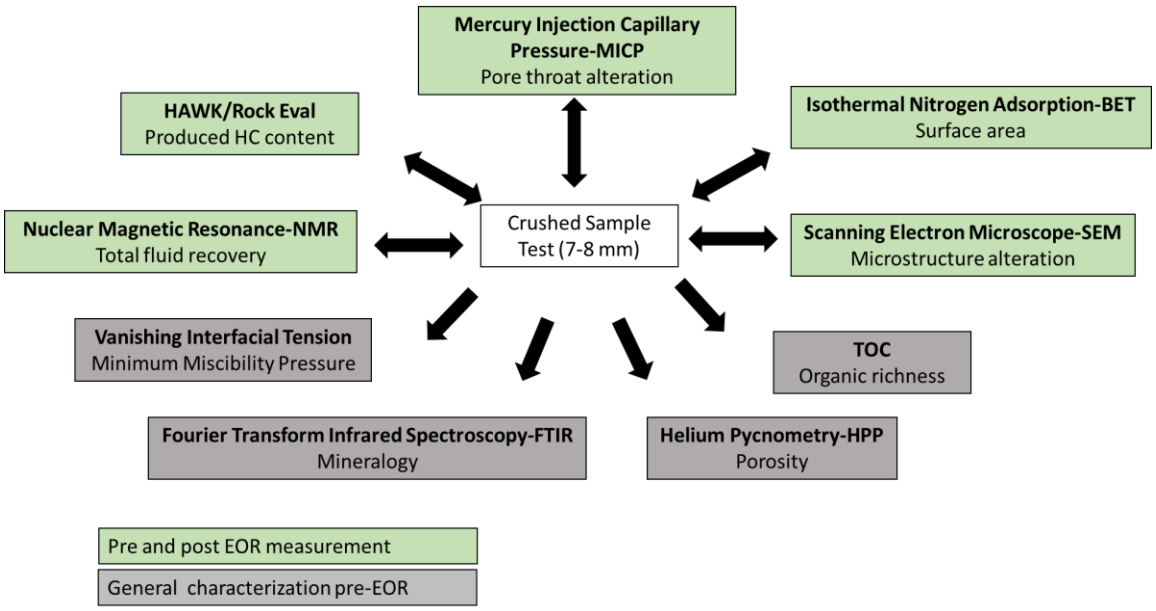

Figure 25 - Experimental apparatus/techniques used to measure EOR HnP performance. The green color represents measurements carried before and after EOR, and the grey color represents measurements used for initial petrophysical characterization.

3.2 Experimental procedures

The experimental setup for huff-n-puff testing is illustrated in **Fig.26**. The apparatus consists of a pressure high-pressure/high-temperature cell (rated for 6,000 psi at 200°F(93°C)) inside a temperature-controlled oven. A Teledyne ISCO Model 100DM Syringe Pump in series with a Teledyne ISCO D-Series Pump Controller is used for pressurizing rated for a maximum pressure of 10,000 psi. A commercially mixed mixture of methane and ethane (72:28 ±2 mol%) is used as the injected solvent. An in-house computer control system software is used to automatically open/close a Vindum valves inside the oven. The solid black line on the schematic represents the gas line, while the orange dashed line shows the communication between the instrument and the computer.

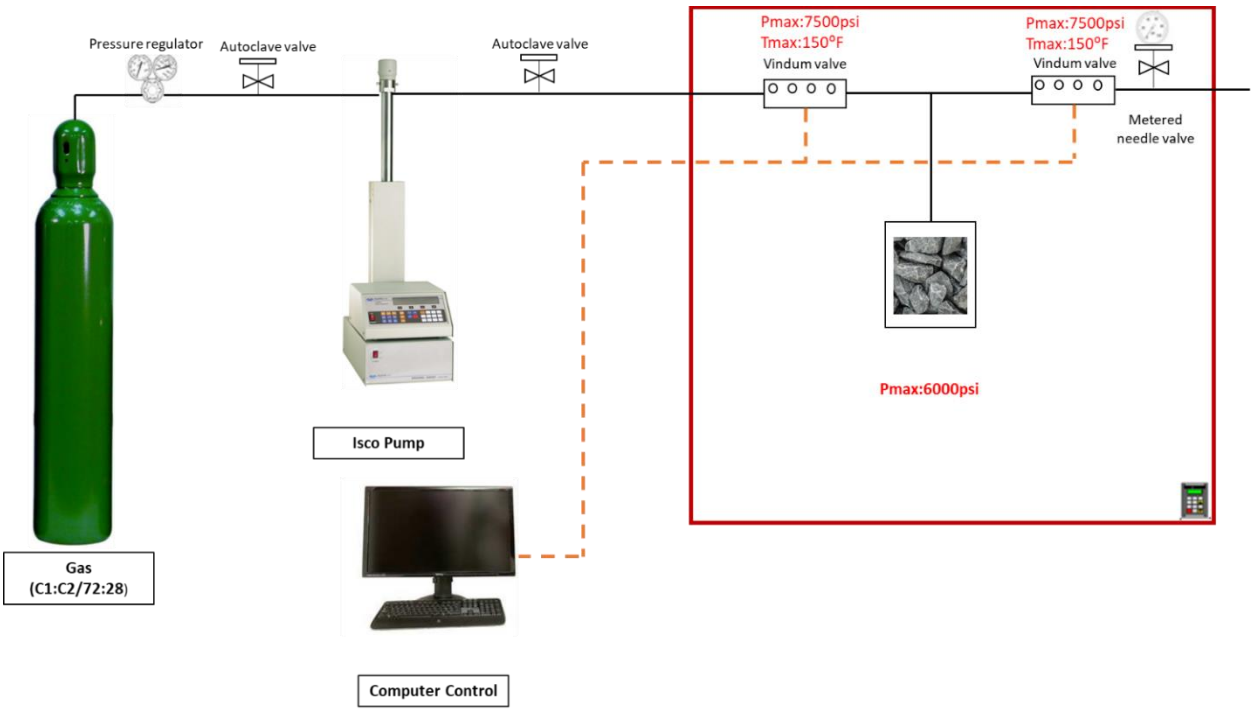

Figure 26 - HnP experimental schematic. The crushed sample is placed inside a high-pressure cell, located within an oven. A mixture of methane: ethane (72:28 ±2%) is injected into high pressure cell via a pump station with precise pressure control; the pressure vessel outlet has a peioduction choke to control production rate and production time.

Crude oil saturation is not required because the experiments are conducted on a "preserved" or "as received" state. NMR is used to monitor the fluid (hydrocarbon and water) content after each cycle. This method improves fluid sensitivity readings particularly when residual volume and porosity are small. The steps used in this experiment are listed in the appendix B.

Cumulative recovery is computed by subtracting the pre and post EOR NMR T_2 spectrum. T_1-T_2 maps are compared to determine which fluids are liberated during the huff-n-puff experiment. **Fig.27 (a & b)** shows an example of NMR HnP response pre- and post- EOR.

$$Recovery\ (\%) = \frac{(NMR\ vol_{pre\ EOR} - NMR_{vol\ after\ cycle\ x})}{NMR\ vol_{pre\ EOR}} x100 \quad (1)$$

Table 4 - 12Mhz Oxford Geospec2 NMR T_2 and T_1-T_2 measurement parameters.

	Time/Number of scans (NSA)	Tau (μs)	T_2 max (ms)	T_1 max (ms)
T_2	**Time=8 minutes**	**57**	**100**	
T_1/T_2	**NSA=32**	**57**	**100**	**200**

a)

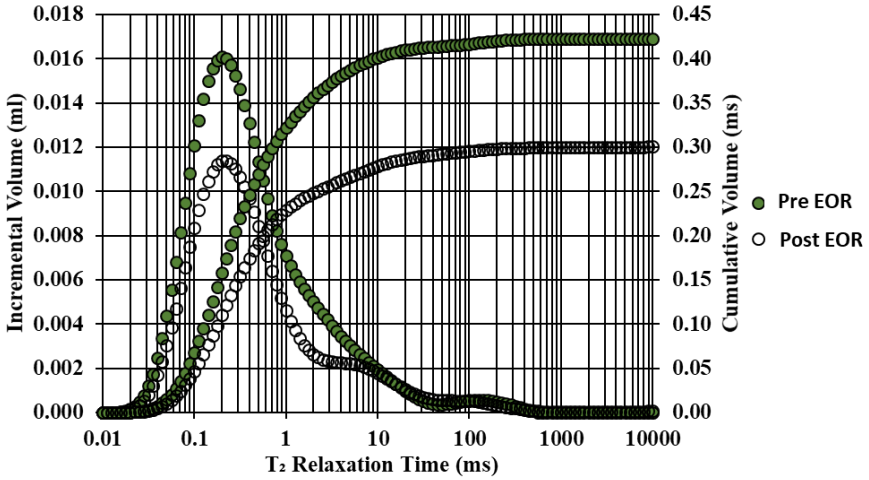

b)

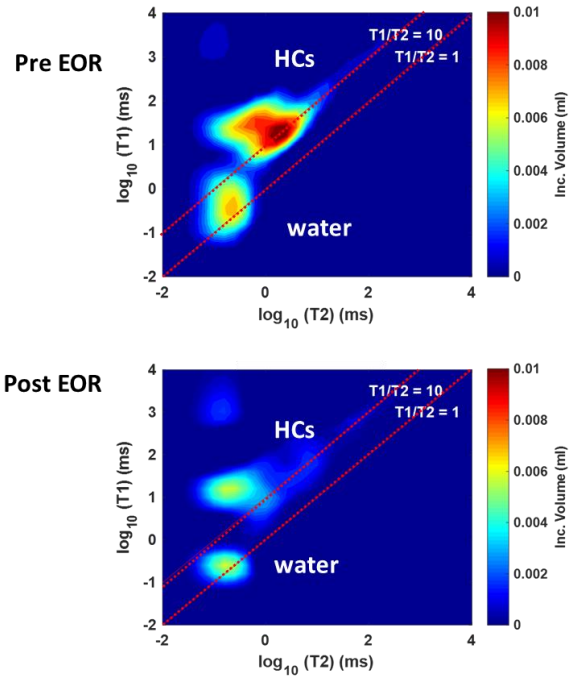

Figure 27 – a) Example of NMR T_2 relaxation pre- and post- HnP for the same crushed sample. The graph shows incremental distribution of the left axis and cumulative distribution on the right axis. The difference between the two spectra represents the total fluid produced. b) Associated T_1-T_2 maps for the same crushed samples pre- and post- EOR. In both maps HC and water can be discriminated by separating signal clusters. 1:1 line is traditionally associated with low viscosity fluid such as brine. While, HCs tends to have larger T_1:T_2 ratio. (Dang 2019)

3.3 Instrument and Theory Review

3.3.1 Minimum Miscibility Pressure (MMP)

The minimum miscibility pressure is a major optimization parameter during HnP to achieve maximum HC production. To determine the injection pressure for a successful huff-n-puff experiment, we needed to determine the MMP. This pressure is measured using the Vanishing Interfacial Tension (VIT) approach (Hawthorne et al., 2014). The traditional methods consist of measuring the Multiple Contact MMP (MC-MMP), where capillary height at different pressures from ambient to near MMP pressure is measured, then extrapolated the zero capillary height to determine the pressure at which the interfacial tension no longer exists. However, for tight rocks with nano scale pore throat size the First Contact Miscible (FC-Miscible) is preferred where the interfacial tension completely vanishes and is not extrapolated as seen in **Fig.28**. This method ensures minimal capillary pressure effect (Dang 2019). A summary of FC-MMP is shown in **Fig.29** at 150 ^{o}F.

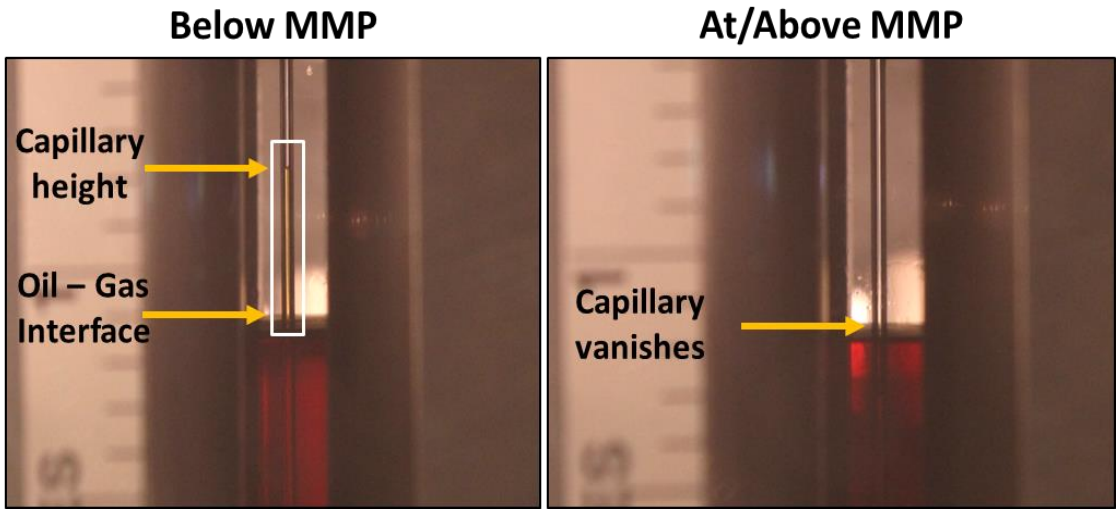

Figure 28 - Example of FC-MMP between a mixture of C_1:C_2 (72:28 mol%) and a crude oil from Meramec (3.5±0.03 cP at 150 ^{o}F). Above MMP capillary height is visible however at or below MMP (3500 psi) the capillary height vanishes (Mukherjee 2020). The measurement is carried in a high-pressure and high-temperature cell (Pmax=10,000 psi and Tmax=350°F).

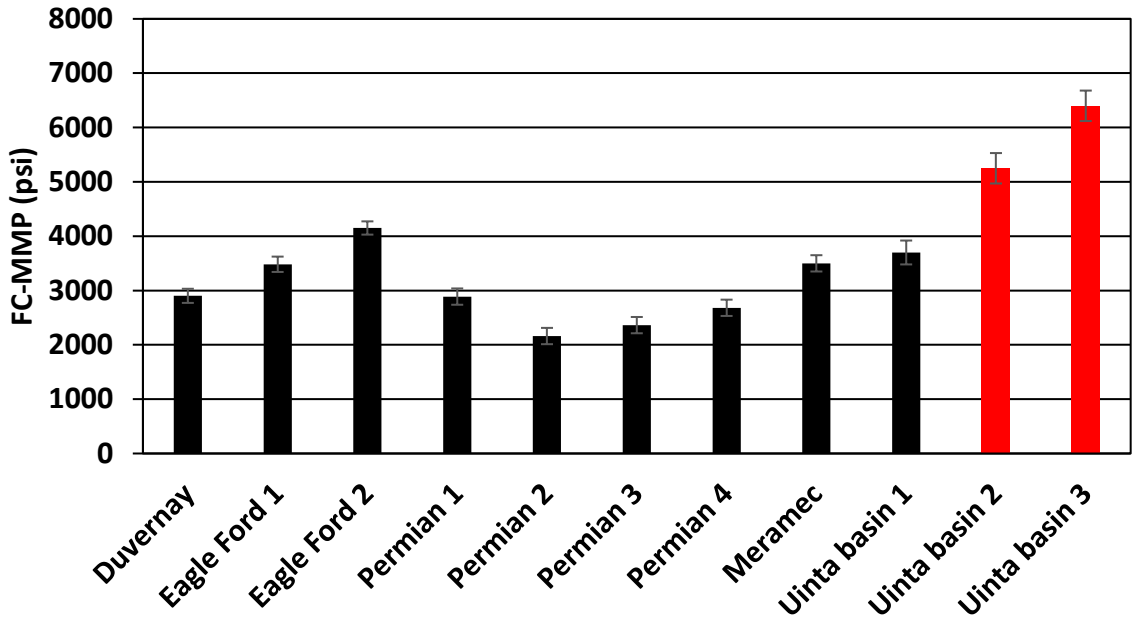

Figure 29 - FC MMP between several produced oil and a mixture of C_1:C_2 (72:28 mol%) measurement at 150 ºF (black) and 185 ºF (red). At 150 ºF Uinta basin oil 2 and 3 were below pour point, hence MMP was determined at 185ºF. The MMP values are used to determine injection pressure during HnP. In this study the injection pressure was kept at 1000 psi above MMP.

3.3.2 Nuclear Magnetic Resonance (NMR)

NMR has been used extensively in the laboratory and field to determine petrophysical properties of saturated (oil or water) rocks. It is a direct method that is largely independent of the host rock influence. NMR theory is based on the excitation and relaxation of hydrogen nuclei present in pore fluid. When a pulse is applied to hydrogen nuclei, they align and precess with a characteristic Larmor frequency. The behavior of the hydrogen nuclei is quantified using the rate of magnetization buildup, also known as T_1 relaxation rate, and the decay rate also known as T_2 relaxation. Both relaxations are a function of pore size and pore fluid chemistry. Theorical estimation of T_1 and T_2 as function of viscosity (Bloembergen et al., 1948) shows that viscous fluid will have shorter T_2 and longer T_1, while less viscous, moveable, fluid will have $T_1 = T_2$.

These two parameters when combined allow *in situ* fluid characterization known as T_1-T_2 mapping, when fluid viscosity contrast is large enough (Hirasaki and Mohanty 2008)

For fluid inside a porous media, three independent relaxation are involved, which affect T_1 and T_2:

- Bulk relaxation, T_{bulk}

  Controlled by the physical properties of the fluid, such as fluid composition and viscosity

- Surface relaxation, T_{surf}

  Interaction between fluid-solid interface, it is strongly affected by mineralogy and is needed to determine the ratio of pore surface to volume.

- Diffusion, T_{diff}

  Diffusion induced relaxation generated by a gradient magnetic field.

T_1 and T_2 relaxation are expressed as follow:

$$\frac{1}{T_2} = \frac{1}{T_{2bulk}} + \frac{1}{T_{2surf}} + \frac{1}{T_{2diff}} \quad (2)$$

$$\frac{1}{T_1} = \frac{1}{T_{1bulk}} + \frac{1}{T_{1surf}} \quad (3)$$

Other parameters of interest for our study is the Signal to Noise Ratio (SNR) during NMR relaxation acquisition. SNR determines the sensitivity of the NMR spectrometer for a sample measurement. It is strongly dependent on amount of *in situ* fluid present.

In this section, the NMR sensitivity is evaluated using bulk dodecane oil (density = 0.75g/cc). A series of 10 dodecane volume (0.1, 0.2, 0.3, 0.5, 0.75, 1, 2, 3, 4 and 5 cc) were prepared inside glass vials using a digital scale. For each volume, the weight was taken 4 times before NMR T_2

relaxation acquisition and 1 time after T_2 acquisition to monitor fluid loss during NMR measurement. Overall dodecane loss during NMR T_2 was negligible (less than 0.005cc). The number of scan (NSA) was kept constant at a value of 16 for T_2 relaxation acquisition. The spectrum is shown on **Fig.31**. The average gravimetric volume was compared to the NMR T_2 relaxation volume **(Fig.32)**. The same figure shows that NMR is accurate in measuring bulk fluid volume, with a 2% error between the two measurements. Additional regression analysis using the EXCEL LINEST function, yield a standard error of 0.002cc and 0.006cc in the slope and in the y-intercept, respectively, which means that NMR is sensitive enough to capture bulk fluid volume up to 0.1cc. The calculation and regression analysis are tabulated and presented in the **Appendix C**.

a)

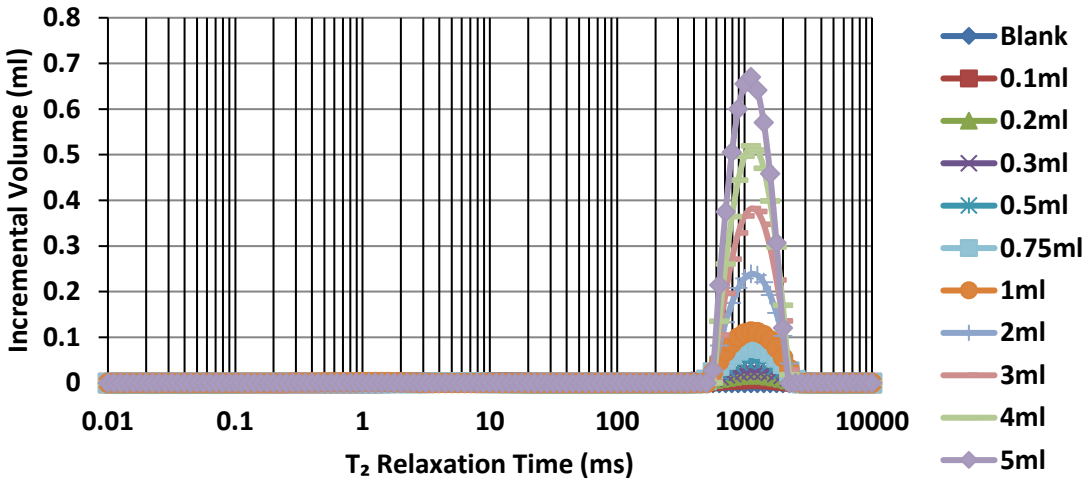

b)

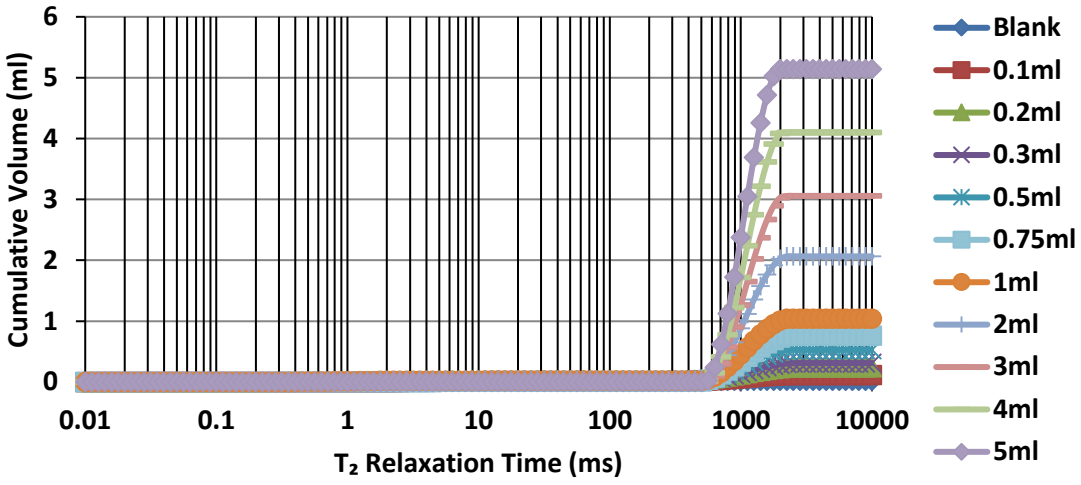

Figure 30 - Incremental (a) and (b) cumulative NMR T_2 relaxation spectrum (NSA=16) for various dodecane oil volume. The glass vial signal was also measured and labelled "blank". Its value was removed during calculation.

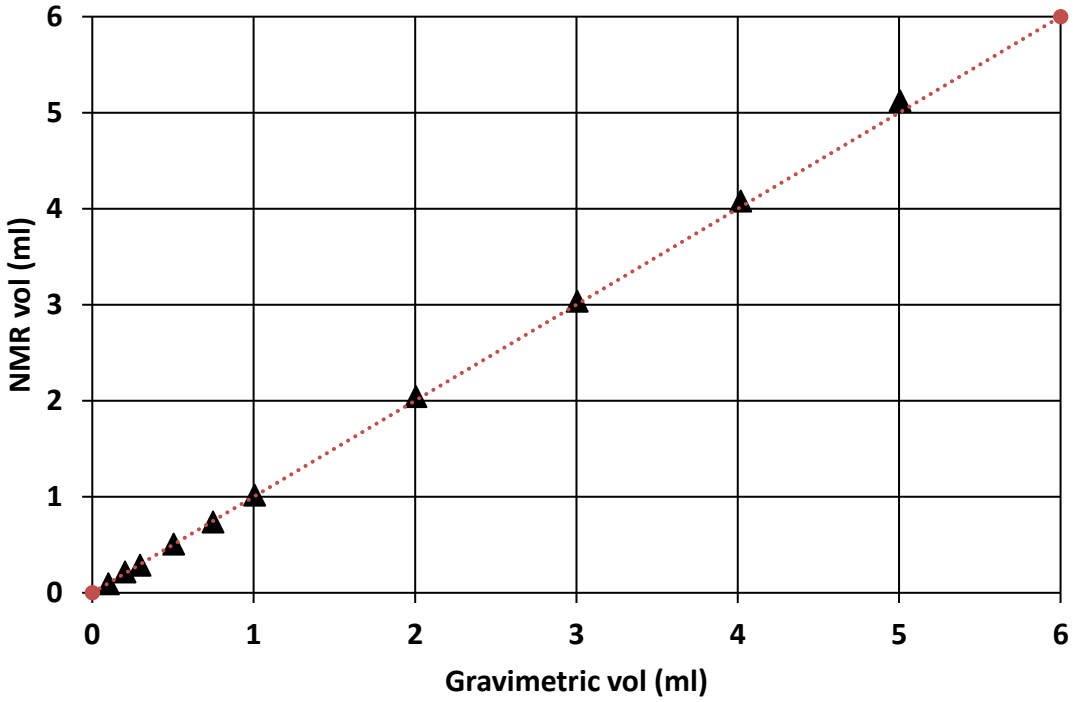

Figure 31 - T_2 NMR relaxation volume as function of gravimetric volume using dodecane oil (0.75g/cc). The red line represents the 1:1 line. NMR is sensitive enough to measure bulk volume up to 0.1cc. Note there is a slight deviation as volume increases.

3.3.3 Source Rock Analysis / HAWK

Source rock analysis includes thermal maturity indicator and organic richness assessment (TOC) method. These can be determined through pyrolysis where a few milligrams of powdered crushed sample are heated in stages. The amount of gas given off is measured as function of time. An example SRA pyrogram is given in **Fig.32**. Where S1 represent the amount of volatilized HC, S2 represents the pyrolysis of kerogen and its associated temperature T_{max} is an indicator of thermal maturity and S3 represents the release of trapped CO_2.

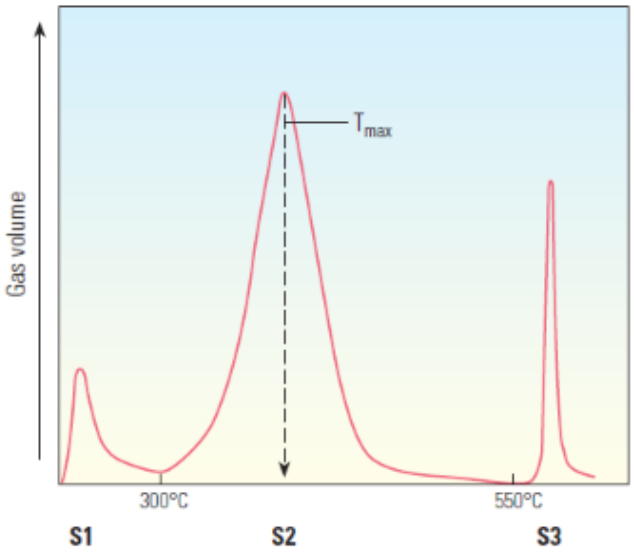

Figure 32 - Traditional source rock analysis pyrogram. S1 represent the volume of free HC that is producible up to 300 ºC. S2 represents the amount of HC generated by thermal cracking, its temperature Tmax is a thermal maturity indicator, from 300-550 ºC. The S3 peak is the amount of CO_2 by kerogen, up to 600 ºC (Boyer et al., 2006)

We used a HAWK® (Hydrocarbon Analyzer With Kinetics) instrument from Wildcat Technologies to characterize more accurately hydrocarbon fraction produced during recovery. Using HAWK, the traditional source Rock Eval pyrolysis program is modified by breaking down the moveable HC in S1 into 4 stages with smaller temperature ramps which divides S_1 into S_{11}, S_{12}, S_{13} and S_{14}. An example of the new pyrogram is presented in **Fig. 33b** with the associated HCs

volatized fraction in **Table 5**. **Fig.33a** shows the response pyrogram to the standard heating protocol. In **Fig.34** the same crushed sample (oil window) was run 5 times to determine instrument accuracy using the 4-steps protocol. Overall, the instrument shows great repeatability with an error in determining total hydrocarbon of ±2%.

(a)

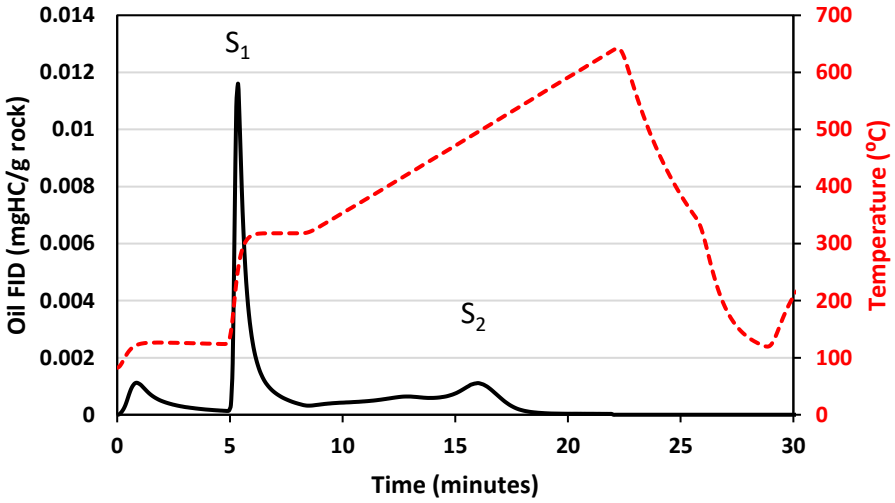

(b)

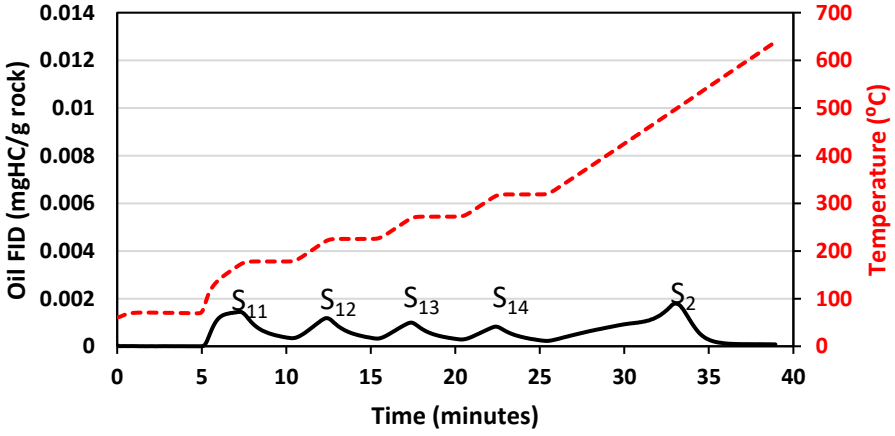

Figure 33 - HAWK pyrograms of a shale using traditional pyrolysis (a) and the modified 4-steps procedure (b). The traditional source Rock Eval pyrolysis program is modified yielding a finer resolution of the S1 peak into: S_{11}, S_{12}, S_{13} and S_{14}.

Table 5 - Correspondence between modified Rock Pyrolysis and HCs fraction (Abrams et al., 2017)

Peak	S_{11}	S_{12}	S_{13}	S_{14}
Temperature Step, ºC	100-150	150-200	200-250	250-300
HCs cutoff	< C_{13}	C_9-C_{17}	C_{13}-C_{24}	C_{17}-C_{27}

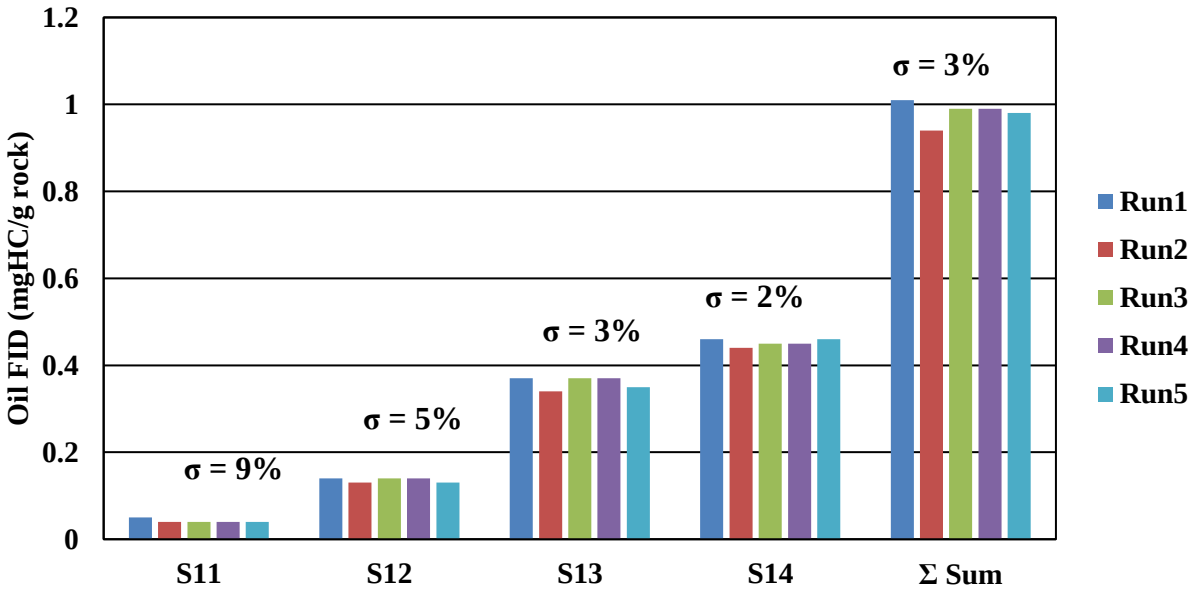

Figure 34 - HAWK sensitivity analysis, where the same shale sample was 5 runs using 4 heating steps. The plot shows a decreased in oil FID standard deviation as the HC becomes heavier. Overall HAWK measurement displays excellent accuracy (±2%) in hydrocarbon characterization on shale samples.

3.3.4 Mercury Injection Capillary Pressure

Mercury Injection Capillary Pressure (MICP) measurement is used to monitor pore throat size alteration created by the injection of the organic solvent. The pore throats are critical elements that affect fluid transport and solvent capacity to carry hydrocarbon, they represent the "door" to larger pore volumes. 12g of sample (7-8mm) from Batch1 in the experimental procedure is placed inside a penetrometer then pressurized in the low pressure (14-27 psi) system of Micrometrics Autopores IV. Then, the penetrometer is inserted into the high-pressure system of the instrument, where the mercury is pressured up to 60,000 psi. Mercury being a non-wetting fluid will penetrate the pores when the capillary pressure is exceeded. The penetration as a function of pressure yields a pore

throat size distribution. Finally, the measurement is repeated in the same fashion after HnP. **Fig.35** shows the impact of mixture of C_1:C_2 (72:28) on a Duvernay shale sample at 150 ^oF after 10 cycles at injection 1000 psi above MMP. The solvent opens significantly more pore throats after EOR.

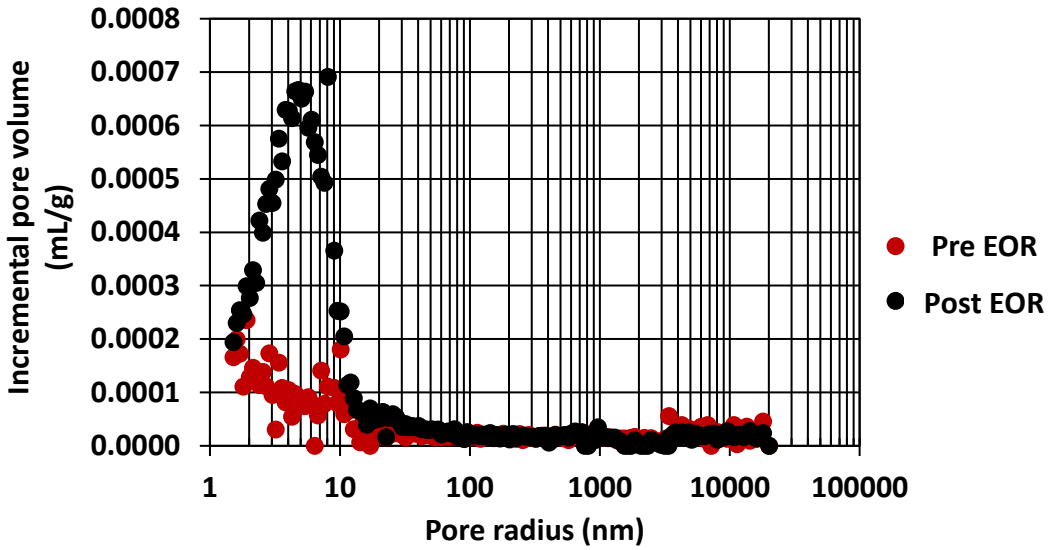

Figure 35 - Example of pore throat size alteration after 10 HnP cycles on a Duvernay shale at 150 ^oF. The experiment was carried at 1000 psi above MMP by cyclically injecting a mixture of C_1:C_2 (72:28). Large increase in pore throat sizes < 10nm after EOR shows that the solvent could open smaller pore throats which could provide access to larger pore bodies. (Dang 2019)

3.3.5 Isothermal Adsorption and Pore Size Distribution

Low pressure nitrogen isothermal adsorption is used to measure internal surface area changes, or the "room" created by the HnP experiment. Adsorption is the process by which molecules are attracted and retained by a surface (Barnes and Gentle 2005). In our experiment a Micrometrics Tristar 2 is used to characterize surface area based on Brunauer, Emmett and Teller (BET) theory (1930) and pore size distribution (PSD) using a Density Functional Theory (DFT) model with a liquid nitrogen as adsorbate at 77.36 K, from 0.05 – 1 relative pressure (P/P0). Most of tight rocks have an average pore size distribution in the nanometer range (<100nm). BET can be used to determine surface area of pores between (2-200nm) (Sinha 2017). For PSD inversion DFT model assuming slit pore instead of BJH (Barret-Joyner-Halenda) assuming cylindrical pore is preferred

for our study. **Fig.36** is an example of PSD pre- and post- EOR on the same Duvernay sample using C_1:C_2 (72:28). Like MICP the graph shows substantial increase in pore size distribution with a BET surface area doubling from 1.4 to 2.7 ±0.2 m^2/g after EOR.

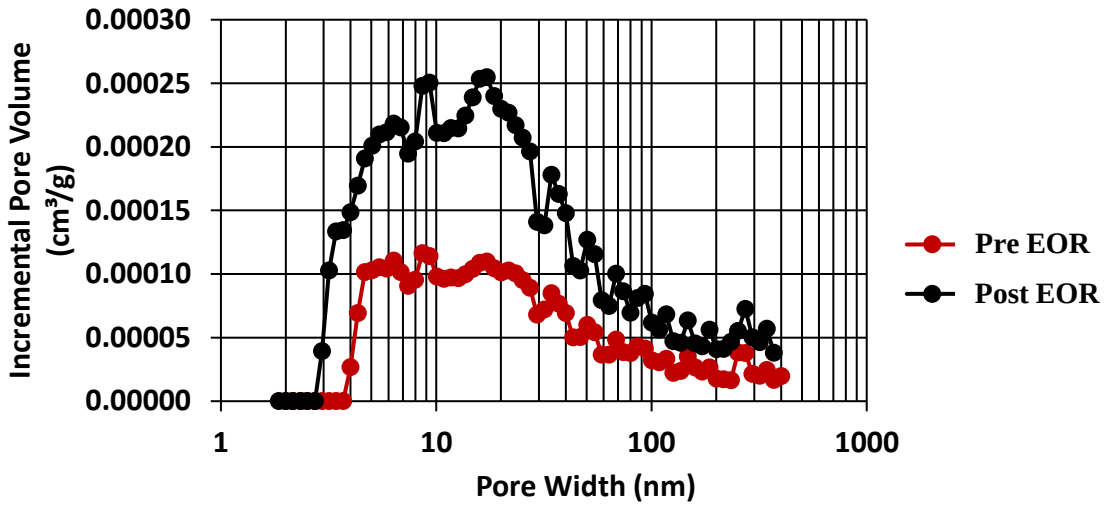

Figure 36 - Pore size distribution alteration after HnP using DFT slit pore inversion on a Duvernay shale. Huff-n-puff was carried at 150 ºF using a C_1:C_2(72:28) as injectate at 1000 psi above MMP. The BET surface area is increased by almost a factor of two after EOR from 1.4 to 2.7±0.2 m^2/g showing that the solvent was capable to open larger or more pore bodies after EOR.

3.3.6 Scanning Electron Microscope (SEM)

A FEI Quanta 200 scanning electron microscope is used in this study to analyze microstructural alteration pre- and post- HnP. Small rock chips (7-8mm) are used. A focused beam of electrons scans the surface of the sample and a signal is generated and detected at each point along the scan. The back-scatter detector (sensitive to atomic number contrast) is used to outline contrast between organic and inorganic matter. Before imaging, the sample is polished using emery paper with increasing grit size (180,600,1200) to create a flat cross-sectional surface. Then, the sample is mounted on an aluminum stub using Crystal Bond adhesive and placed inside a broad beam argon ion mill for 3-hours. An area of a few millimeters in size is milled by two rotating ion guns in order to create a perfectly smooth surface. Traditional SEM imaging requires samples to be coated with

a thin gold layer to provide a good signal and avoid charging issues but for our application only the post HnP samples are coated, to avoid altering the interaction between the injected solvent and organic matter.

3.3.7 Total Organic Carbon

Total organic carbon (TOC) measures the richness in organic content of a rock. It is used in this work as a general petrophysical parameter to assess hydrocarbon potential pre- EOR measurement. LECO C844 is used to measure in wt% TOC of a crushed sample (particle size <35mesh). Roughly 1g of sample is treated with 35% hydrochloric acid to remove inorganic carbonates from the sample. Then, the powdered sample is placed inside the Leco C844 carbon analyzer, where the sample is combusted inside a furnace at 1200 °C, the organic content is measured by quantifying the IR signal of the combustion products.

3.3.8 Helium Pycnometry

The total porosity is measured on plug samples of at least 10 cc bulk volume by summing the effective porosity and the NMR porosity on a dried sample. The sample is dried inside an oven at 100 °C for several days, while NMR T_2 relaxation is used to monitor *in situ* fluid volume decrease. When the *in-situ* volume does not change (±1pu), Boyle's Law helium pycnometry is used to measure the grain volume and the effective porosity with **Equation 4**.

$$\emptyset = \frac{V_b - V_G}{V_b} \quad (4)$$

Where V_b is the bulk volume of the plug measured by mercury displacement and V_G is measured grain density from helium pycnometry.

3.3.9 Fourier Transform Infrared Spectroscopy (FTIR)

The mineralogy was measured using transmission Fourier Transform Infrared Spectroscopy (FTIR) (Sondergeld and Rai 1993). The FTIR responds to vibrational energy from covalent bonds, each vibration mode results in an infrared absorption at a particular wavenumber. The sum of these produces an absorption spectrum which is characteristic of a mineral. An infrared beam is transmitted through the sample, where the amount of energy loss measured as absorbance is measured by a detector. The energy loss or attenuation is dependent on the mineral types and their concentrations. The total absorbance is related to the sum of singular mineral and their concentration by the Beer's Law in **Equation 5**.

$$A(v) = bk_i(v)C_i \quad (5)$$

where: b = pathlength

k_i = absorptivity of the ith component

C_i = Concentration of the ith component

The "as received sample" is crushed and powdered. The powder is dried at 100 ºC for 12-hours and plasma ashed for 12-hours to remove organic content. The samples are heated for at least 5 h at 100 ºC before measurement. Finally, 0.0005 g of sample is mixed with 0.3000 g of KBr and pressed into pellet which has a constant thickness. The pellet is placed inside Nicolet 6700 FTIR instrument for analysis.

CHAPTER 4: RESULTS AND DISCUSSION

In this section we evaluate the EOR performance of different shale plays. The first objective is to determine the best candidates for HnP and then determine possible parameters controlling recovery based on the crushed rock protocol established in Chapter 2. A total of 7 wells were studied: 1 well from Eagle Ford, 1 well from Duvernay, 2 wells from Uinta basin, 2 wells from Montney and 1 well from Meramec.

4.1 Sample Description

The mineralogy and petrophysical properties of all the sample is presented in **Table 6**. All samples have porosity ranging from 5-9%. They are organic rich with TOC >2 wt%, except the Meramec sample (TOC <0.8 wt%). Thermal maturity for the samples is measured based on the HAWK 4 step protocol as opposed to the traditional pyrolysis T_{max}. All samples in this study are in the oil window except Meramec and Montney 2 sample, which are immature (T_{max}<435°C).

Table 6 - Petrophysical properties of the 7 samples presented in this study.

Sample (State)	Total Porosity (%)	TOC (wt%)	T_{max}(^{o}C)	Total Clays (wt%)	Total Carbonates (wt%)	Quartz + Feldspar (wt%)	Others (wt%)
Eagle Ford (Preserved)	5	5	460	16	62	13	8
Duvernay (Preserved)	6	5	460	33	18	48	0
Uinta 1 (Non preserved)	5	5	460	5	81	11	3
Uinta 2 (Non preserved)	7	5	459	32	48	20	0
Montney 1 (Non preserved)	5	2	445	23	12	64	2
Montney 2 (Non preserved)	9	3	415	0	39	59	2
Meramec (Non preserved)	4	1	-	13	22	63	1

4.1.1 Pre-HnF pore throat and pore body size

MICP response in the samples can be grouped into two categories (**Fig.37**). A group with small pore throats (<20 nm) which includes Eagle Ford, Duvernay, Uinta 1 and 2 and a group of samples with larger pore throats (>20nm) such as Montney 2 and Meramec. Montney 2 stands out with an abundance of large pore throats of the micrometer size. Additional SEM images confirm large pores in the order of μm in **Fig.38** in Montney 2 compared to tight sample such as Eagle Ford, where the pores are in nanometer size (5-20nm) inside the OM (**Fig.39**).

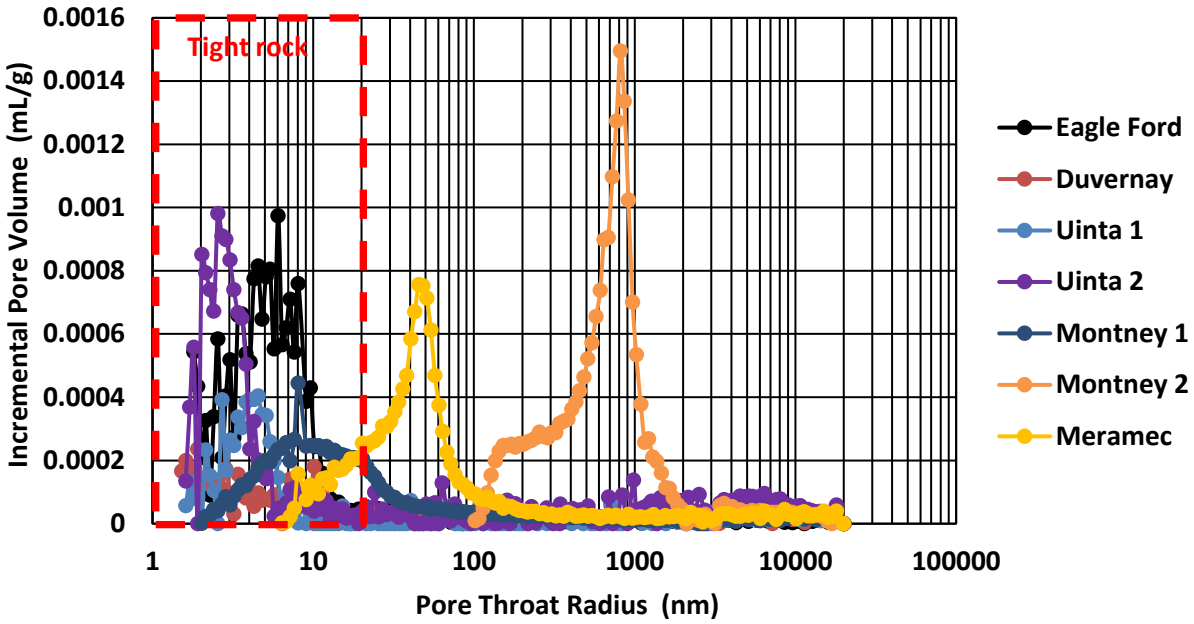

Figure 37 - Mercury injection capillary pressure measurements of the samples used in this study. Eagle Ford, Duvernay, Uinta 1 and 2 appear tighter with pore throats <20nm compared to the Montney 2 and Meramec formations, which have larger pore throats.

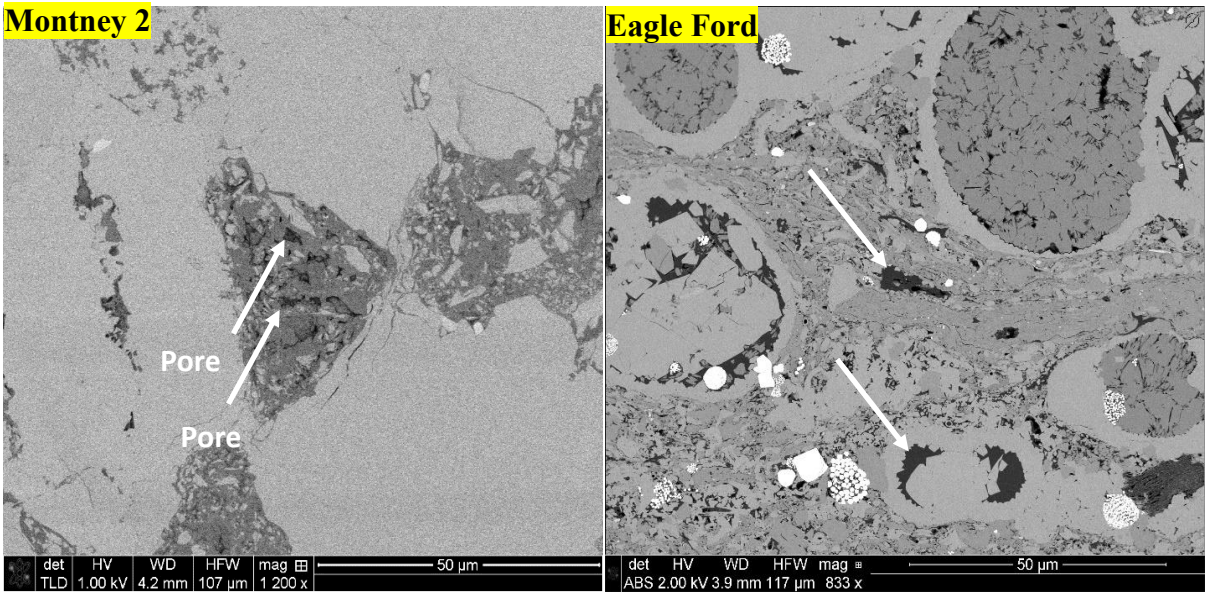

Figure 38 - SEM images showing pore body size contrasts between Montney 2 (Left) and Eagle Ford (Right) on the same scale. Large µm size pores are visible inside the OM of the Montney 2 sample (white arrows).

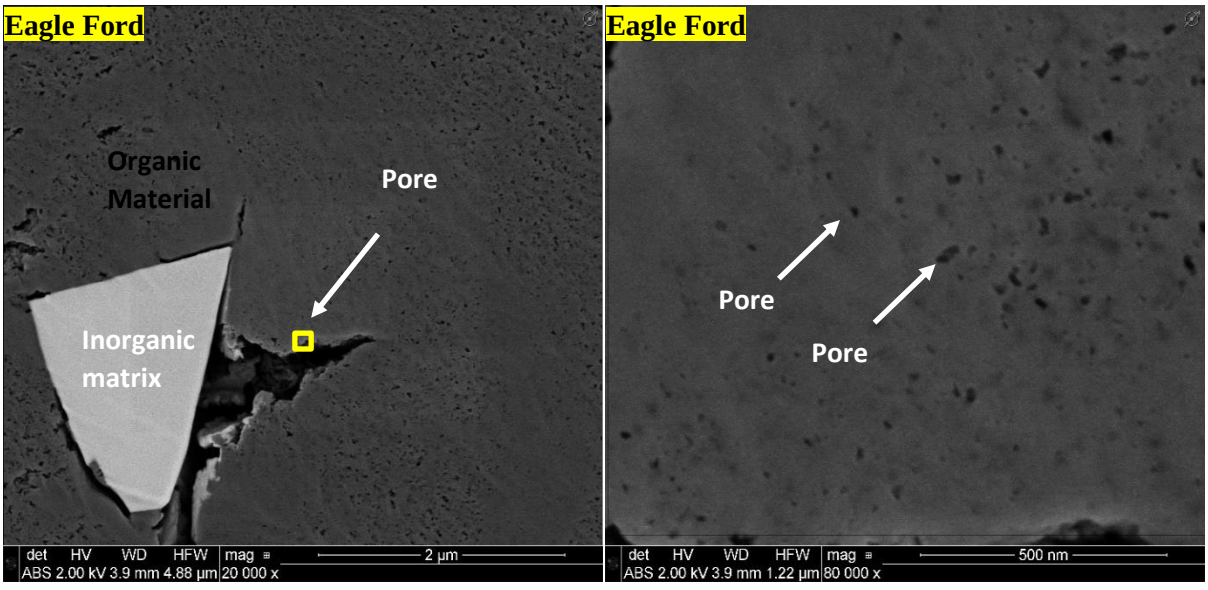

Figure 39 - Porous region in the Eagle Ford sample to the left. Magnified in image of the same sample showing pore bodies ranging from 5-20nm inside the organic material.

4.1.2 As received fluid saturation

Fig.40 shows HAWK analysis of the residual fluid inside the rock pre- EOR. Preserved rock (Eagle Ford and Duvernay) tends to have higher concentration of lighter components S_{11} and S_{12} (< C_{17}) compared to other formations.

In addition, T_1-T_2 maps were also collected to determine fluid type before EOR. Traditionally T_1-T_2 ratios for water ~1-10 and for oil ~ 10-20. **Fig.41** shows T1-T2 maps for the samples. Eagle Ford, Duvernay, Uinta 1 and Montney 2 are HC rich with low residual water, while Uinta 2, Montney 1 and Meramec have low oil saturation with mostly residual water.

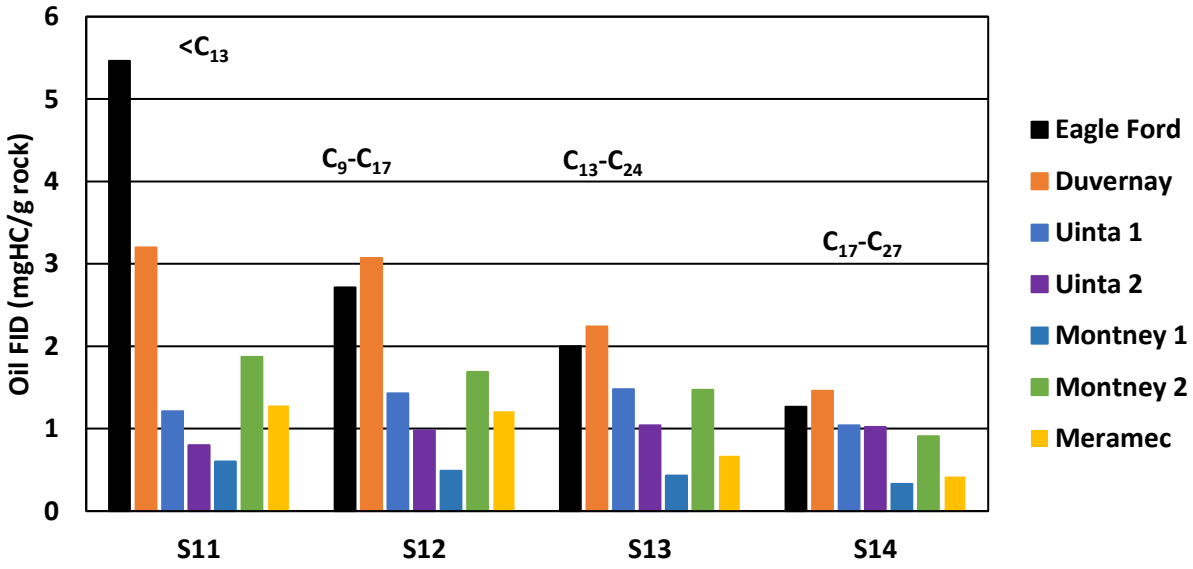

Figure 40 - HAWK analysis using the 4-step heating protocol on the as received samples. Notice that preserved sample (Eagle Ford and Duvernay) have the highest HC saturation, mostly made of lighter HC, S_{11}. The HC concentration of others sample is lower but more homogeneous.

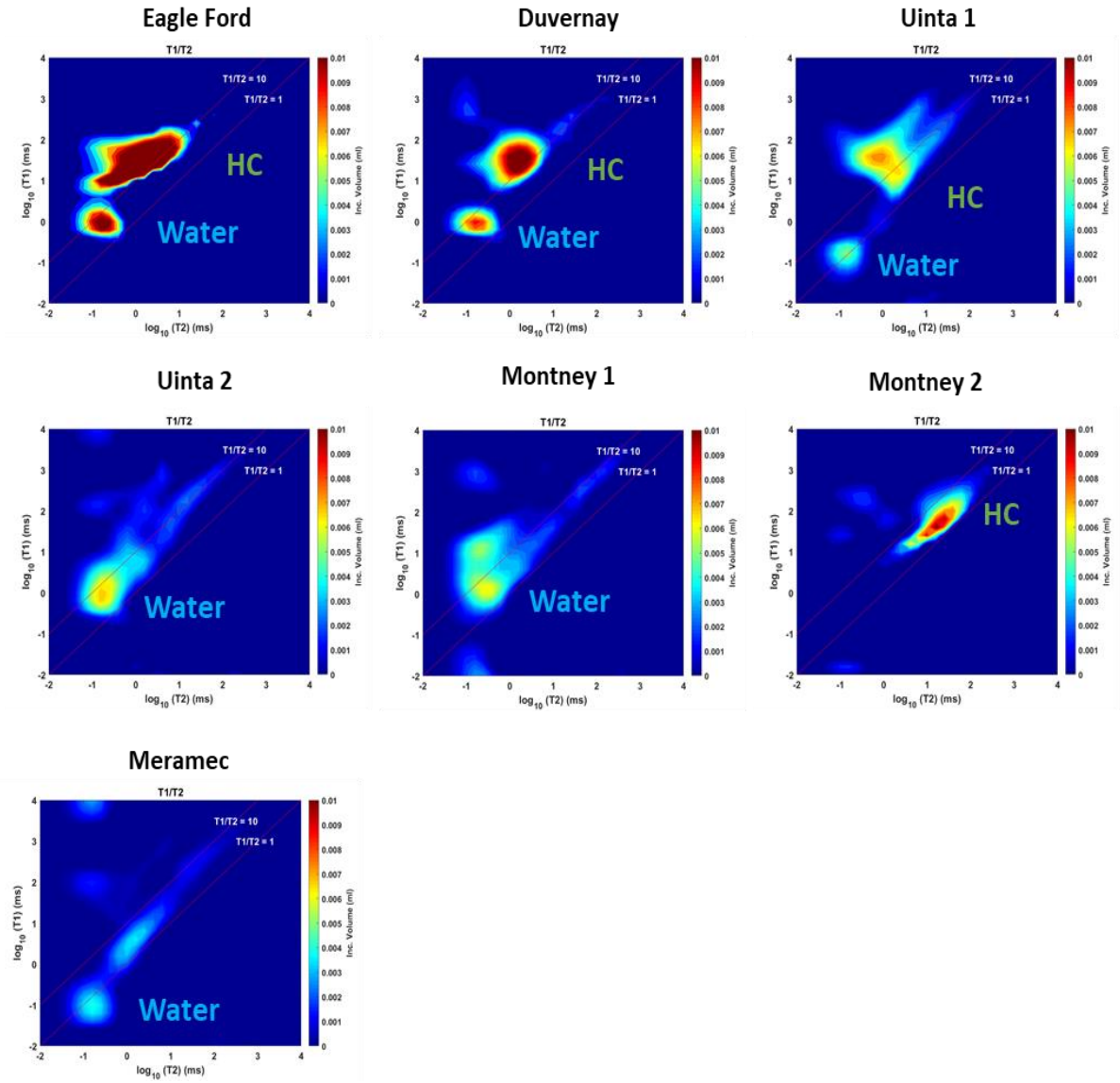

Figure 41 - As received T_1-T_2 maps of crushed samples on the same scale. Notice Eagle Ford, Duvernay and Montney 2 have the highest oil saturation. Low residual oil saturation is observed in Uinta 2, Montney 1 and Meramec with high water saturation.

4.1.3 Water signal identification

After T_1-T_2 map acquisition it is important to verify that the water signal recorded between T_1-T_2~1-10 is water. In this section we propose a procedure that uses manganese chloride solution ($MnCl_2$) to dope water signal. Previous study from Gannaway (2014) showed that 65% $MnCl_2$ solution has no measurable NMR volume and does not mix with oil. A Preserved Eagle Ford plug

(1x1in) was imbibed into a 70% $Mncl_2$ for 96-hours to monitor water and oil signal **(Fig.42).** Fig.42 shows an initial increase in water level after 2-hours imbibition in $MnCl_2$ from 0.32 ml to 0.43 ml mainly because of a filtration effect; the sample is initially imbibing water with no $Mncl_2$ ions. After 24-hours the water volume starts to decrease as the $MnCl_2$ ions are mixing with the water inside the sample. Then, the water volume reaches 0.29 ml after 96-hours, which is lower than the native water volume of 0.32 ml. The same plot also shows that the oil volume stays constant from 0.33 ml to 0.32 ml after 96-hours, confirming that $MnCl_2$ is not mixing with oil and that T_2~1-10 is water. Finally, T_1-T_2 maps on **Fig.43** shows a general reduction in water signal after 96-hours imbibition in $MnCl_2$.

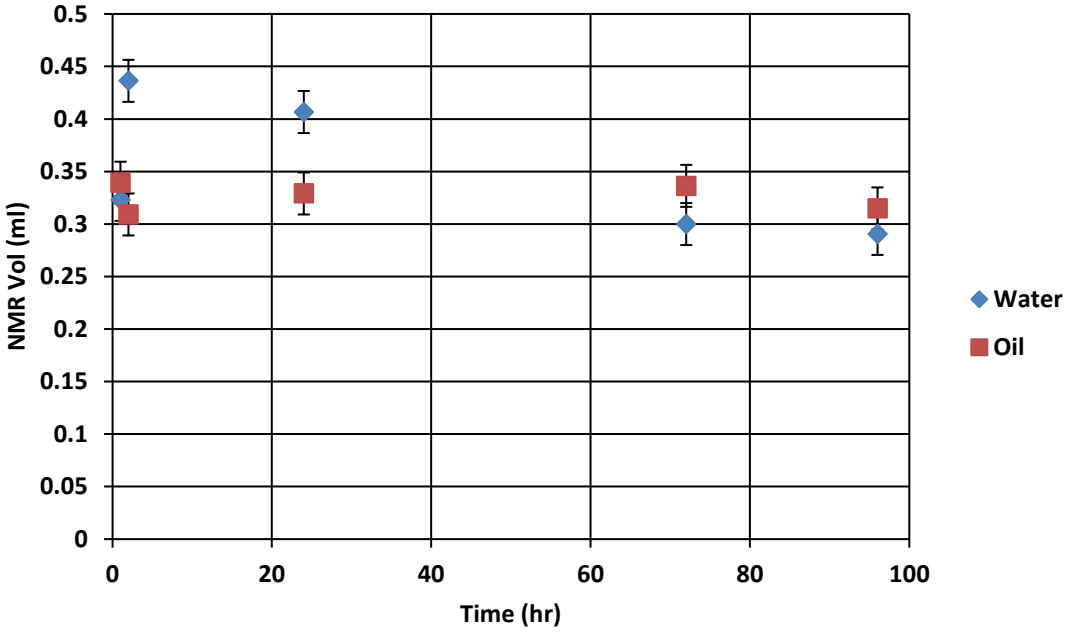

Figure 42 - Water and oil volume after 96-hours imbibition in 70% $MnCl_2$ solution based on T_1-T_2 maps. The water signal initially increases as water is entering the rock with no $MnCl_2$ ions, after 24-hours $MnCl_2$ ions are mixing with the water inside the sample resulting in a decrease in NMR volume. After 96-hours the water volume drops below its initial value. However, the oil volume remains constant as the $MnCl_2$ does not mix with the oil inside the sample.

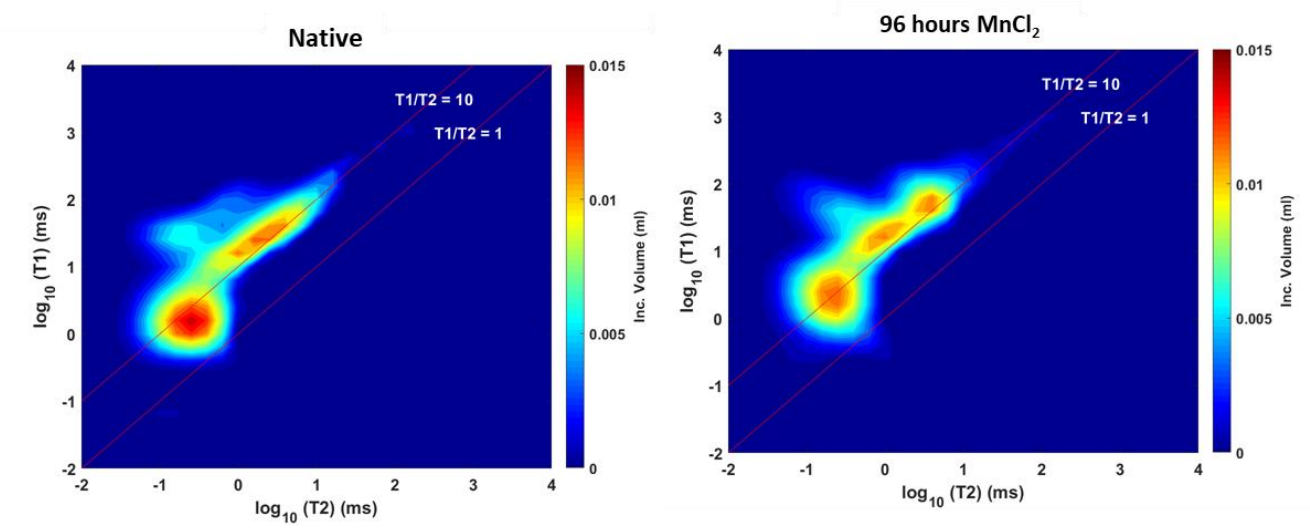

Figure 43 - T_1-T_2 of preserved Eagle Ford before and after 96-hours imbibition in 70% Manganese chloride solution. The maps show a general decrease in the intensity of the T_1-T_2~1-10 peak, confirming that this signal is water.

4.1.4 MMP and oil viscosity

Fig.44 shows MMP and viscosity of the produced oil from each reservoir. All MMP's were measured with the rich gas of C_1:C_2 (72:28) at 150 ^oF. Unfortunately, no oil from Montney formation was available for this study. Therefore, MMP was determined through molecular simulation using Montney 1 oil composition (Courtesy of Ovintiv). Overall a positive trend is observed between the produced oil viscosity and MMP (**Fig.45a**). The heavier the oil the higher the MMP. The same trend is also observed with the residual oil composition. This statement is also supported by comparing HAWK heaviest fraction S_{13} and S_{14} to MMP on **Fig.45b.** Previously, Minh (2018) and Dang (2019) showed that the mixture of C_1:C_2(72:28) can mobilize efficiently S_{11} and S_{12} oil fractions in the Eagle Ford. Hence a HAWK heaviness ratio can be defined as seen in **Equation 6** by comparing HC fraction left behind by C_1:C_2(72:28) to the total HC content.

$$HAWK\ Heaviness\ Fraction = \frac{S14}{S11+S12+S13+S14} \quad (6)$$

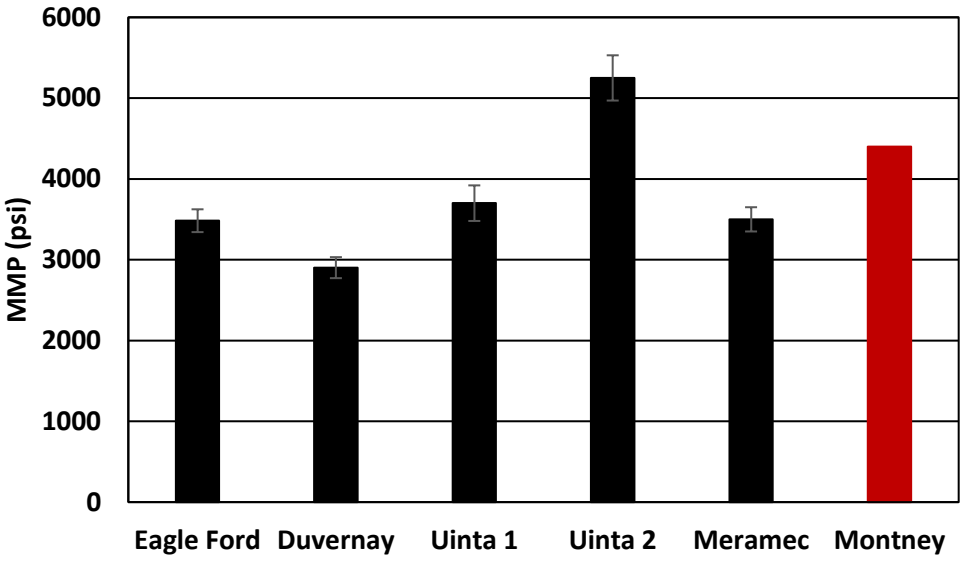

Figure 44 - MMP at 150 ºF with mixture of C_1:C_2 (72:28). No oil was available for Montney so the MMP was calculated using molecular simulation of Montney 1 oil composition(red). These MMP values will be used as injection pressure reference during HnP performance evaluation.

a)

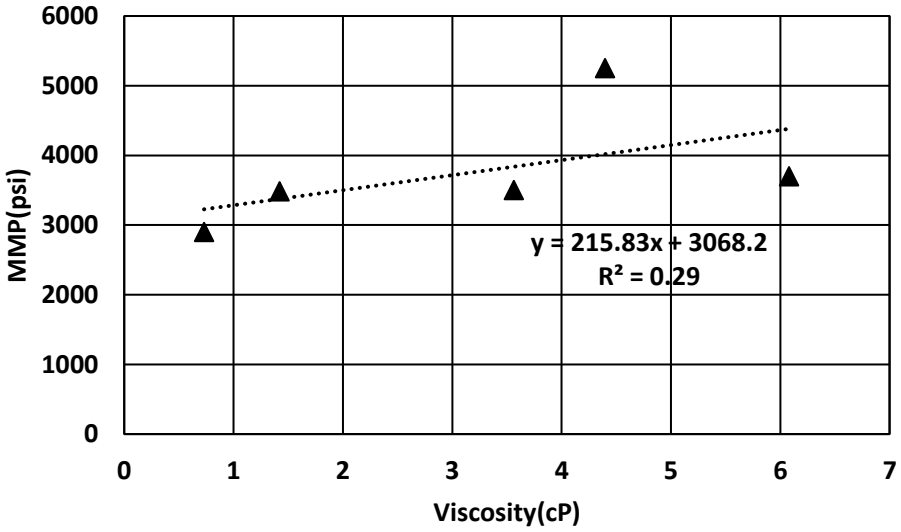

b)

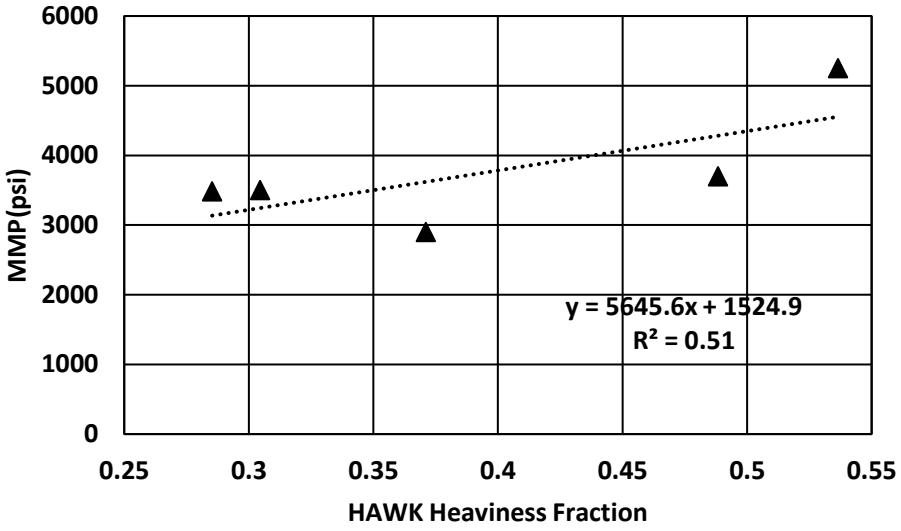

Figure 45 - Positive relationship between MMP and a) produced oil viscosity at 150 ºF and b) residual rock heaviness fraction from HAWK. Overall, the heavier the oil the higher the MMP. Hence the higher the compression pressure required to achieve efficient HC mobilization HnP

4.2 Case study

4.2.1 Eagle Ford (Preserved)

Recent success of EOG in the Eagle Ford has raised a lot of interest in understanding the mechanism behind HnP EOR. Hence, Eagle Ford shale has been the focus of extensive experimental and simulation studies. The fundamental question is what rock/fluid properties make this play a major success. This section reviews Eagle Ford crushed sample performance during HnP with the mixture of C_1:C_2 (72:28) at 150 ºF and 4500 psi injection pressure.

SARA (Saturate, Aromatic, Resin and Asphaltene) analysis (**Fig.46**) compares produced oils and extracted core HC from the same Eagle Ford reservoir. The ternary diagram shows that the Eagle Ford reservoir is rich in saturated alkanes (>65%) with low resins and asphaltenes contents (10-20%). Additional viscosity tests show that at our HnP test temperature of 150 ºF, the produced oil

is very light with viscosity of 1.42±0.02 cp and API gravity of 45.7±1.6°API; this oil will clearly be moveable.

NMR results pre- and post- HnP show that most of the oil is preferentially extracted from the larger pore bodies with very little water production (**Fig.47 and Fig.48**). The produced oil is rich in lighter end alkanes < C_{13} (**Fig.49**) and after 24-hours residence time (12 cycles) 45% recovery is achieved (**Fig.50**). In this sample there were little changes in the pore throat size distribution in **Fig.51b;** instead it opened smaller pores (<200nm) shown by an increase in BET internal surface area from 0.8 to 2.8m^2/g. (**Fig.51a**). Those small alterations are visible at the interface between organic and inorganic matter on **Fig.52** SEM**,** where we observe an increase in porosity.

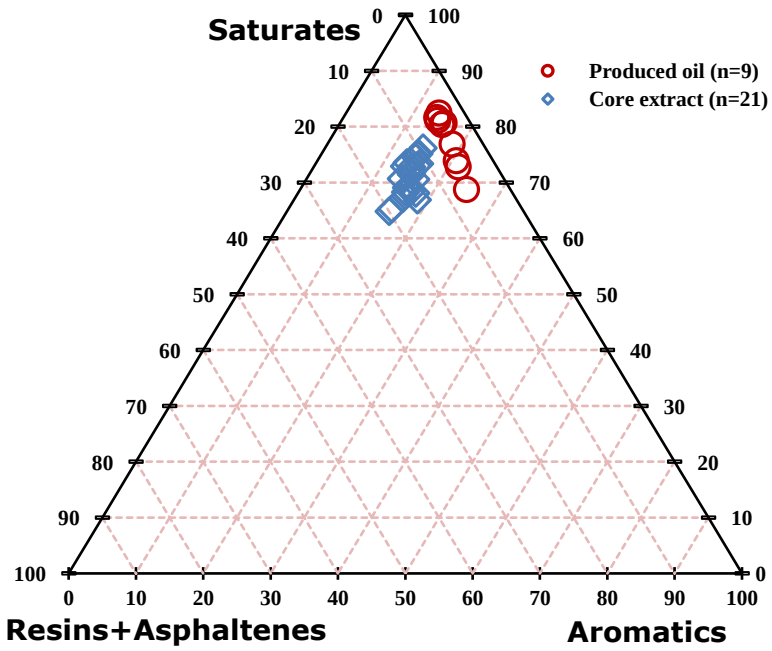

Figure 46 - SARA analysis of Eagle Ford produced oils from the same well pad in red and core plug extract from 200 ft core sampled from the same well. Note both produced oils and residual extract oil have a composition rich in saturated alkanes with limited resins and asphaltenes. (Courtesy of Ovintiv)

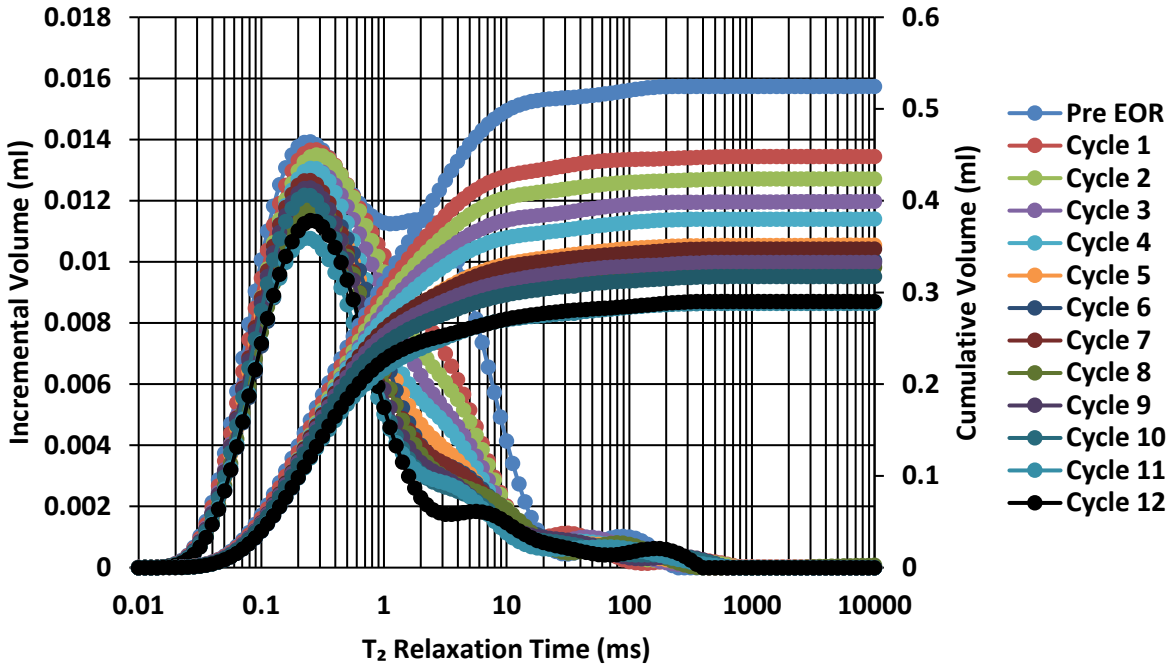

Figure 47 - NMR T_2 spectra for 12 cycles of HnP for the Eagle Ford sample. Hydrocarbon recovered are preferentially from the larger pore bodies (1-10ms). HnP cycles were conducted using a rich gas mixture of C_1:C_2 (72:28) at 4500 psi (1000 psi above MMP) and 150°F. One cycle corresponds to 1-hour soak and 1-hour production (Minh 2019).

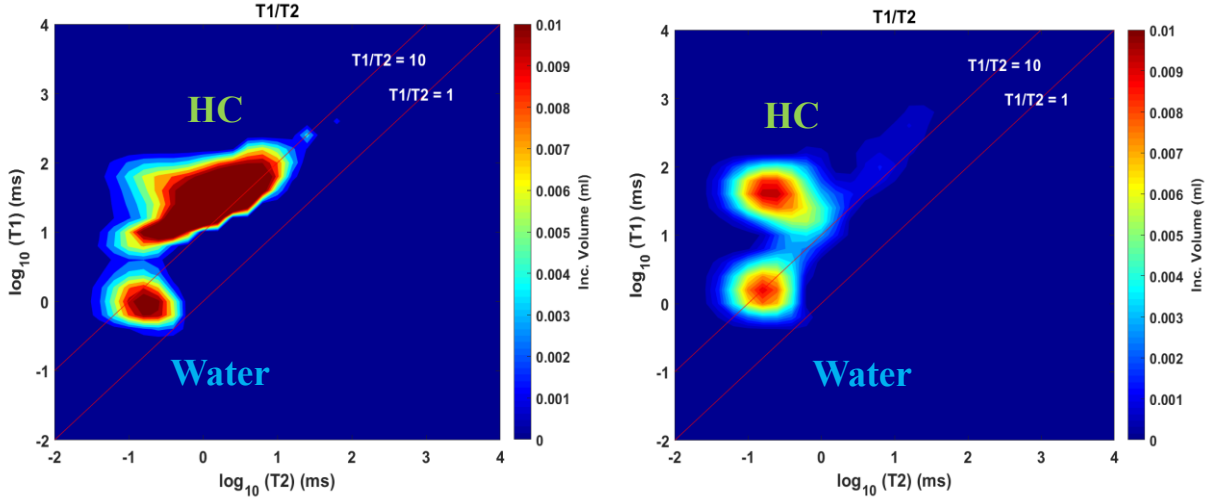

Figure 48 - 2D T_1-T_2 maps of the Eagle Ford sample pre- and post- EOR. Comparison of fluids signal shows that 73% of the fluid production is oil and 27% is water. For this sample the solvent C_1:C_2 (72:28) can mobilize both oil and water.

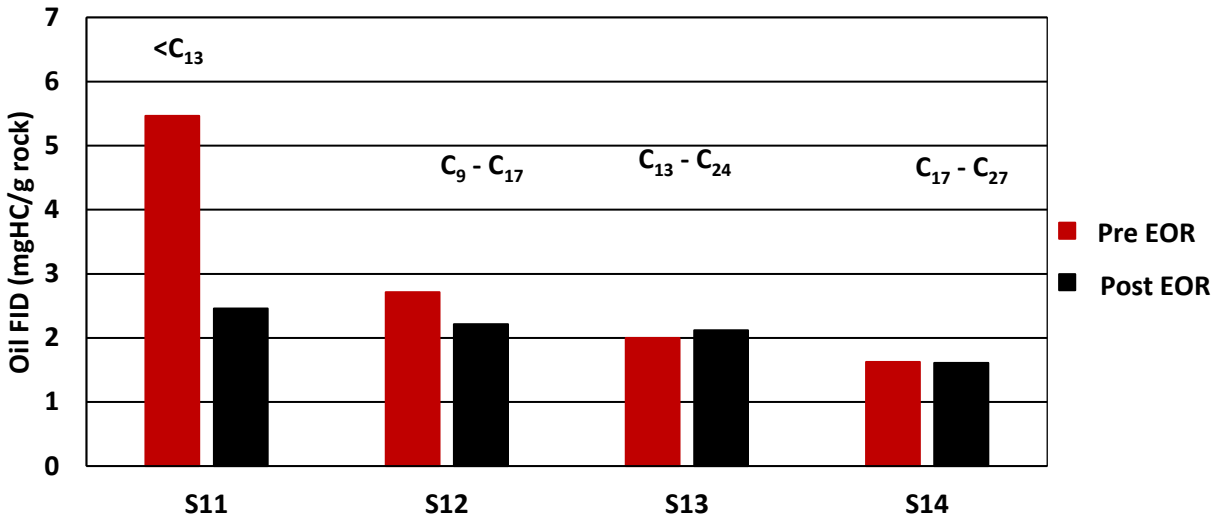

Figure 49 - HAWK pyrolysis pre- and post- HnP on Eagle Ford crushed sample using the same conditions. Note only light HC fractions S11 and S12 are mobilized after 12 cycles of HnP.

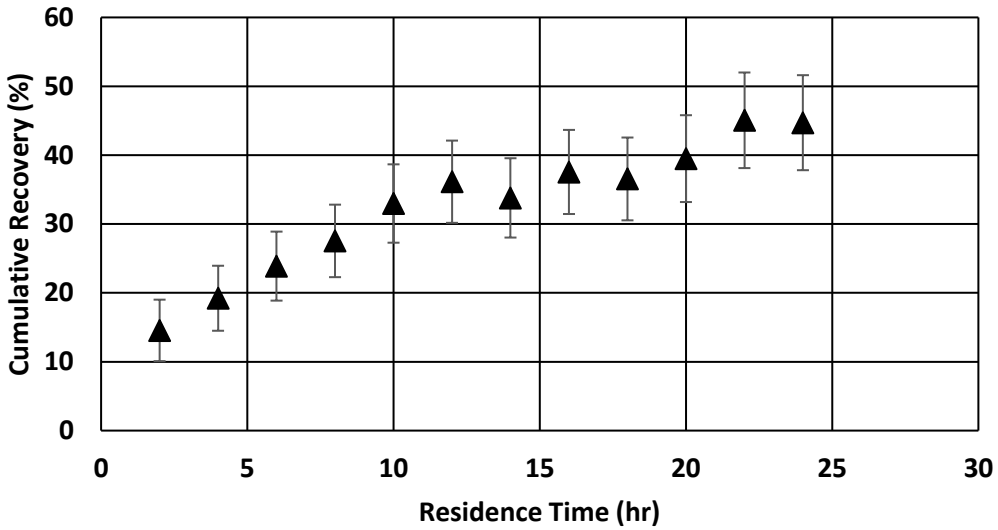

Figure 50 - Cumulative recovery as function of residence time for Eagle Ford crushed sample. Note the solvent was able to mobilize 45% of the *in-situ* fluid (Minh 2019)

a)

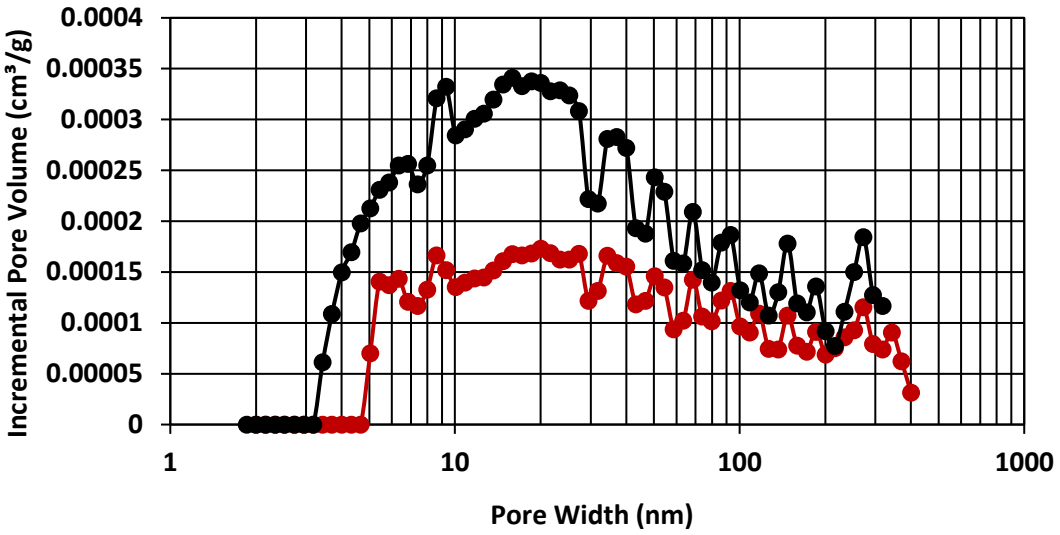

b)

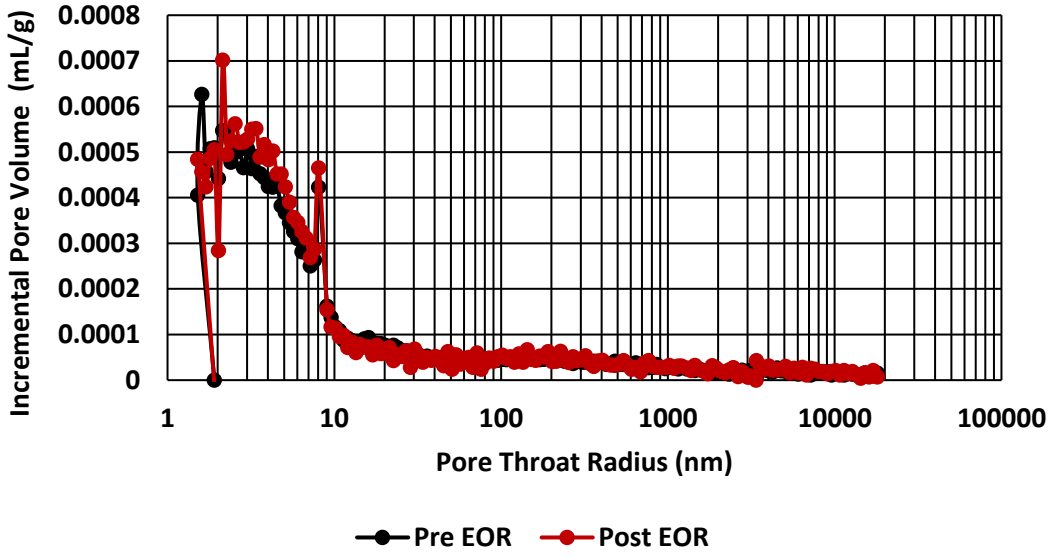

Figure 51 - a) Isothermal nitrogen BET adsorption measurement pre- and post- EOR for an Eagle Ford sample. Nano-pores around 2nm were opened after HnP. BET shows cleaning of smaller pores <200nm and an increase in surface area from 0.8 to 2.8m^2/g. b) MICP does not show significant change in pore throat size (Dang 2019)

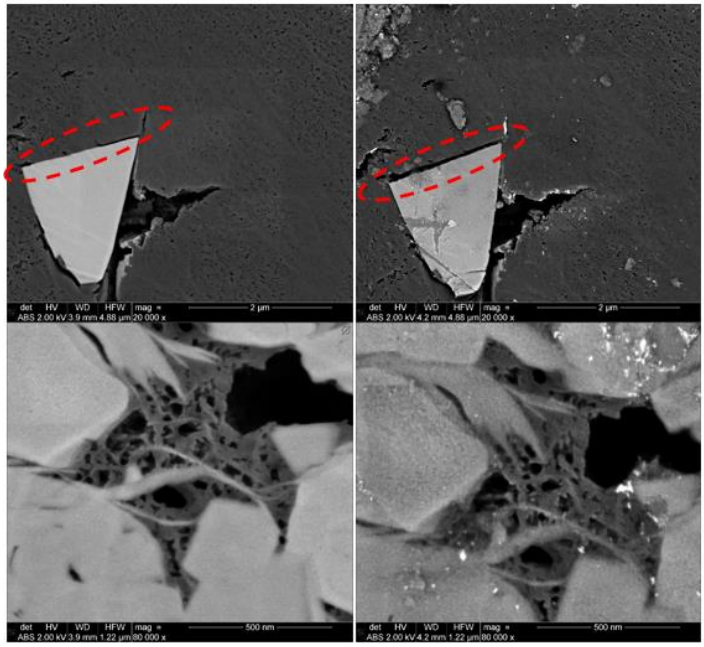

Figure 52 - SEM image pre- (left) and post- (right) HnP. No significant microstructural alteration was observed in the OM. However, we observe porosity generation between organic and inorganic interfaces, which might alter the rock wettability and fluid recovery (oil/brine) during HnP.

4.2.2 Duvernay (Preserved)

The Duvernay shale is an organic rich shale deposited as basin-filling fine grain sediments (argillaceous, calcareous and siliceous muds) overlain by calcareous shales and argillaceous limestone. It is considered as the source rock for several oil and gas reservoir in Alberta, Canada and is considered a major target for unconventional production (Marshall et al., 2019).

Like the Eagle Ford previously studied, Duvernay produced oil is very light (52.3±1.0°API and 0.73±0.02 cp at 150 °F). However, the residual HC is not as rich in lighter component S_{11} and S_{12} ($<C_{17}$) as Eagle Ford. Both formations have porosity and organic content that are similar (TOC ≈ 5 wt% and ø = 5-6%) and average pore throat size distribution between 2-10nm. After HnP the cumulative recovery is close to Eagle Ford, i.e. around 43% **(Fig.53 and Fig.54)** with HC fraction up to C_{27} being mobilized **(Fig.55).** Most of the fluid production is HC as can be seen in the T_1-T_2 maps (**Fig.56**). Duvernay shows substantial microstructural alteration after gas injection with large

increase in pore surface area and pore throat size distribution **(Fig.57).** In other words, the solvent opened initially smaller pore throats to access additional HC locked inside different pore bodies. Those observation are confirmed by the SEM image in **Fig.58**, which shows an increase in size of the organic matter pores after gas injection.

Additionally, when the differential NMR T_2 spectra (ie: every single cycle is subtracted from its the subsequent cycle) are plotted as function of T_2 relaxation times, the main T_2 relaxation shift back and forth between fast and slow relaxation and sometimes both as can be seen on **Fig.59.** The same figure shows that fluid comes out from different pore body sizes after each cycle. The solvent cleans out a certain group of pore bodies, then after cleaning a pore throat, it can contact new fluid from a different pore size body.

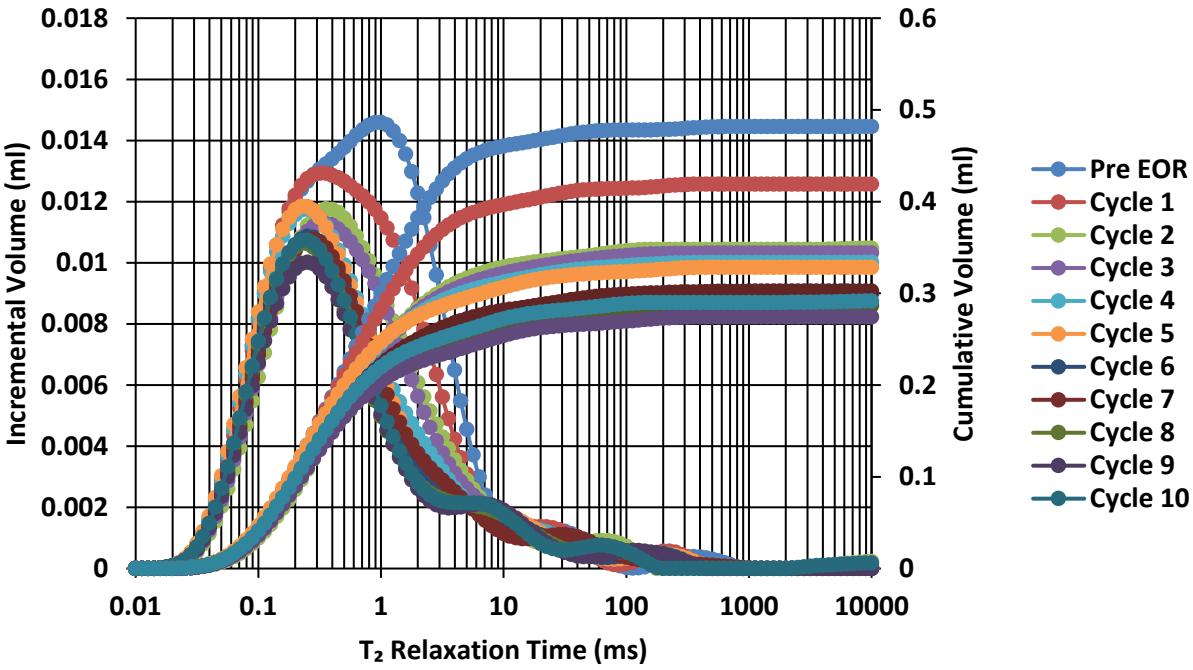

Figure 53 - NMR T_2 spectra during HnP for Duvernay crushed sample. 10 cycles were conducted using a rich gas mixture of C_1:C_2 (72:28) at 3900 psi (1000 psi above MMP) and 150°F. One cycle corresponds to 1-hour soak and 1-hour production (Dang 2019).

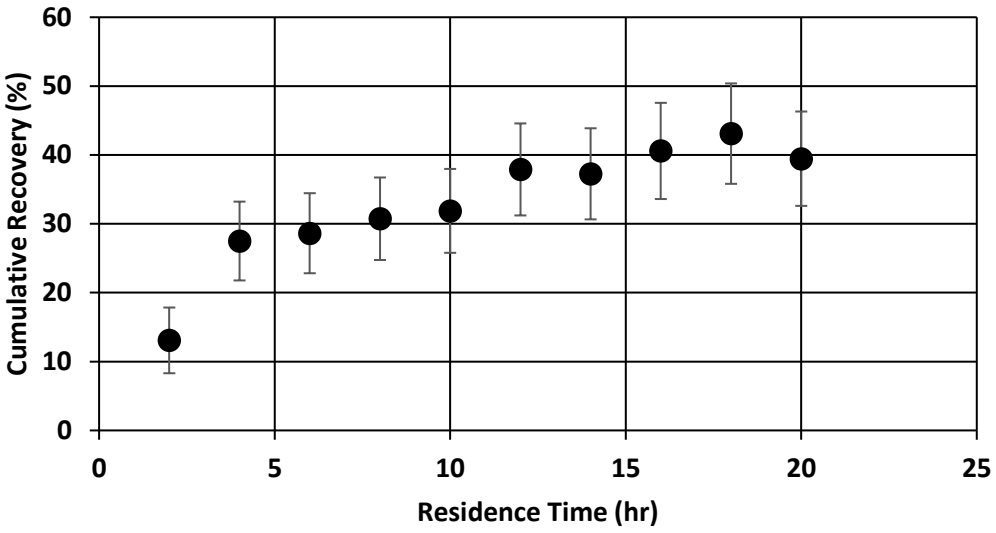

Figure 54 - Cumulative recovery as function of residence time for Duvernay sample crushed sample. Note the solvent was able to mobilize 43% of the *in-situ* fluid.

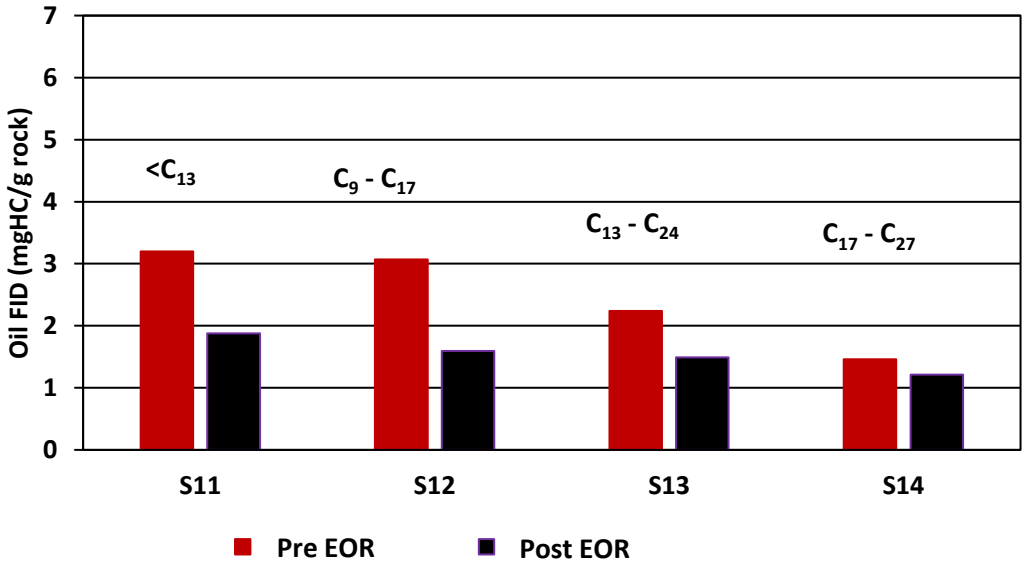

Figure 55 - HAWK pyrolysis pre- and post- HnP on a Duvernay crushed sample. Note the solvent was able to mobilize HC fraction up to C_{27}.

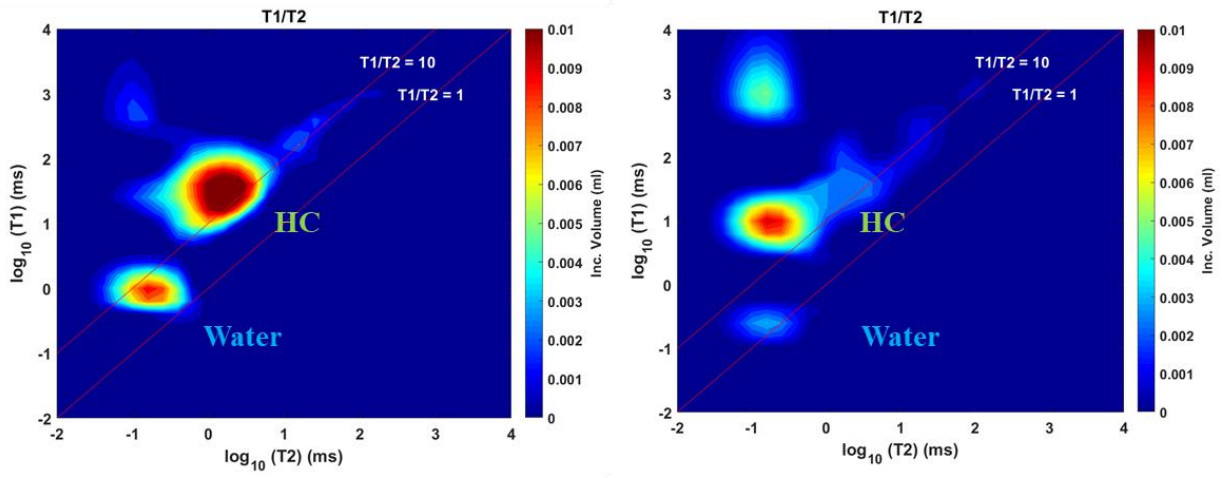

Figure 56 - 2D T1-T2 maps of the Duvernay sample pre- (left) and post- (right) EOR. Mostly oil is produced during this test (83%) with some water (17%).

a)

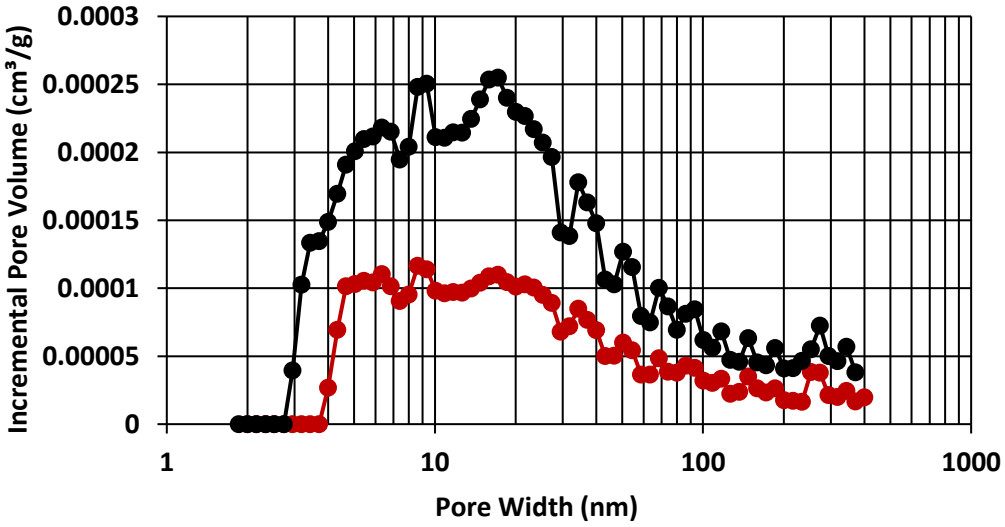

b)

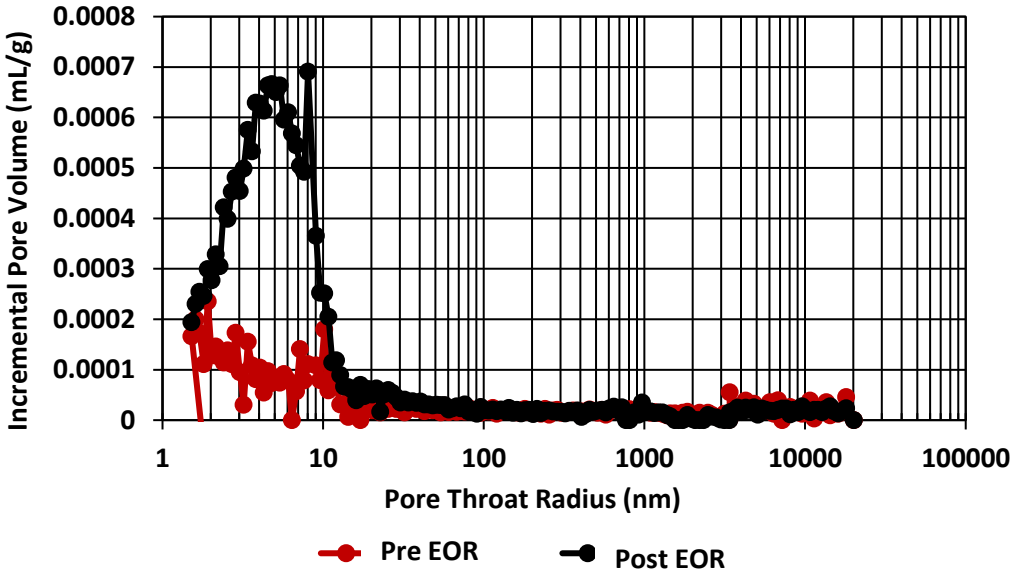

Figure 57 - a) Isothermal nitrogen adsorption before and after EOR showing opening of smaller pores and surface area increases from 1.4 m^2/g to 2.7 m^2/g. b) MICP shows increase in pore throat size by almost 4 times after EOR.

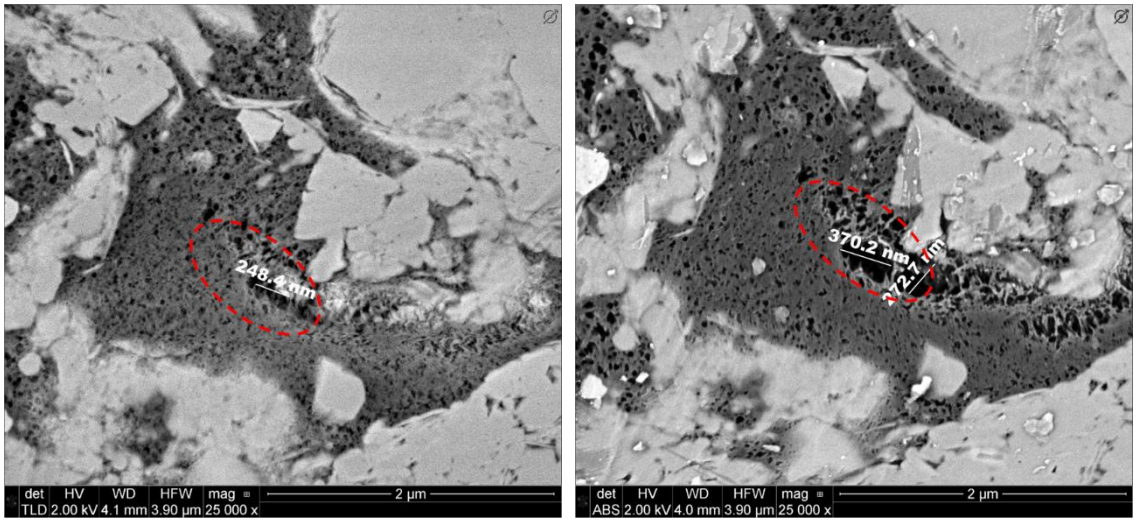

Figure 58 - Pre- (left) and post- (right) EOR SEM images taken on the same scale, showing dissolution of the organic matter resulting in an increase by 50 % of the organic pore size after solvent injection.

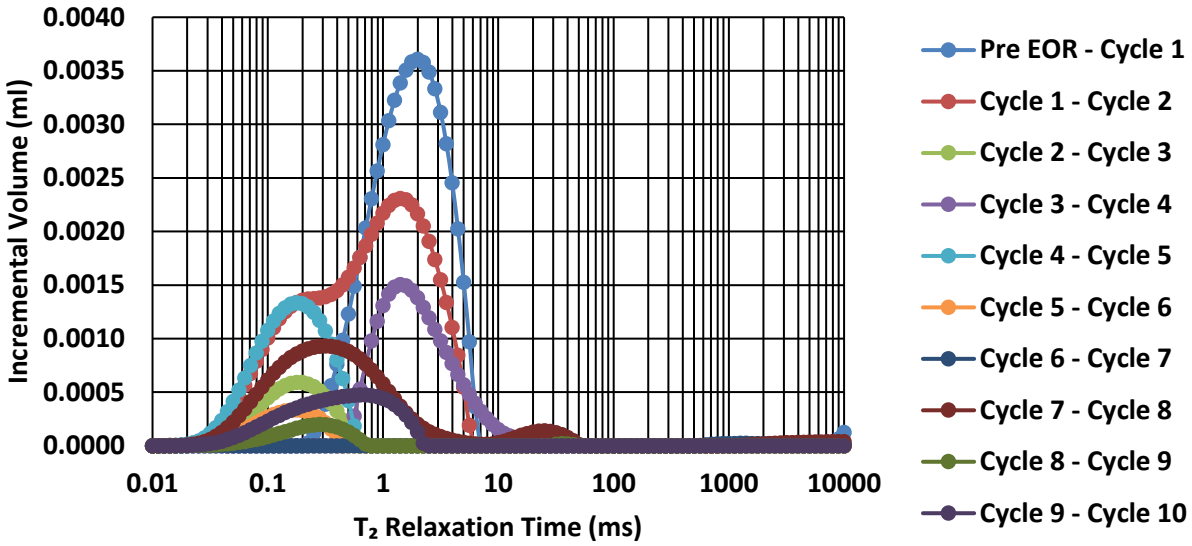

Figure 59 - Subtracted incremental T_2 spectrum from Figure 48 of Duvernay shale showing produced volume during each cycle of HnP. This figure shows that HC production is not bias toward fast or slow relaxation times, HC comes out of both fast and slow relaxation times (i.e. small and large pores) with progressive HnP cycles.

4.2.3 Uinta Basin 1 (Non-Preserved)

Uinta 1 sample presented in this study is from the Uteland Butte formation. It is the basal carbonate of the Green River formation deposited during the first and extensive lake-level rise deposition of the Wasatch formation (Morgan et al., 2002). **Fig.60** shows the general stratigraphy of the Uinta Basin. It is considered a good "tight reservoir" reservoir with thin dolomite beds having porosity ranging from 8-15% and permeability less than 1mD (Ramakrishna et al., 2012)

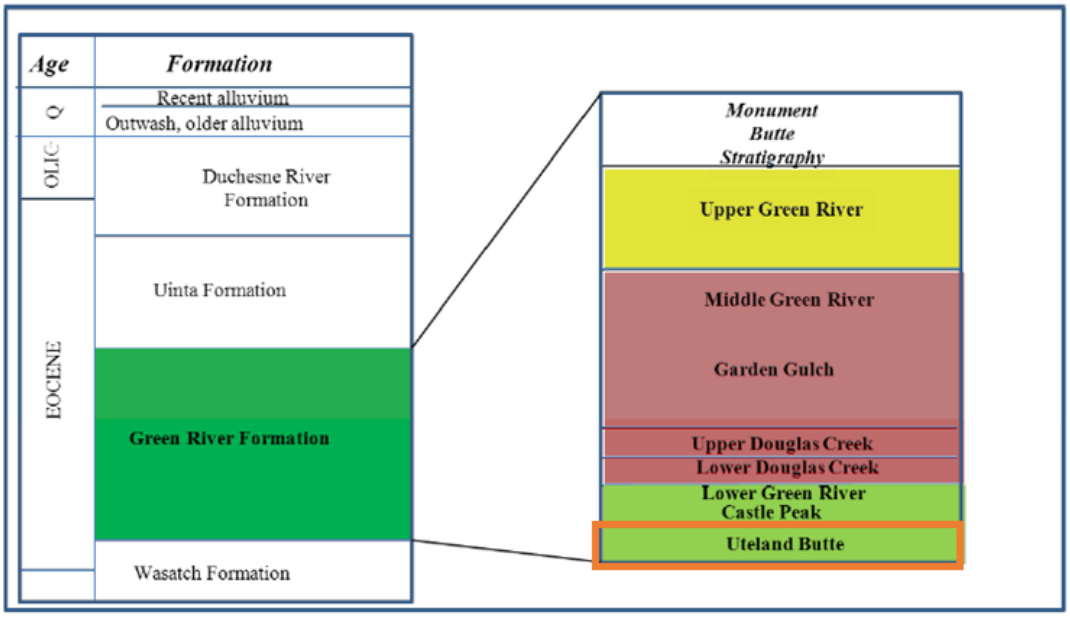

Figure 60 - Regional stratigraphy of the Uinta basin. The Uteland Butte is the basal green carbonates of the Green River formation (Ramakrishna et al., 2012)

For this reservoir similar experiments were conducted at the same conditions of the Duvernay and Eagle Ford (1-hour soak, 1-hour production, 150 °F, 1000 psi above MMP (4700 psi)). The significant difference with this formation is that the oil received from the Uinta basin courtesy of Ovintiv was in waxy state at room temperature. Pictures of the two waxes at room temperature are shown in **Fig.61.** These waxes are clearly viscous and immovable at room temperature. Their T_2 relaxation spectra are shown in **Fig.62.** After EOR very low HC recovery is observed, around 10% **(Figs.63, 64 and 65**)



Figure 61 - Images of brown and yellow wax received from the Uinta basin at room temperature.

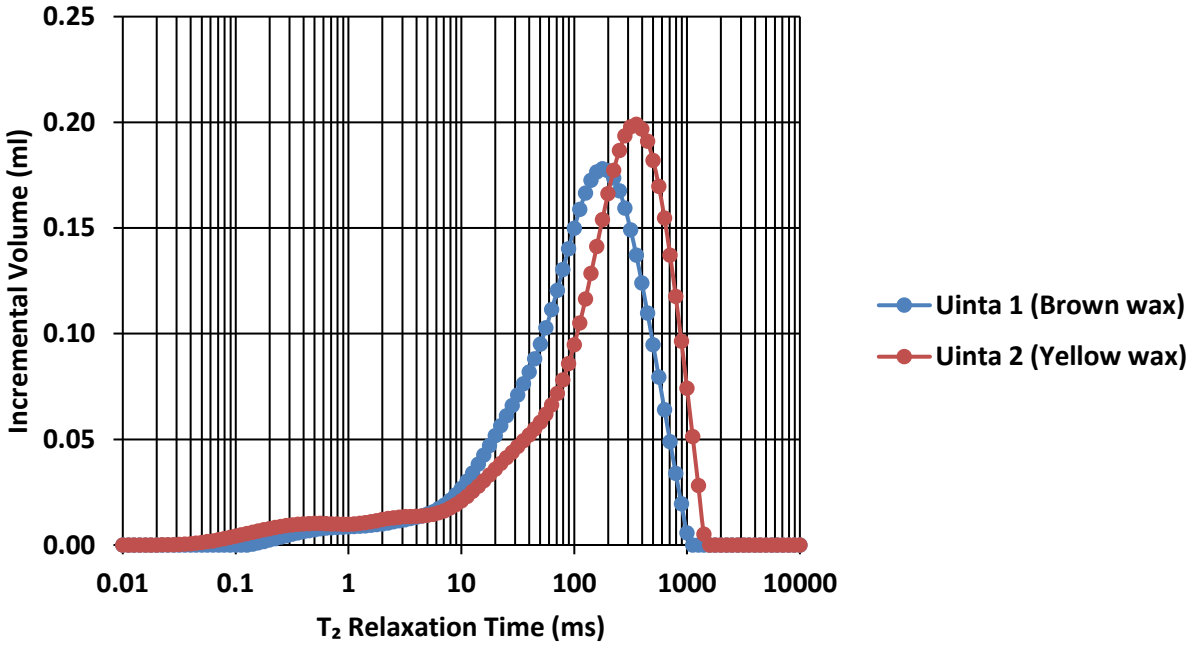

Figure 62 - T_2 relaxation spectra of Uinta 1 and Uinta 2 produced HC. The main peak of Uinta 1 is 220 ms, while Uinta 2 is 400 ms.

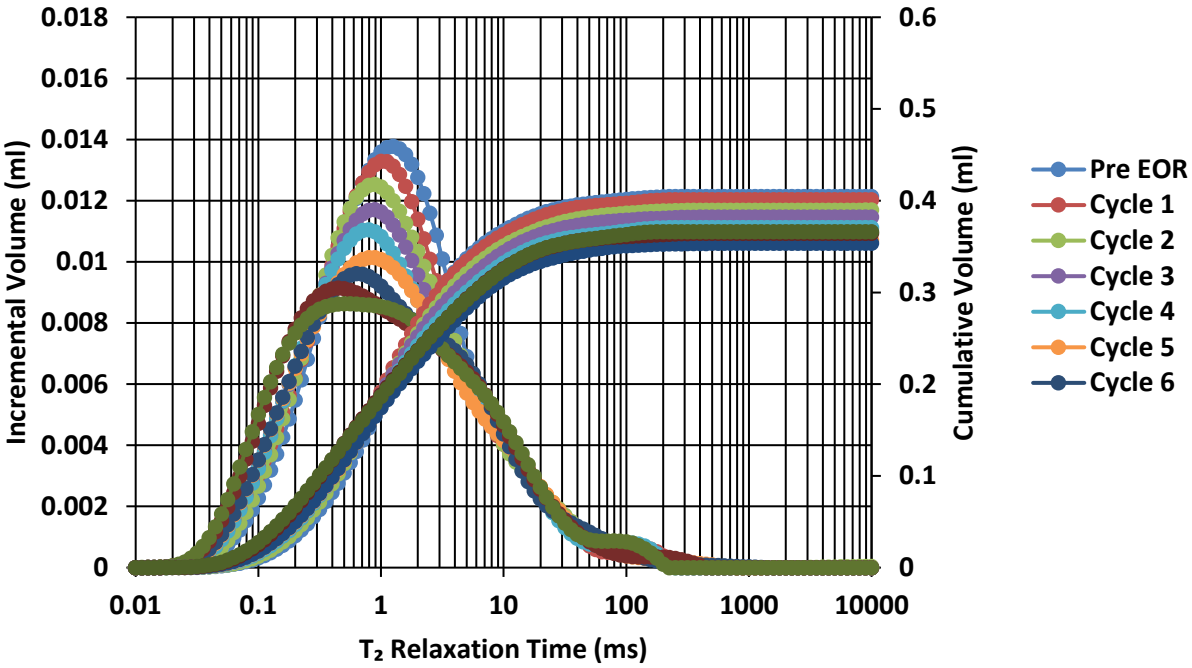

Figure 63 - NMR T_2 spectra during HnP for Uinta 1 crushed sample. Small depletion is observed after EOR. Note that T_2 peaks shifts to the left during HnP signifying that the left-over oil is getting heavier.

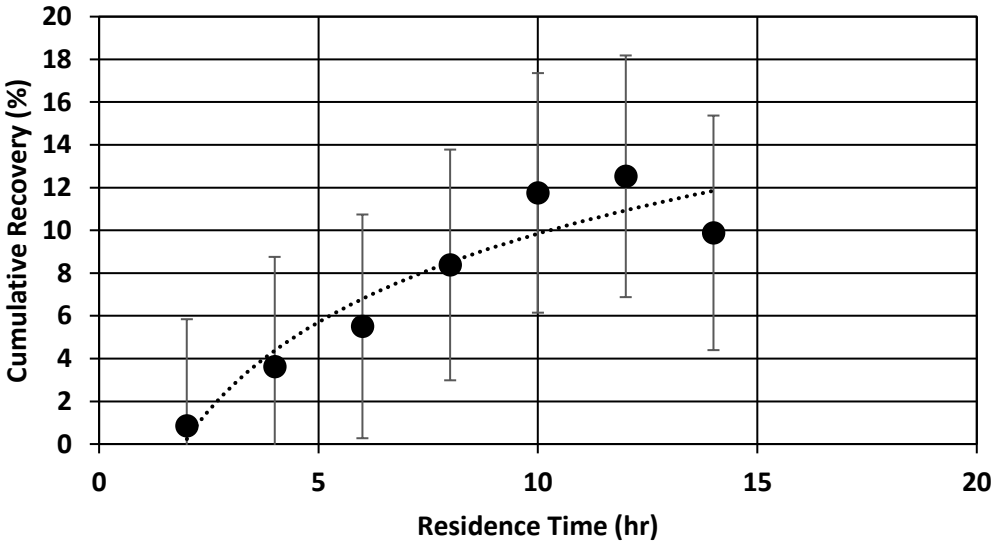

Figure 64 - Cumulative recovery as function of residence time for Uinta 1 sample crushed sample. Note the solvent performance is very poor, only around 10%

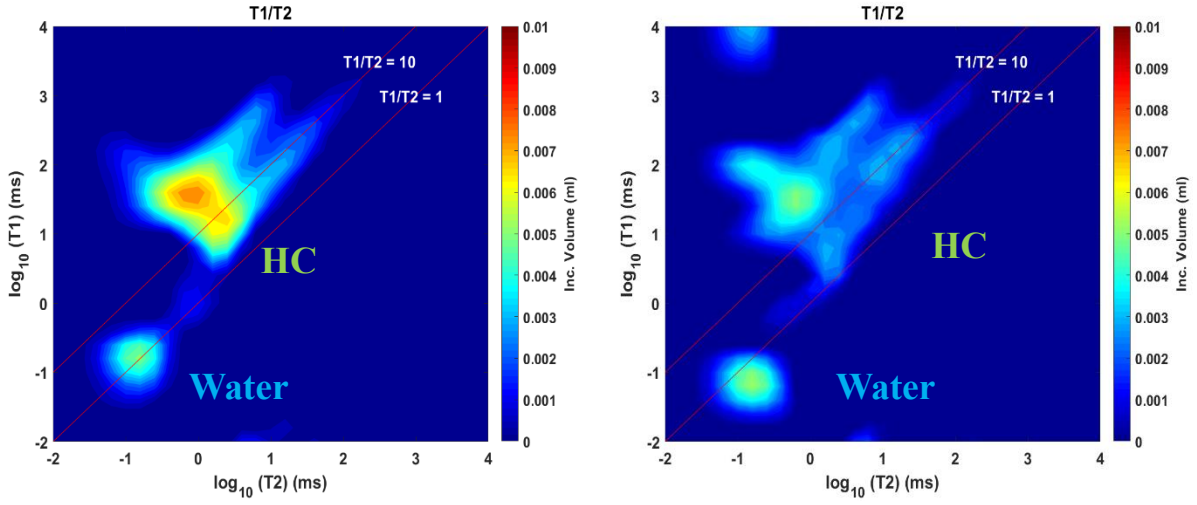

Figure 65 - 2D T_1-T_2 maps of Uinta 1 sample pre- (left) and post- (right) HnF. After EOR only HC is produced.

HAWK analysis (**Fig.66**) shows that significantly heavier HC S_{13} and S_{14} are left behind after EOR. This poor EOR performance is confirmed by BET, MICP and SEM with no changes in internal surface area, pore throat size distribution and micro-structure alteration of OM **(Fig.67 and Fig.68).**

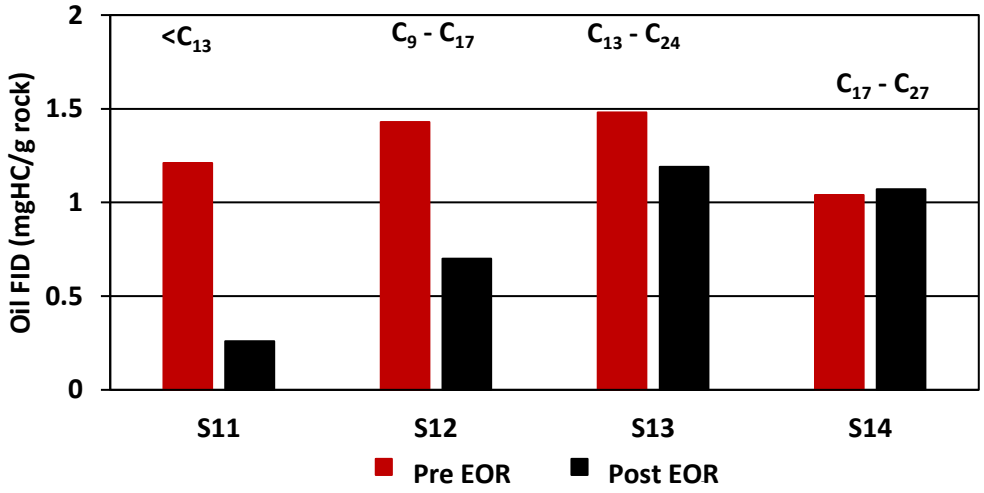

Figure 66 - HAWK pyrolysis pre- and post- HnP on Uinta 1 crushed sample. Note mostly S_{11} and S_{12} are produced but there is a large volume of S_{13} and S_{14} left behind.

a)

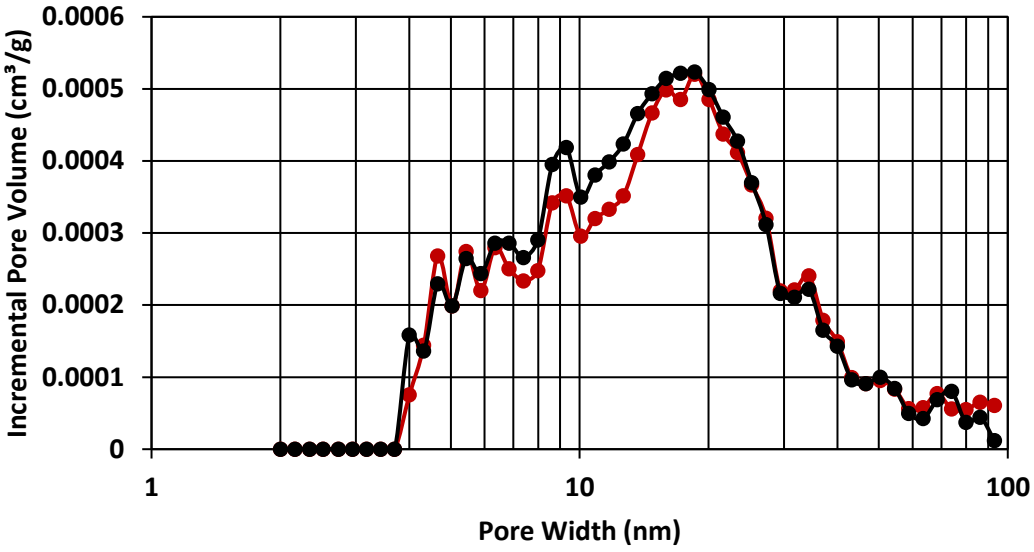

b)

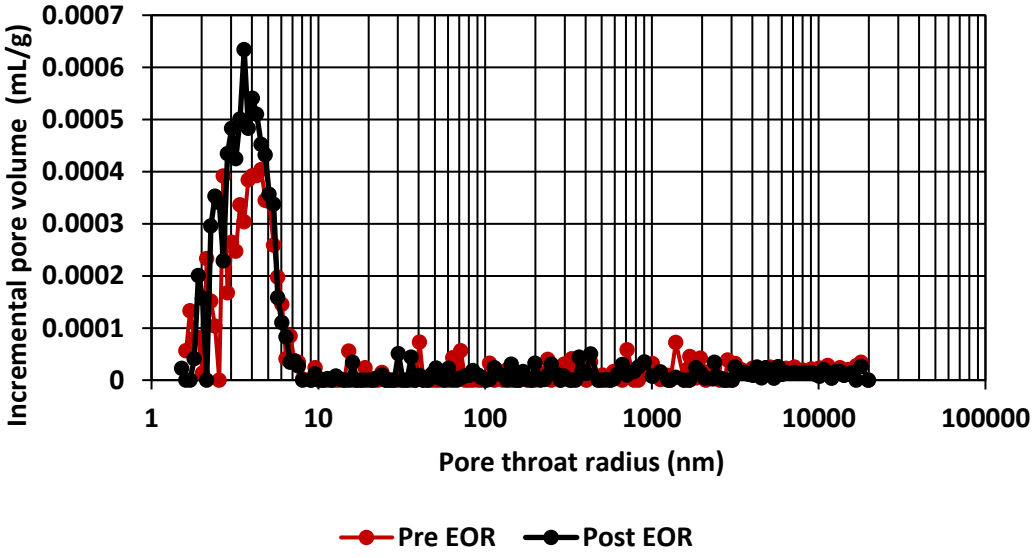

Figure 67 - a) Isothermal nitrogen adsorption before and after EOR showing modest increase in surface area (<10%) from 2.5 m^2/g to 2.8 m^2/g. b) MICP shows modest increase in pore throat radius as well.

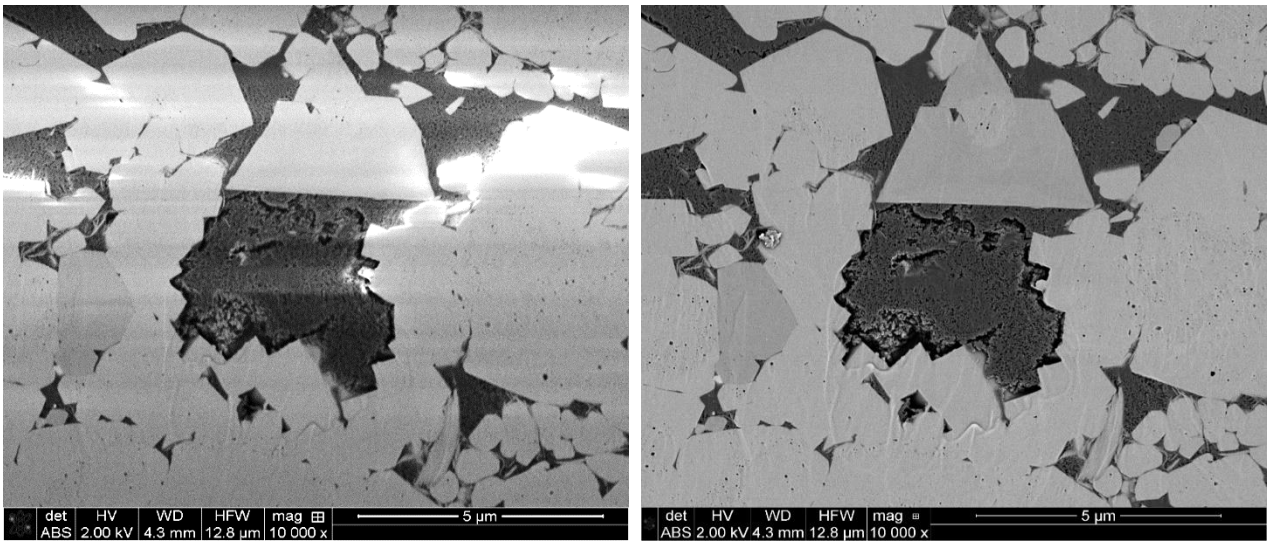

Figure 68 - SEM image pre- (left) and post- (right) HnP show no significant microstructural alteration was observed in the OM.

4.2.4 Uinta Basin 2 (Non-Preserved)

Uinta sample 2 is from the Wasatch formation (Fig. 60). It is predominantly made of sandstones and variegated red, green, and gray shale deposited in a fluvial setting (Johnson 2003). Its porosity is higher than Uinta 1 (7% versus 5%). There is initially low HC saturation as can be seen in the T_1-T_2 map. Most of the residual fluid is water **(Fig.69).** A cumulative recovery of 28% is observed after only 12-hours residence time **(Fig.70 and Fig.71).** The small volume of HC produced is rich in HC up to C_{27} **(Fig.72).** BET and MICP **(Fig.73)** show that this produced fluid comes from very small pores (<10nm). SEM images **(Fig.74)** show substantially more clay than Uinta1 suggesting that the produced water might be clay bound water carried out by thesolvent.

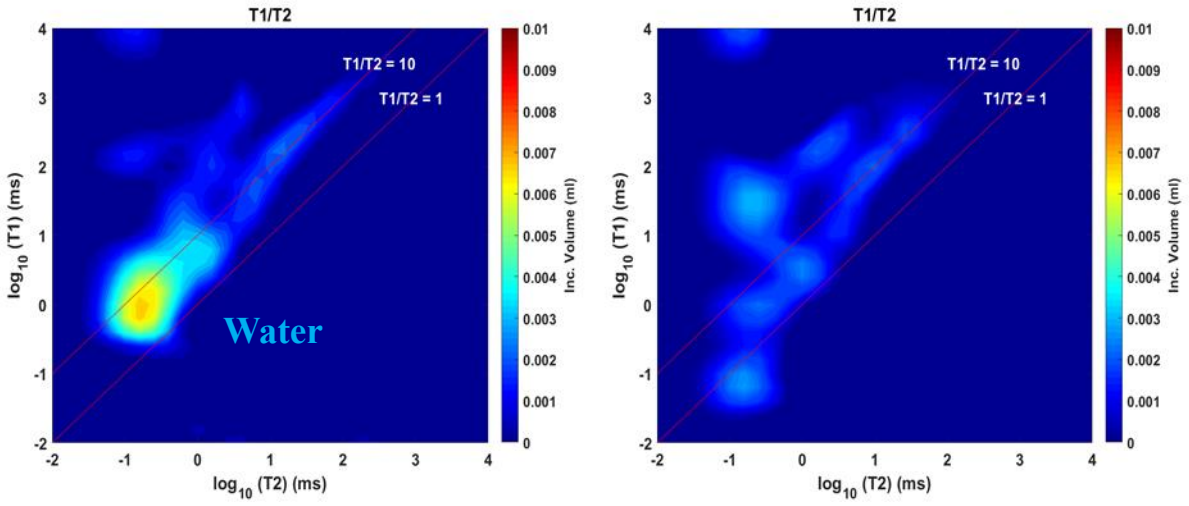

Figure 69: 2D T_1-T_2 maps of Uinta 2 sample pre- (left) and post- (right) HnP. Very low HC present in the sample pre- EOR. Note after EOR mostly water is produced.

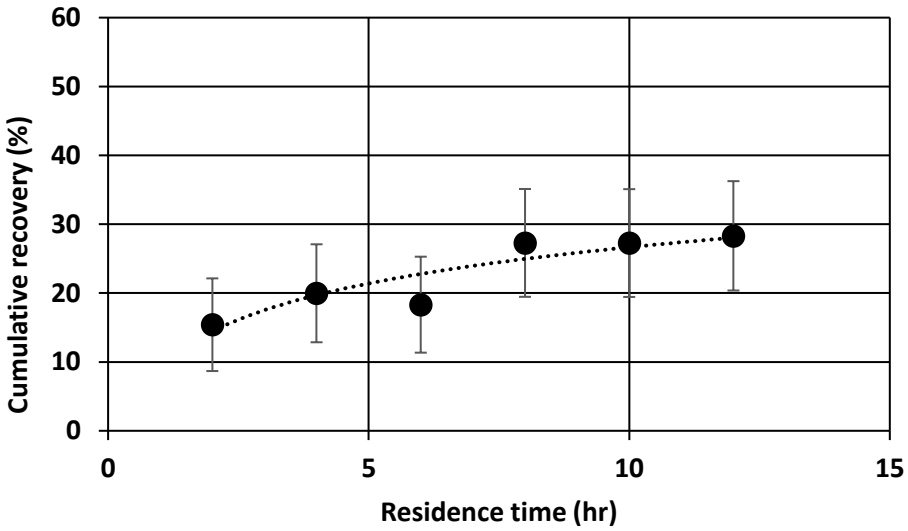

Figure 70 - Cumulative recovery as function of residence time for Uinta 2 crushed sample. Note the cumulative production is around 28 % but most of the fluid produced is water.

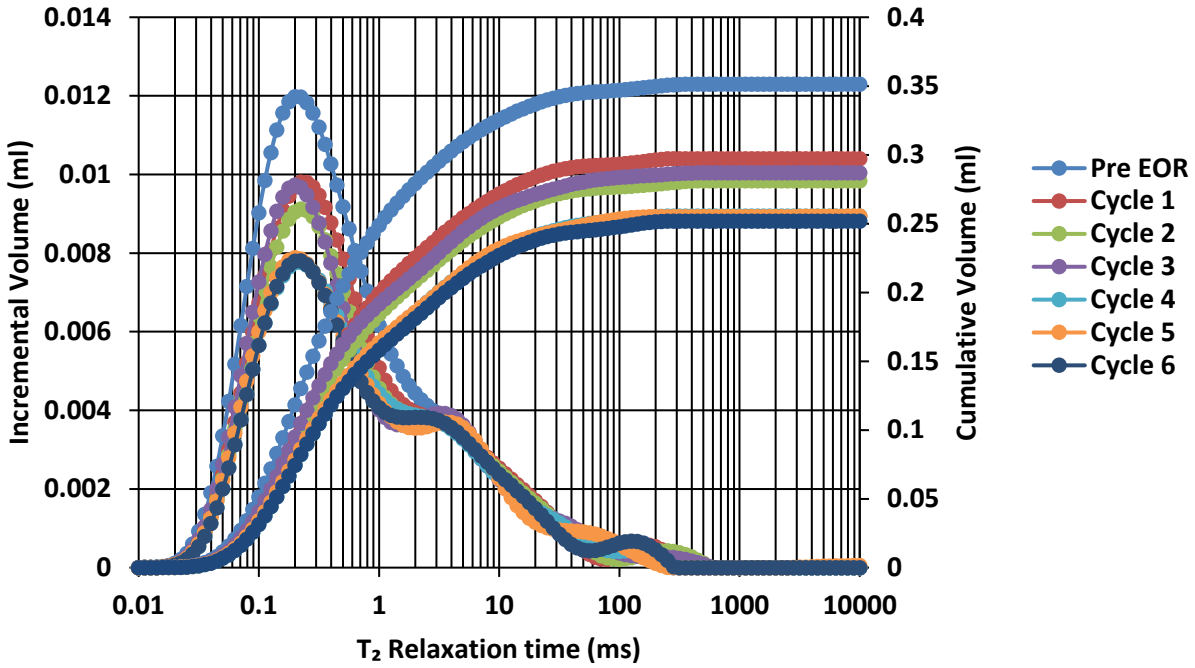

Figure 71 - NMR T_2 spectra during huff-n-puff for Uinta 2 crushed sample. Relatively smaller pore bodies (<1ms) are depleted during EOR.

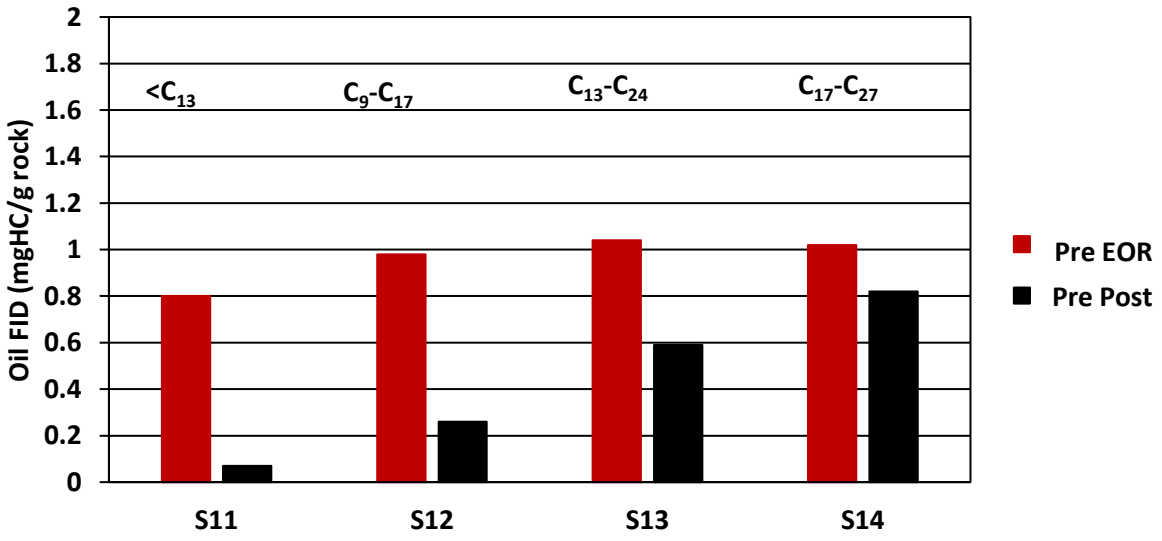

Figure 72 - HAWK pyrolysis pre- and post- HnP on Uinta 2 crushed sample. After EOR HC fractions up to C_{27} are produced. Note the overall oil FID is substantially lower than the other formations.

a)

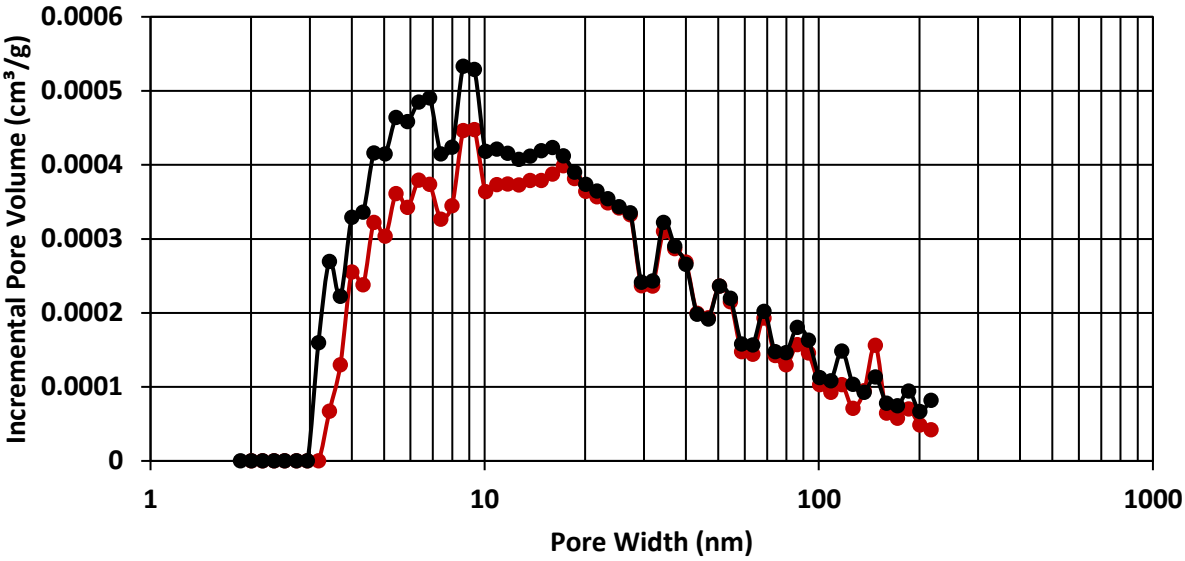

b)

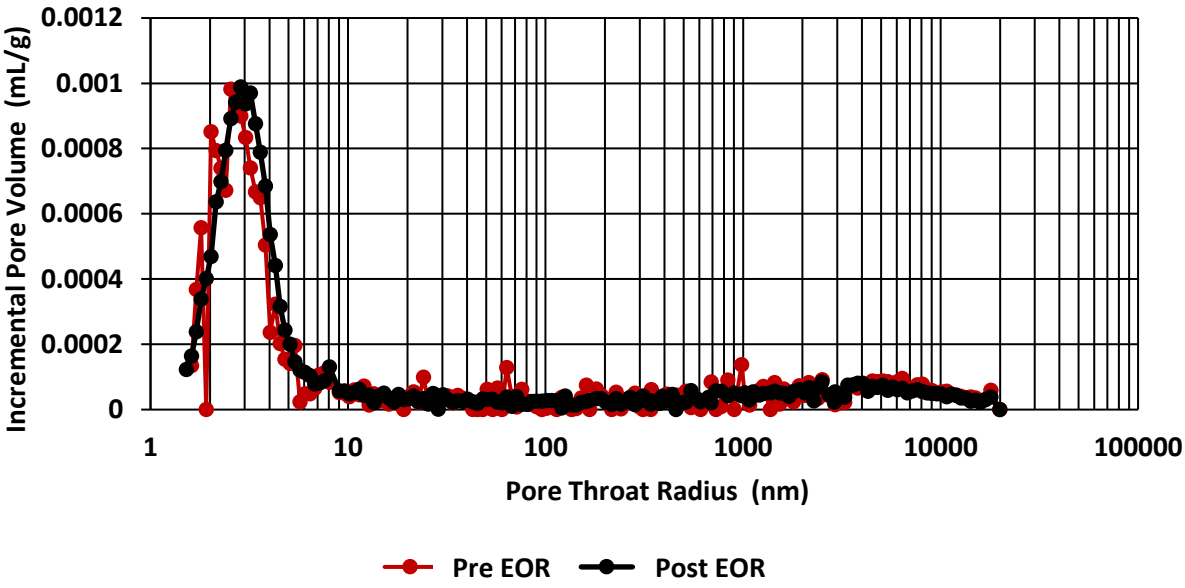

Figure 73 - a) Isothermal nitrogen adsorption before and after EOR showing 30% increase in surface area from very small pores (<10nm). b) However, MICP shows no major change in pore throat radii.

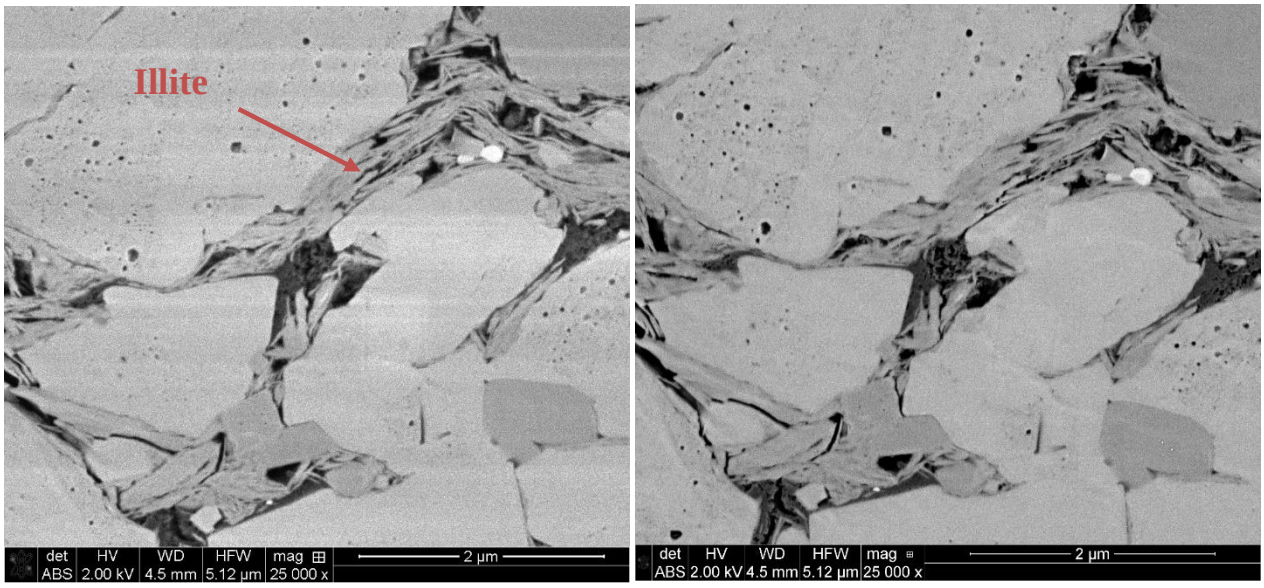

Figure 74 - SEM image pre- (left) and post- (right) HnP. No significant microstructural alteration was observed in the OM. Note Uinta 2 has significantly more clay than Uinta 1.

4.2.5 Montney 1 (Non-Preserved)

The Montney shale is also a major unconventional reservoir in Canada. It is a thick and extensive siltstone rich reservoir extending between British Columbia and Alberta; this formation is estimated to contain 449 Tcf of marketable gas, 14,521 MMbbl of marketable natural gas liquid and 1,125 MMbbl of marketable oil (National Energy Board 2013).

Post HnP, NMR results **(Fig.75, Fig.76 and Fig.77**) show that for Montney 1, both water and HC are produced with a cumulative production of 23%. The first cycle produced 19% recovery. Like Uinta 2 HAWK results shows that the solvent is effective in moving HC up to S_{13} ($<C_{24}$) **(Fig.78)**. BET show in increase in the surface area by a factor of 4, from 0.4 m^2/g to 1.6 m^2/g in very small pores (4-5nm) **(Fig.79).** Observations that agrees well with SEM images showing no microstructural alteration except for extensive amount of rock debris on the surface of the sample, which might reduce porosity **(Fig.80).**

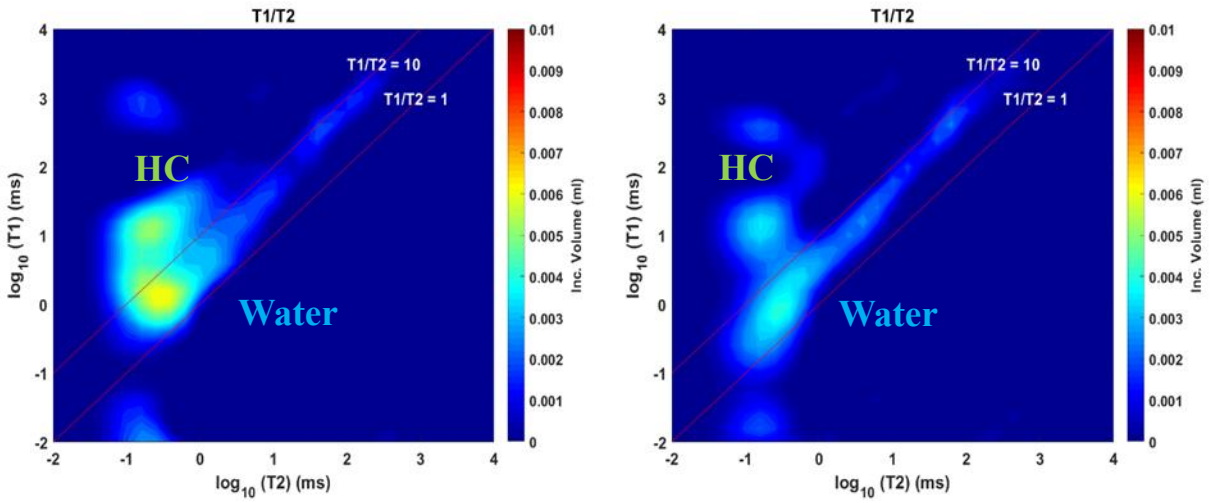

Figure 75 - 2D T_1-T_2 maps of Montney 1 sample pre- (left) and post- (right) HnP. After HnP 46% of oil and 54% of water was produced.

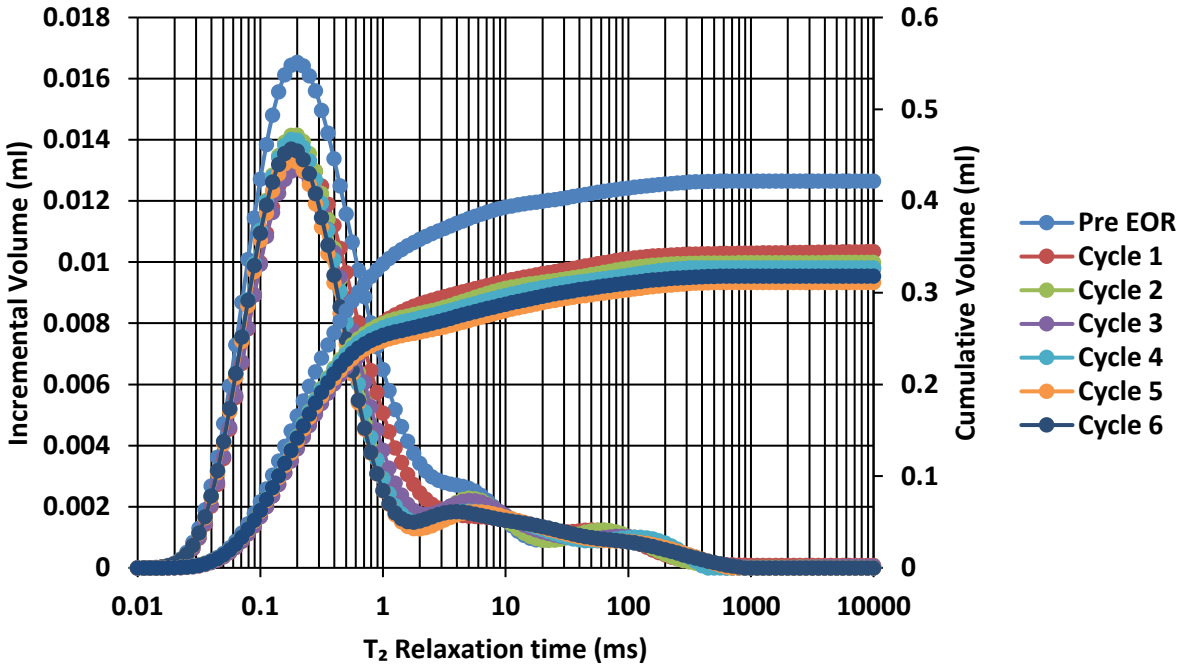

Figure 76 - NMR T_2 spectra during HnP for Montney 1 crushed sample. Most of the production happens during cycle 1. Note based on T_2 alone no clear distinction can be made to discriminate fluid type.

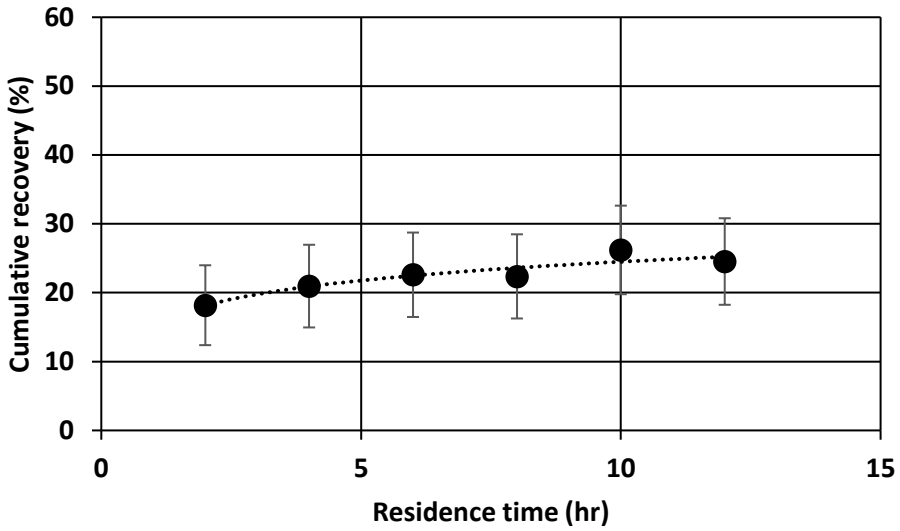

Figure 77 - Cumulative recovery as function of residence time for Montney 1 crushed sample. Note cycle 1 is the most efficient with almost 20% recovery. The ultimate recovery ~24% is achieved after 12-hours.

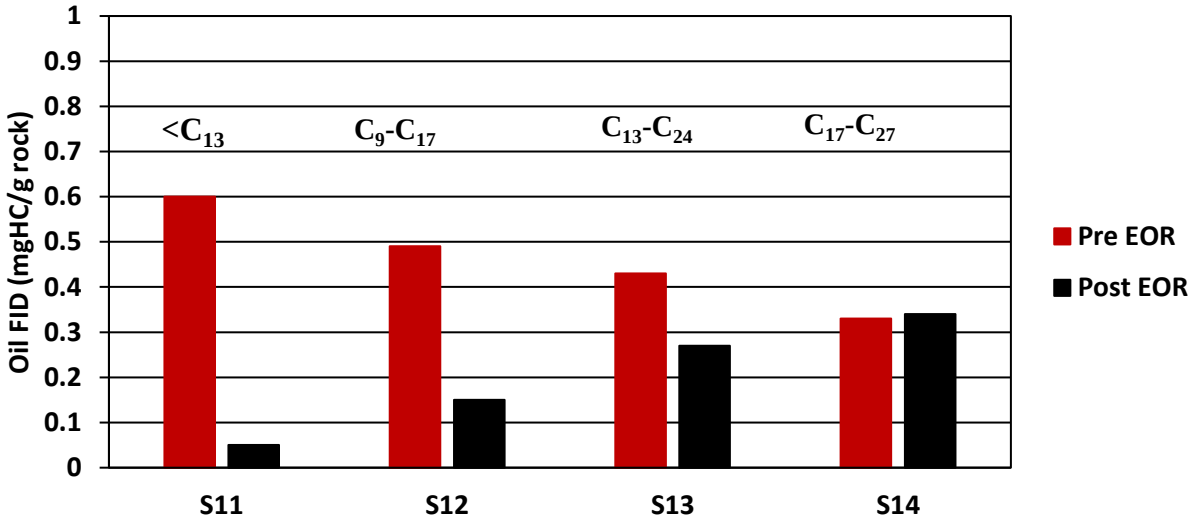

Figure 78 - HAWK pyrolysis pre- and post- HnP on Montney 1 crushed samples. After EOR HC fraction up to C_{24} are produced, but most of the oil mobilized are lighter HC ($<C_{17}$)

a)

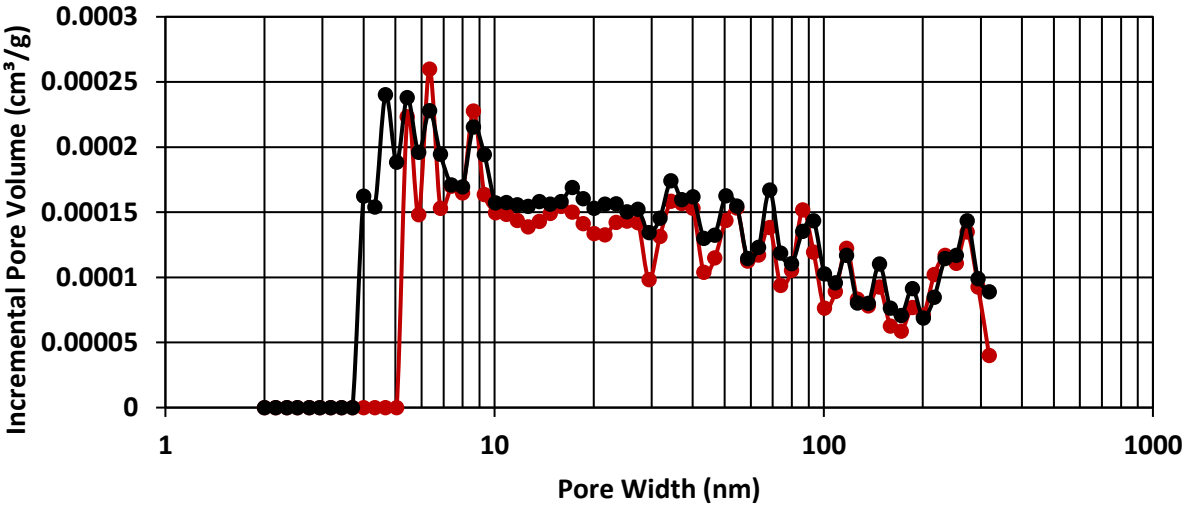

b)

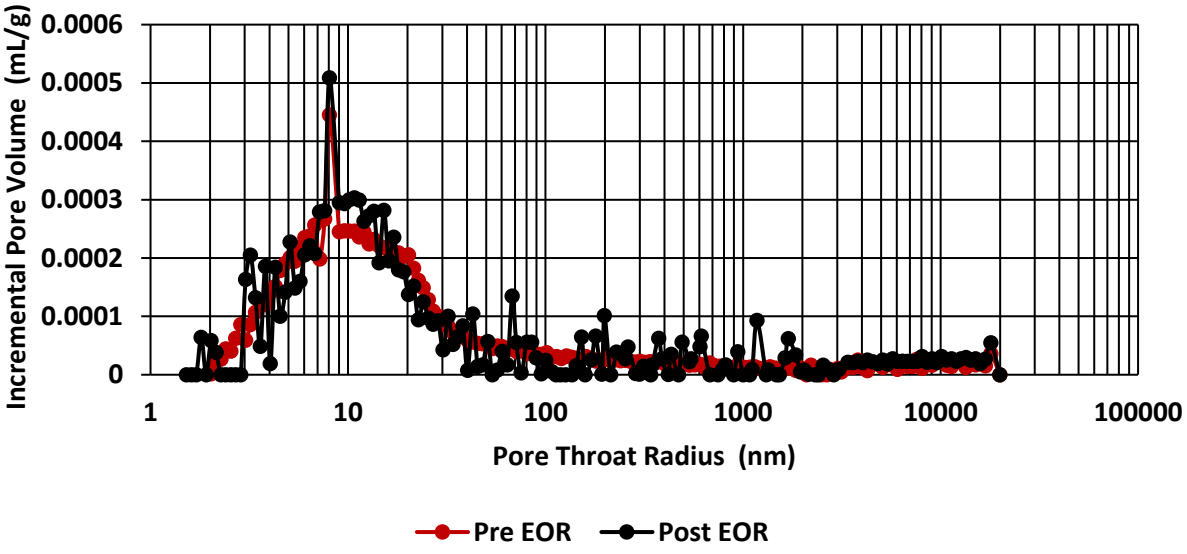

Figure 79 - Isothermal nitrogen adsorption before and after EOR showing increase surface area from 0.4 m^2/g to 1.6 m^2/g coming from very small pores (4-5 nm). b) However, MICP shows no major change in pore throat radii.

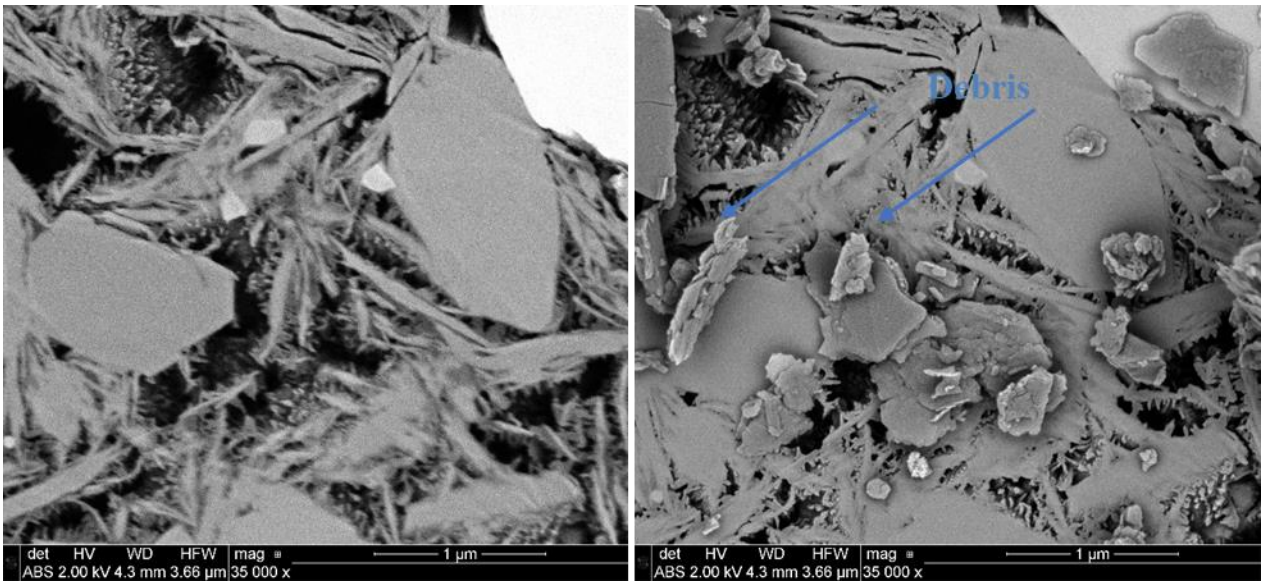

Figure 80 - SEM image pre- (left) and post- (right) HnP. No microstructural alteration is observed after EOR. Note the extensive amount of debris after EOR, which plug pores and reduces recovery.

4.2.6 Montney 2 (Non-Preserved)

A cumulative HC recovery of 50% is achieved after 20-hours of residence time with a gradual depletion rate (**Fig.81, Fig.82 and Fig. 83**). The depletion rates seem to be controlled by the large range of pore throat size (0.1-1µm). The residual oil is also moveable with mostly light HC S_{11} and S_{12} ($<C_{17}$), which are the main targets of the rich gas C_1:C_2 (72:28) **(Fig. 84)**. In addition, BET and MICP shows significant increase in pore throat size from 0.8 to 1µm **(Fig. 85).** Observation that agrees well with the SEM images showing in increase in pore size by a factor of 2 after gas injection **(Fig. 86)**

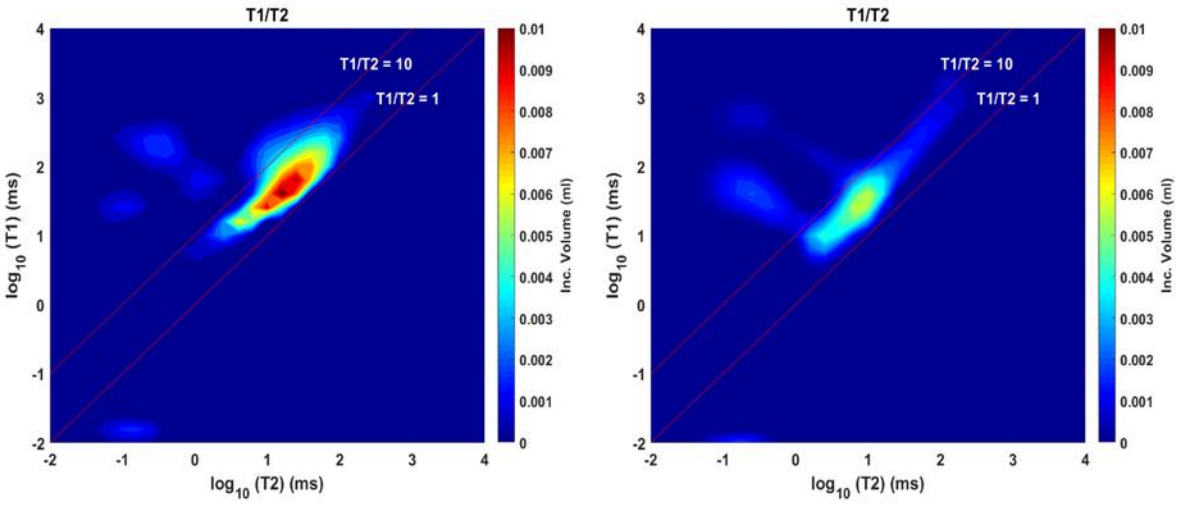

Figure 81 - 2D T_1-T_2 maps of Montney 2 sample pre- (left) and post- (right) HnP. The sample has high initial oil saturation with no residual water. During EOR substantial volume of HC is produced.

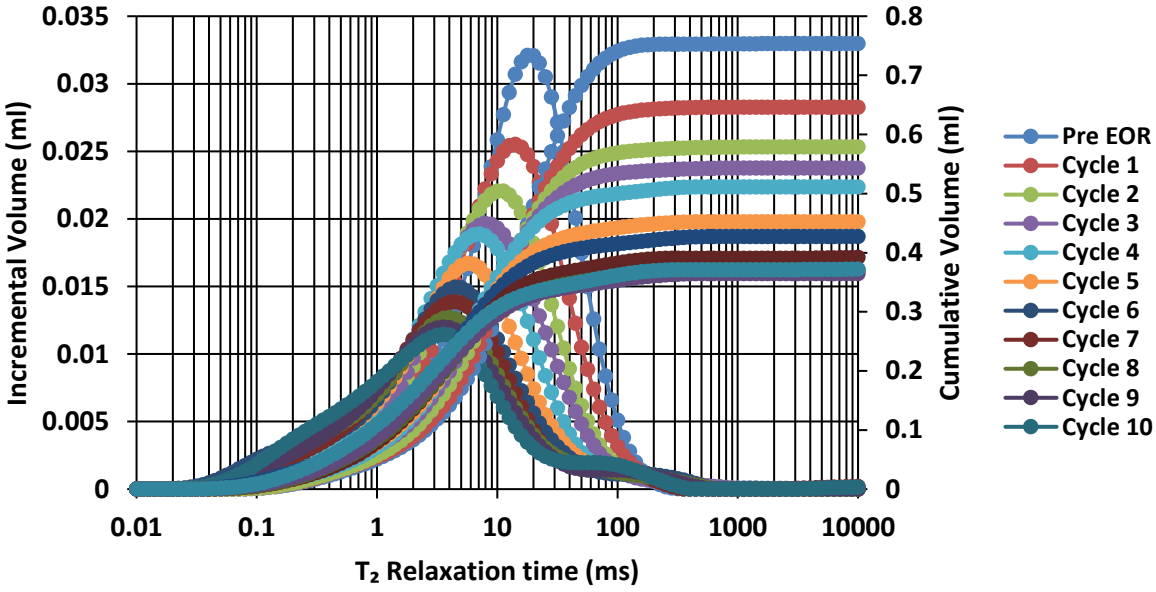

Figure 82 - NMR T_2 spectra during HnP for Montney 2 crushed sample. The depletion in this sample is gradual and well behaved. Note that the main T_2 peaks shift to the left suggesting that the left-over HC is getting heavier.

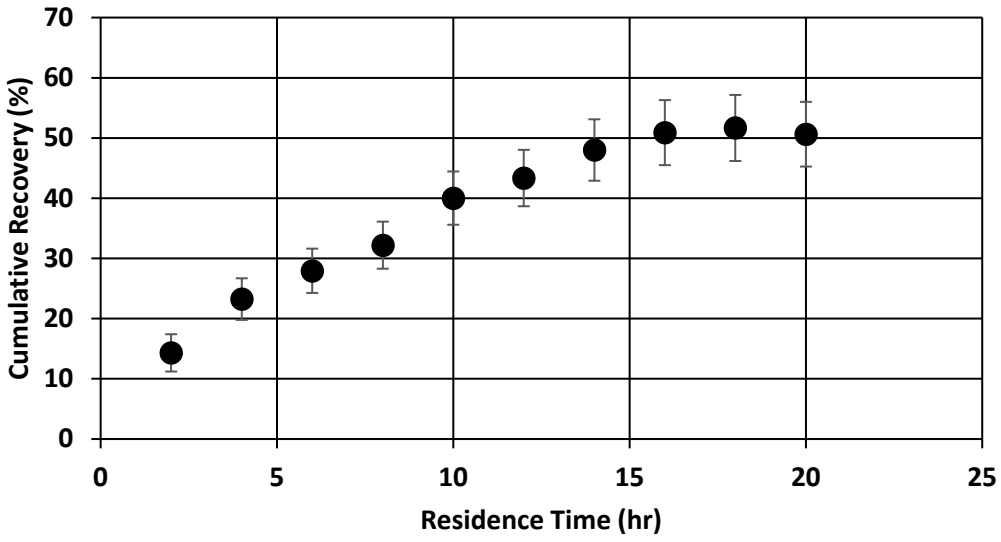

Figure 83 - Cumulative recovery as a function of residence time for Montney 2 crushed sample. Note that after 20-hours, 50% of HC is recovered with a gradual production rate.

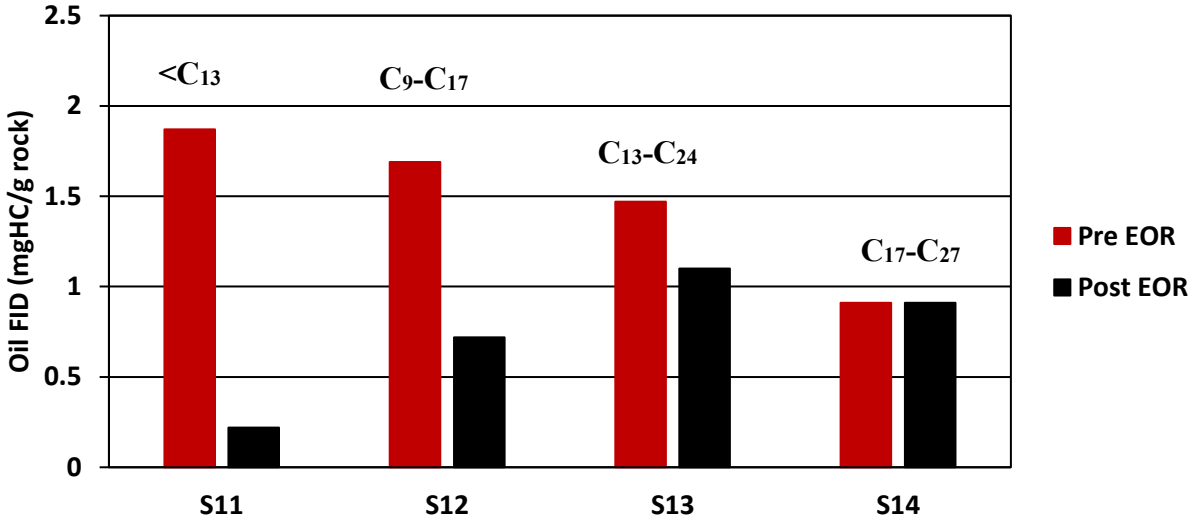

Figure 84 - HAWK pyrolysis pre- and post- HnP on Montney 2 crushed sample. After EOR HC fractions up to C_{24} are produced, but most of the oil mobilized is lighter HC ($<C_{17}$).

a)

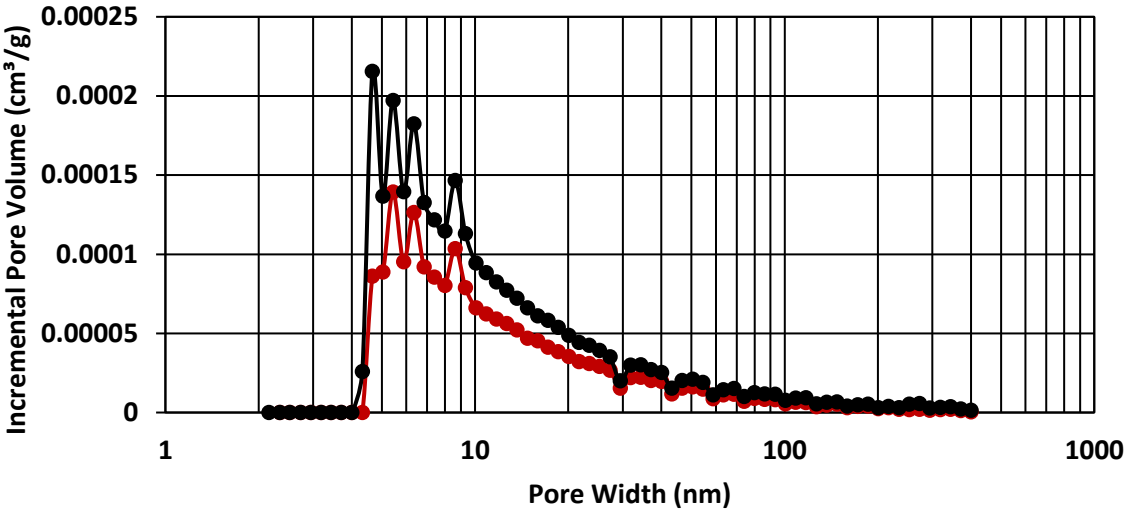

b)

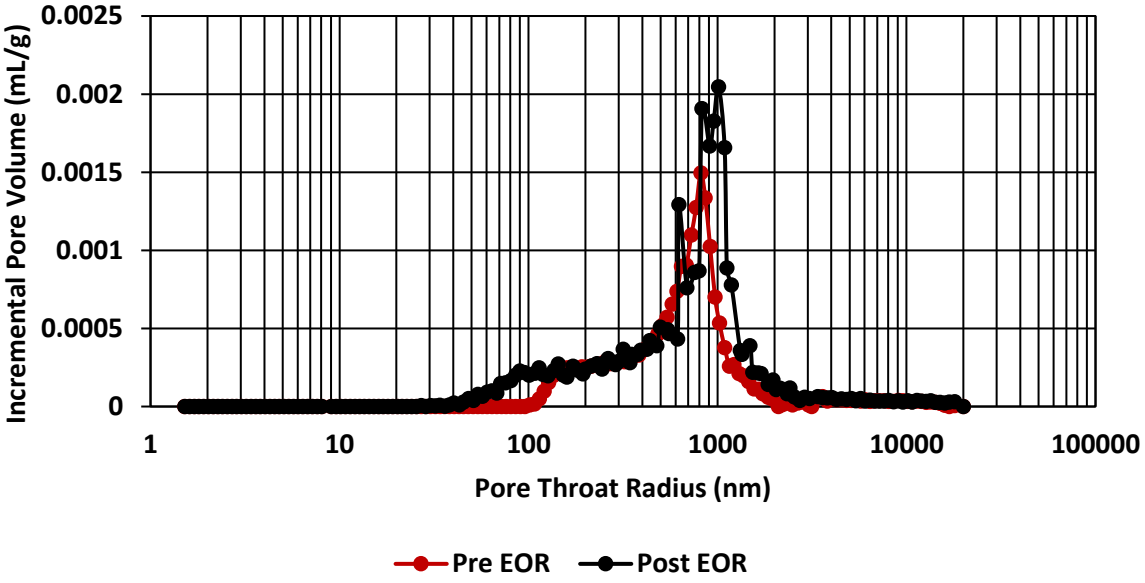

Figure 85 - Isothermal nitrogen adsorption before and after EOR showing small change in surface area; from 0.0018 m^2/g to 0.0075 m^2/g from small pores. b) However, MICP shows large increase in pore throats from 800nm to 1000nm.

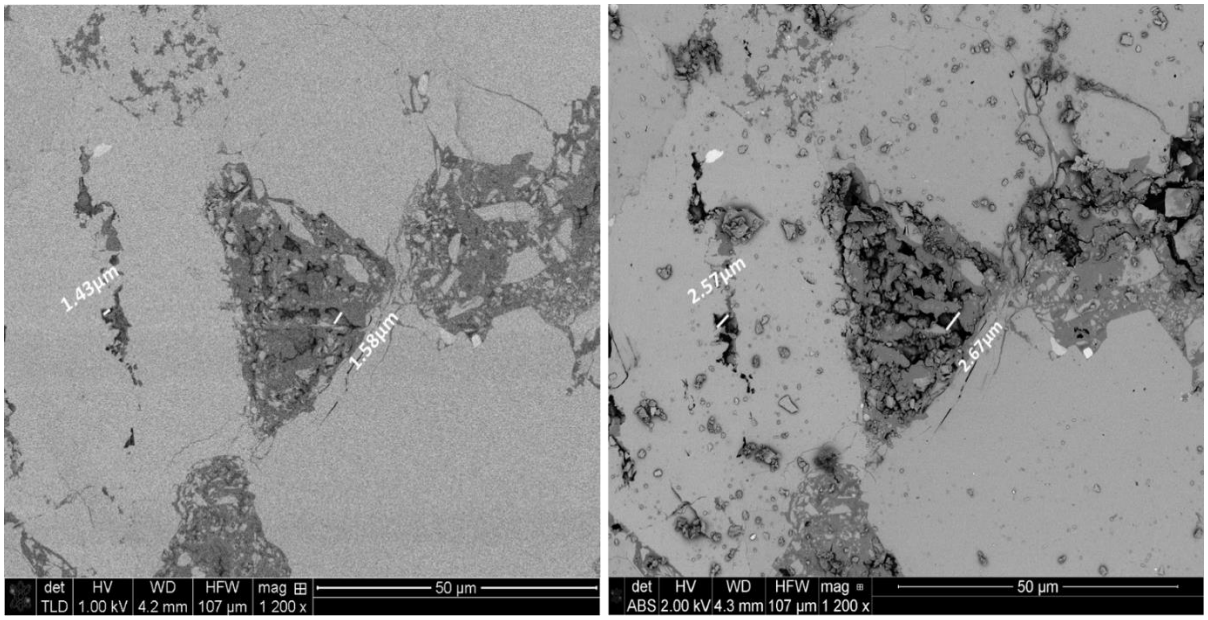

Figure 86 - SEM image pre- (left) and post- (right) HnP showing dissolution of the OM microstructure on Montney 2 after HnP. The increase in pore size agrees well with BET and MICP interpretation. The new dimensions after EOR in the OM are greater by a factor of 2.

4.2.7 Meramec (Non-Preserved)

For the Meramec sample the test was conducted at the same conditions: rich gas solvent C_1:C_2 (72:28) at 4500 psi (1000psi above MMP) and at 150 °F. This sample displays low initial HC saturation and very low TOC (0.8wt%). The T_1-T_2 maps (**Fig.87**) shows clear fluid separation between water and oil, with water in relatively smaller pores, while the residual oil is in larger pores. During EOR oil seems to be produced first from the larger pore bodies first (T_2 ~1-10ms) then smaller pores (T_2<1nm) (**Fig.88**). This fluid production signature is shown by the sudden jump in recovery after 6-hours residence time (**Fig.89**). A cumulative recovery of 44% is observed after 12-hours. After EOR HC fractions up to C_{24} are produced, but most of the oil mobilized is lighter HC (<C_{17}) (**Fig.90**). No significant microstructural alterations are observed with BET, MICP and SEM (**Fig.91 and Fig.92**).

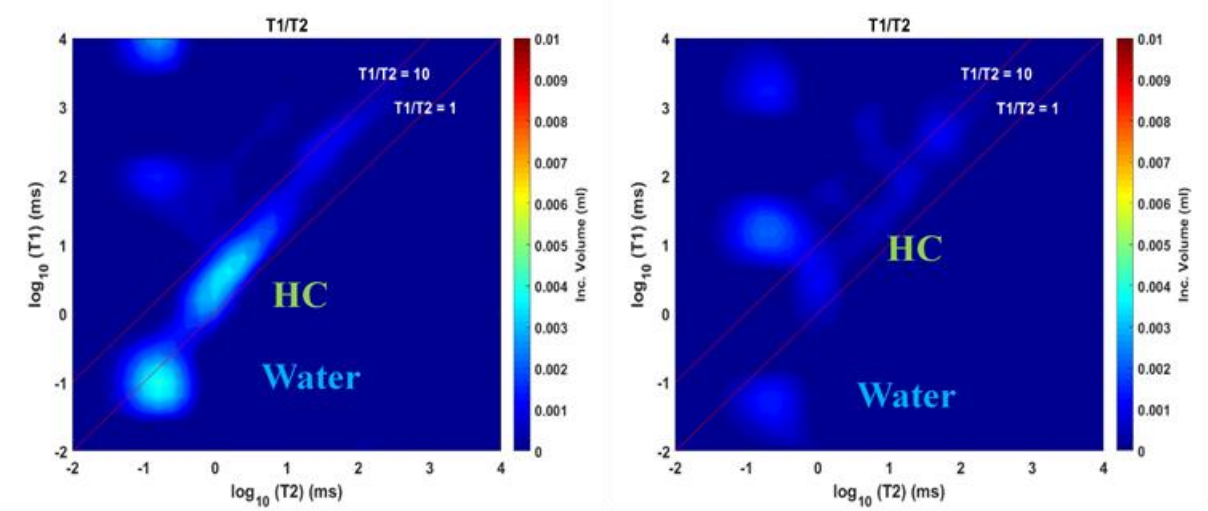

Figure 87 - 2D T_1-T_2 maps of Meramec sample pre- (left) and post- (right) HnP. The sample has very low initial oil and water content. Note the clear separation between the two oil and HC clusters. In this case water in present in relatively smaller pores while the residual oil is in larger pores.

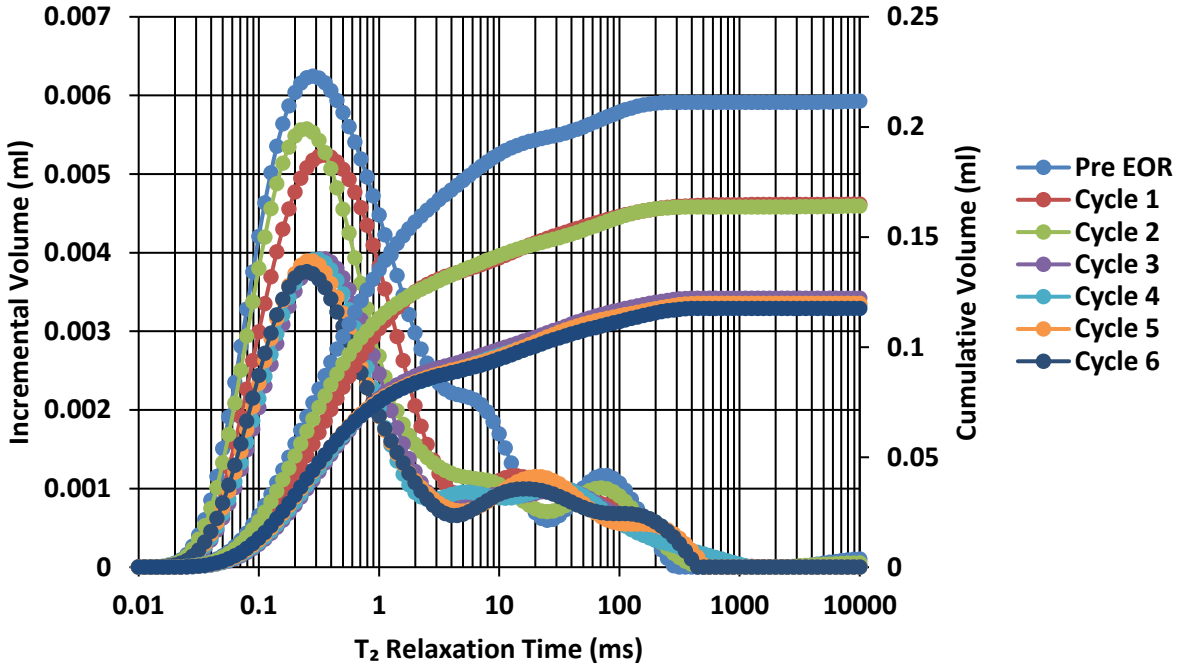

Figure 88 - NMR T_2 spectra during huff-n-puff for Meramec crushed sample. Larger oil wet pores are depleted first (1-10ms) in the first 2 cycles and water pores are depleted in smaller pores (T_2<1ms)

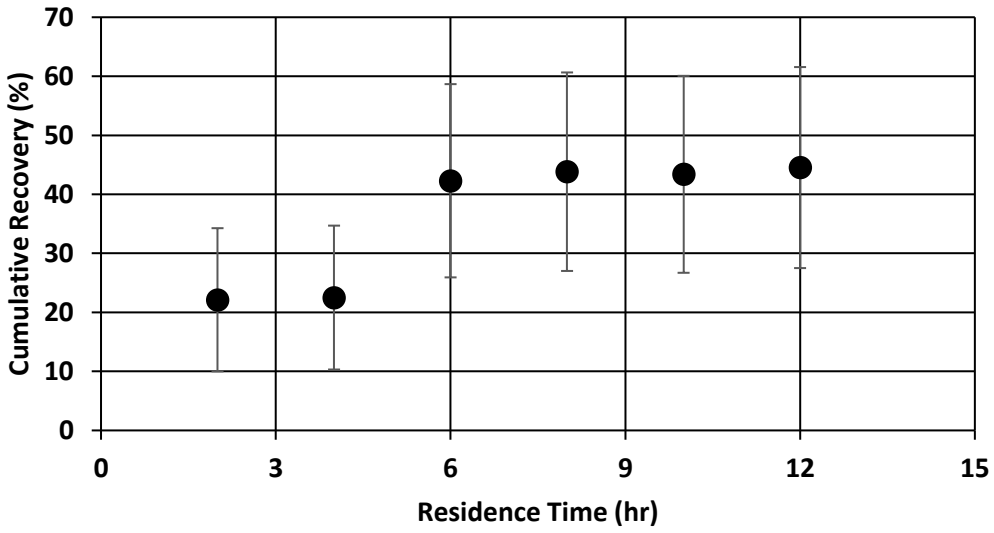

Figure 89 - Cumulative recovery as function of residence time for Meramec crushed sample. A total recovery of 44% is observed after 12-hours. Note that the error bars are large due low initial residual saturation.

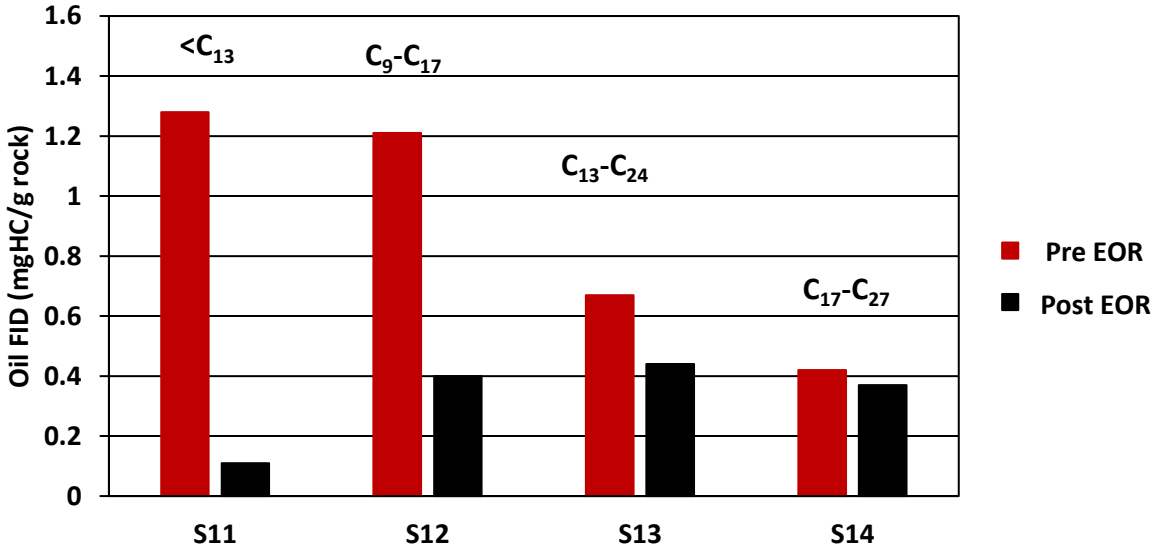

Figure 90 - HAWK pyrolysis pre- and post- HnP on Meramec crushed sample. After EOR HC fractions up to C_{24} are produced, but most of the oil mobilized is lighter HC ($<C_{17}$).

a)

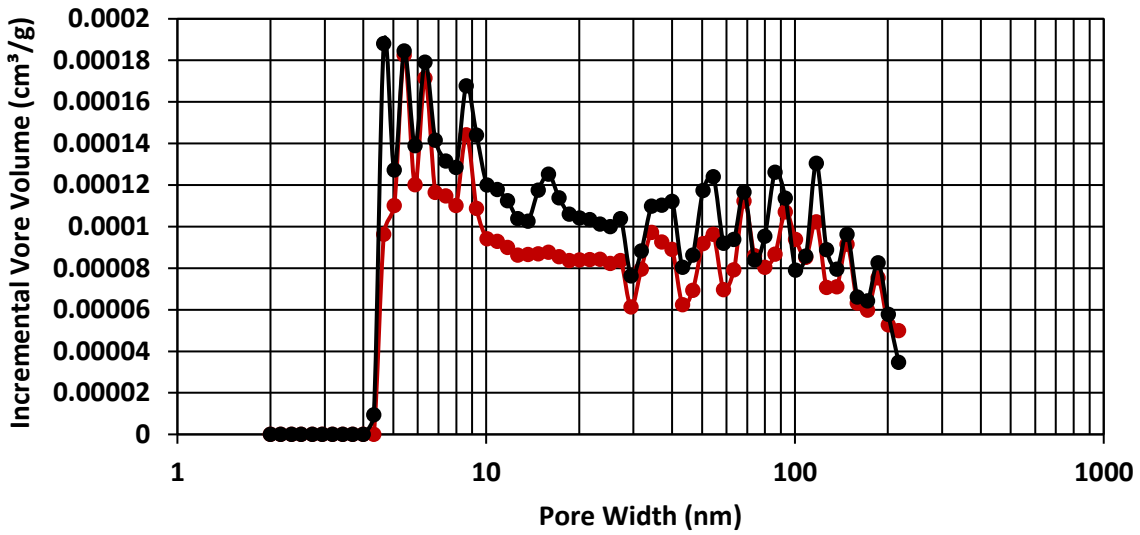

b)

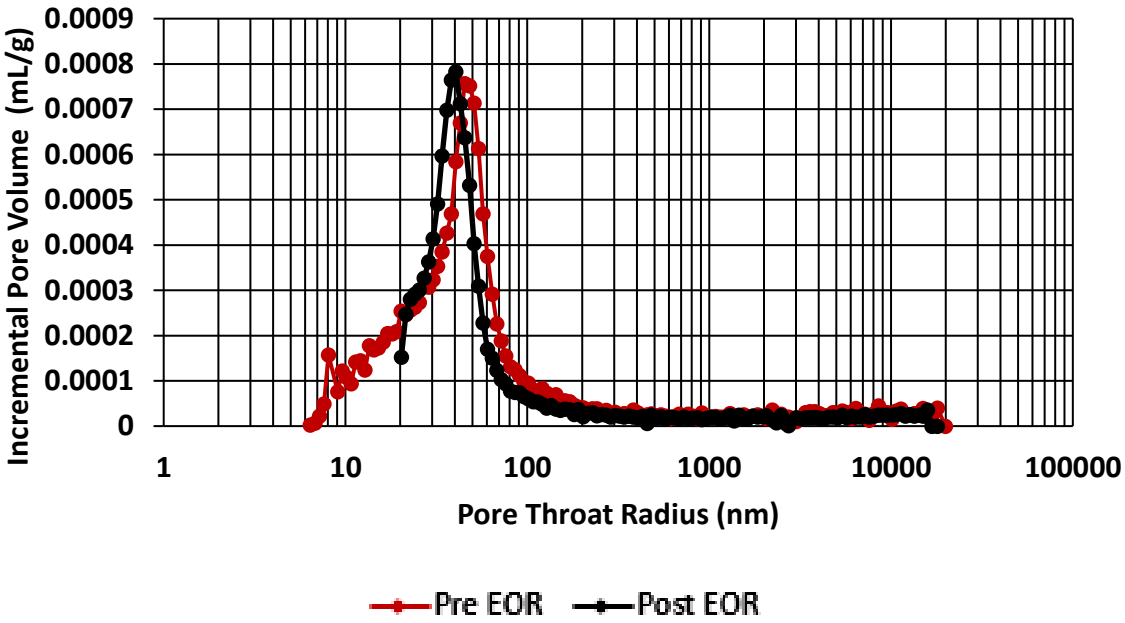

Figure 91 - Isothermal nitrogen adsorption before and after EOR showing little increase in surface area from 0.6 m^2/g to 0.8 m^2/g coming from very small pores (<200nm.) b) MICP shows large pores compared to other tight formation in this study but a slight change in pore throat size distribution from 50 to 40nm is observed after EOR. Note after EOR there no pore throat below 20nm, which could attribute to some pore blockage.

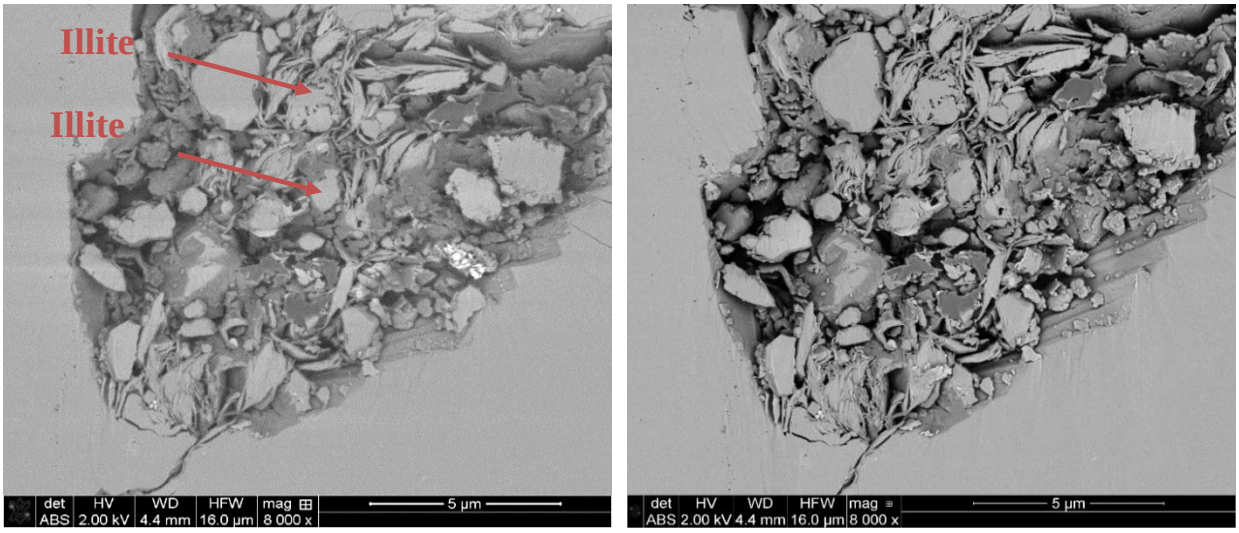

Figure 92 - SEM image pre- (left) and post- (right) HnP showing no microstructural alteration of Meramec. Mostly clay minerals and inorganic material are visible.

4.3 Performance evaluation

To determine the best HnP candidates, the final oil recoveries for every reservoir is compared as illustrated in **Fig.93**. The cumulative oil recovery was corrected based on T_1-T_2 maps pre and post EOR. Fig.93 shows that Montney 2 has the highest recovery of 51±4%, followed by Duvernay 36±6%, Eagle Ford 33±5%, Montney 1 11±6% and Uinta 1 9±5%. Following this work the best candidate for HnP with the mixture of C_1:C_2 (72:28) would be the Montney 2, Duvernay and Eagle Ford. Montney 1 and Uinta 1 would be poor candidates for the solvent C_1:C_2(72:28).

The results shown in Fig.93 clearly indicates different recovery behaviors, which begs the question what properties are controlling HC mobilizations during this process.

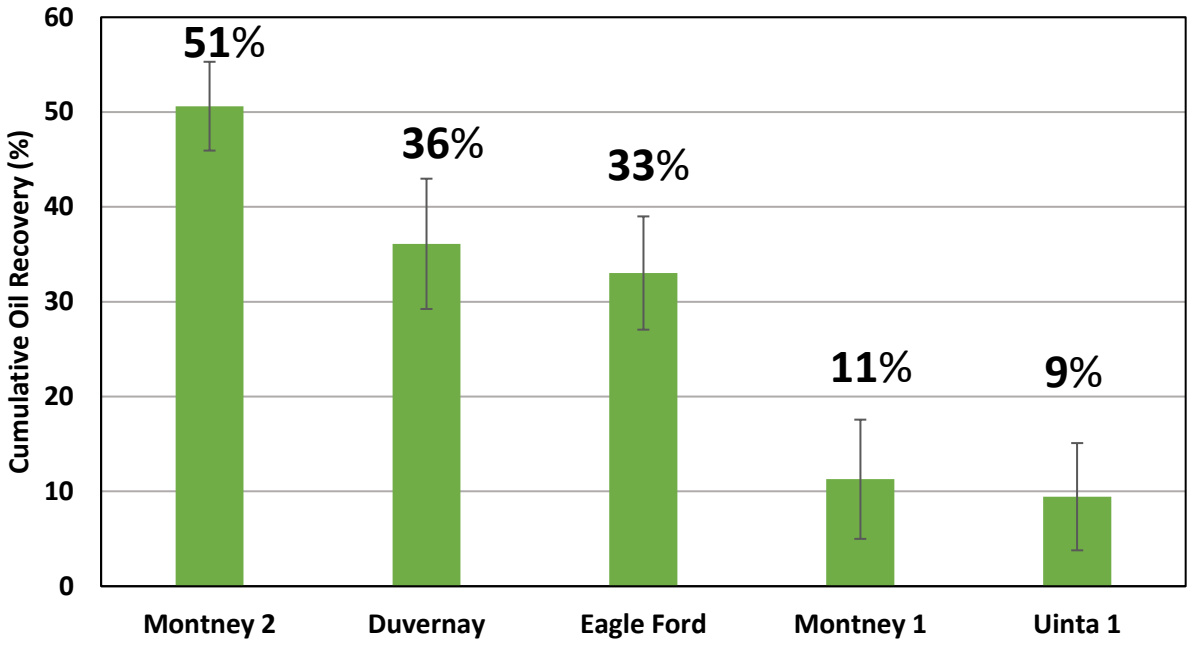

Figure 93 - Summary of cumulative oil recovery after HnP. Montney appears to be the best candidate followed by Duvernay and Eagle Ford.

4.4 Performance control

The previous chapter demonstrated that every reservoir performance with the solvent was unique, significant microstructural alteration have been documented from SEM, HAWK, MICP and NMR after HnP. The next part of the study proposes to compare cumulative oil recoveries to major rock and fluid properties to determine potential relationships. **Fig.94** shows that the oil composition seems to have a strong impact on recovery factor. The produced HC viscosity and HAWK heaviness fraction developed earlier seems to control the solvent capacity to move fluid out of the rock. A reservoir with a light oil and high HAWK S_{11} and S_{12} would be a good candidate for EOR with the rich solvent C_1:C_2(72:28). Rock properties such as the total porosity and the average pore throat size also plays important roles as can be seen on the same figure. Mineralogy, and organic content seems to play a minimal role on oil mobilizations with R^2<1 (**Fig.95**).

From all the reservoirs evaluated the Montney 2 sample stands out with the highest oil recovery compared to Eagle Ford and Duvernay (Fig.93). The Montney 2 reservoir is a siltstone with large pores and pore throats in the micron sizes as can be seen in SEM in Fig.37 and MICP in Fig.38. Therefore, fluid flow in these types of pores is expected to be different from a tight formation such as the Eagle Ford and Duvernay. When this play is removed from the oil recovery versus HAWK heaviness analysis, improved correlation is observed from R^2= 0.44 to 0.76 **(Fig.95 a and b)**. Fig.95 confirms that for the reservoirs studied oil mobilizations seems to be controlled by the oil composition and pore throat size distribution. In the Eagle Ford and Duvernay the oil recovery is governed mainly by the oil composition made of light HC S_{11} and S_{12}, while in the Montney 2 additional contribution is observed because of larger pore throat size. Samples with heavier HC content S_{14} (Heaviness Fraction >20%) such as the Uinta 1 will require a more aggressive solvent than C_1:C_2(72:28).

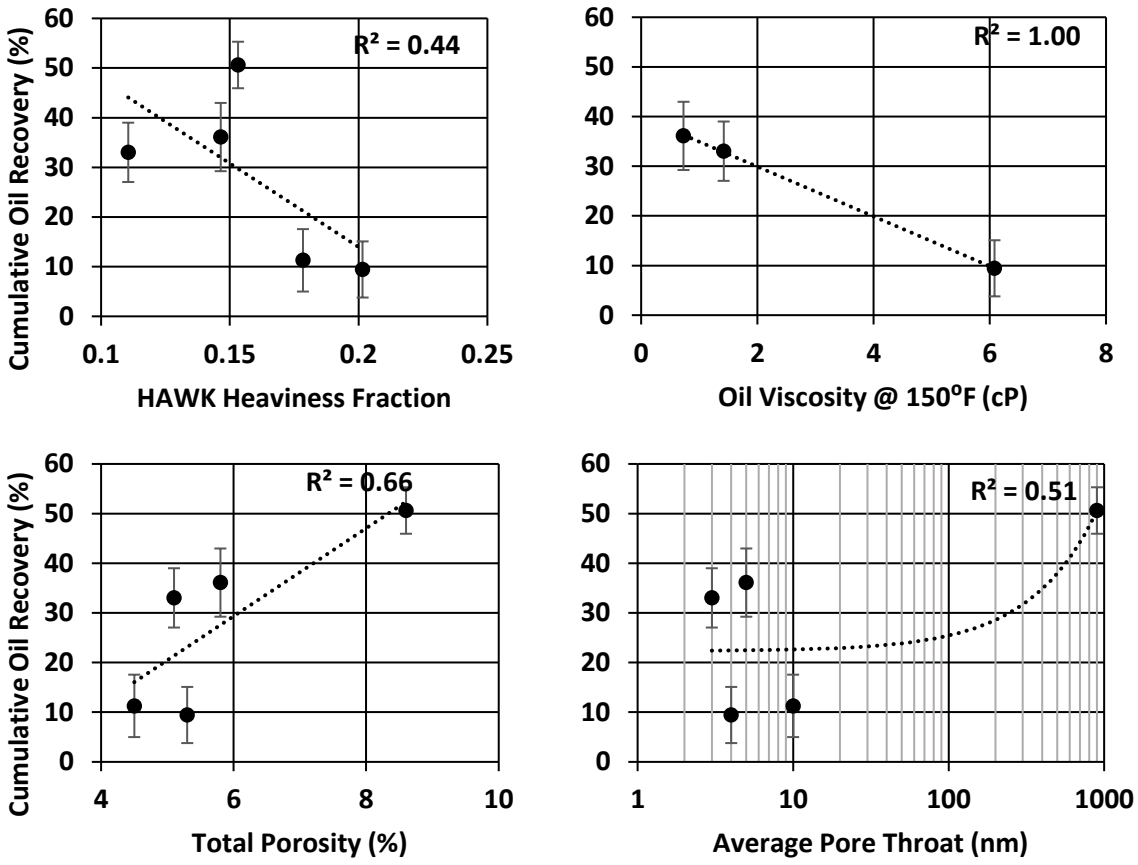

Figure 94 - Relationships between NMR oil recovery with HAWK heaviness fraction, oil viscosity, total porosity and average MICP pore throat size. A strong dependence is observed between the recovery factor and the oil composition (produced oil viscosity and residual oil composition).

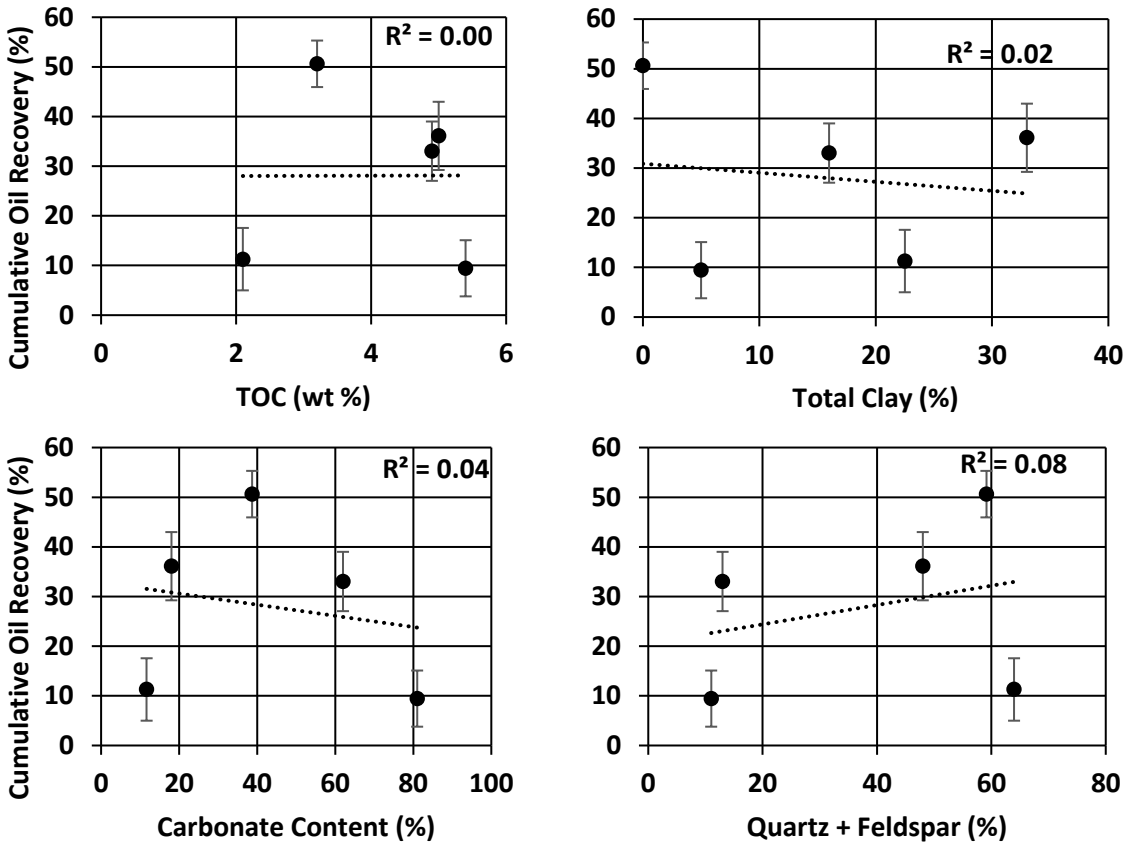

Figure 95 - Relationships between NMR oil with TOC and mineralogy. A weak dependence is observed between the organic content and mineralogy.

a)

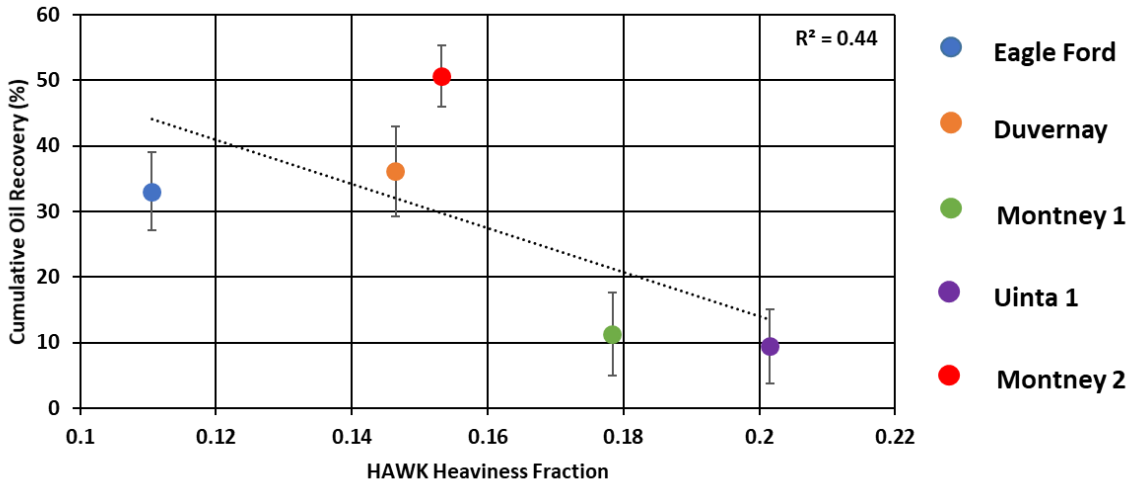

b)

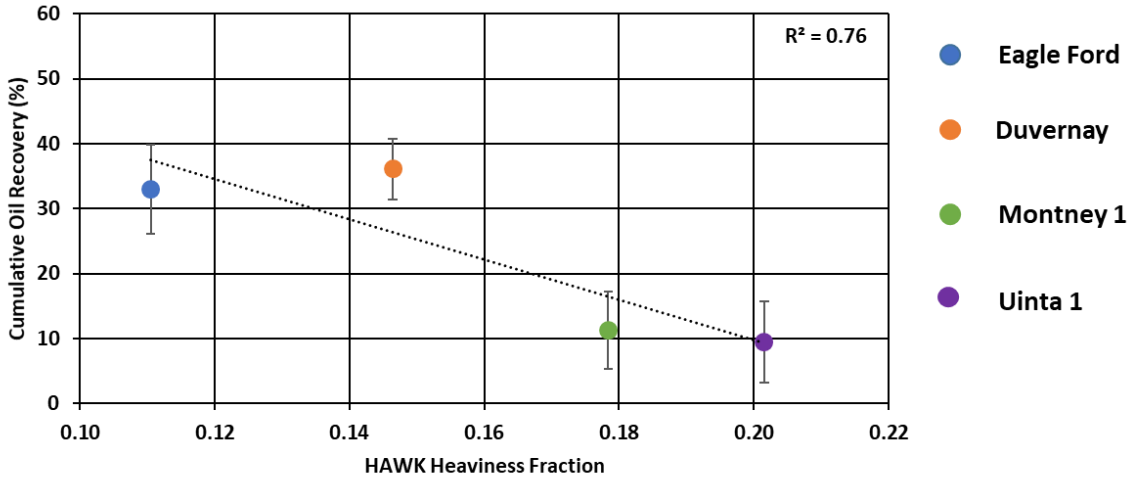

Figure 96 - Oil recovery as function of HAWK heaviness fraction with (a) and without Montney 2 (b). Improved correlation is observed when Montney 2 is removed from the analysis. Oil recovery seems to be controlled by the oil composition and pore throat size.

CHAPTER 5: CONCLUSIONS

5.1 Summary

1. EOR Huff-n-Puff recovery is controlled mostly by the reservoir oil composition and pore throat size distribution. Analysis of the produced oil and residual oil composition can be used as proxy to quickly evaluate possible candidate. Samples with HAWK heaviness fraction >20 % such as the Uinta samples will require a stronger solvent or thermal EOR to remover heavier HCs, hence they will be poor candidates for the mixture of C_1:C_2 (72:28)
2. Pore throat size distribution controls the rate of production during EOR. The tighter the rock (pore throats size distribution <20nm) the more gradual the HC production. However, when the pore throats are large (>20nm) the faster the depletion as can be seen in Montney 2 and Meramec samples.
3. Rock properties such as mineralogy and TOC are second order controls on recovery.
4. SEM results before and after EOR can be used to reveal microstructural alteration that are taking place during EOR. Those changes occur by increasing OM pore body sizes, sometimes by a factor of 2 or by creating porosity between organic and inorganic.
5. A comprehensive EOR efficacy protocol was developed to capture the dynamic changes behind huff-n-puff. This protocol focuses on three major elements, the oil (viscosity and composition), the rock (porosity, pore throat size, pore body size, microstructural change, mineralogy and organic content) and the solvent (MMP).

REFERENCES

Abrams, M.A., Gong, C., Garnier, C., and Stephenson, M.A. 2017. A new thermal extraction protocol to evaluate liquid rich unconventional oil in place and in-situ fluid chemistry. Journal of Marine and Petroleum Geology 88: 659-675.https://dx.doi.org/10.1016/j.marpetgeo.2017.09.014.

Barnes, G. and Gentle, I. 2005. Interfacial Science. Oxford University Press Oxford.

Begum, M., Yassin, M. R. and Dehghanpour, H. 2019. Effect of kerogen maturity on organic shale wettability: A Duvernay case study. Journal of Marine and Petroleum Geology. Canada, Alberta, Edmonton. https://doi.org/10.1019/j.marpetgeo.2019.07.012

Boak, J., Birgenheier, L., and Johnson, R.C. 2011. EMD oil shale committee annual report.

Boyer, C., J. Kieschnick, R. Suarez-Riviera, R. Lewis and G.Waters, 2006, Producing gas from its source, Oil Field Review, 36-49

Brunauer, S., Emmett, P.H., Teller, E. 1938. Adsorption of gases in multimolecular layers. Journal of American Chemical Society 60: 309-319

Bloemberg, N., Purcel, E.M., and Pound, R.V. 1948. Relaxation effects in nuclear magnetic resonance absorption. Phys. Rev 73:679-746.

Coates, G. R., Xiao, L., and Prammer, M.G. 1999. NMR Logging principles & applications, 39-41. Houston, USA, Halliburton Energy Services.

Curtis, M.E., Sondergeld, C.H., and Rai, C.S. 2013. Investigation of the microstructure of shales in the oil window. Presented at the Unconventional Resources Technology Conference, Denver, Colorado, August 13-14. https://doi.org/10.15530/URTEC-1581844-MS

Dang, S.T., Sondergeld, C.H., and Rai, C.S. 2018. Interpretation of NMR response to hydrocarbons: application to miscible EOR experiments in shales. SPE Res Eval & Eng. SPE-191144-PA. https://dx.doi.org/10.2118/191144-PA.

Dang, S.T. 2019. Understanding the fundamental drive mechanism for huff-n-puff enhanced oil recovery in tight formations. PhD dissertation. University of Oklahoma, Norman, Oklahoma

Du, F., and Nojabaei, B. 2019. A review of gas injection in shale reservoirs: enhanced oil/gas recovery approaches and greenhouse gas control. Energies Journal 12,2355, Blacksburg, VA. doi :10.3390/en12122355

Energy Information Administration (EIA). 2019.Weekly U.S. field production of crude Oil, https://www.eia.gov/dnav/pet/hist/LeafHandler.ashx?n=pet&s=wcrfpus2&f=w (accessed 27 March 2020).

Energy Information Administration (EIA). 2016. Initial production rates in tight oil formations continue to rise. https://www.eia.gov/todayinenergy/detail.php?id=24932 (accessed 30 June 2019)

Gamadi, T.D., Sheng, J.J., and Soliman, M.Y. 2013. An Experimental study of cyclic gas injection to improve shale oil recovery. Presented at the SPE Annual Technical Conference and Exhibition, New Orleans, Louisiana, USA, 30 September-2 October. SPE-166334-MS. https://doi.org/10.2118/166334-MS.

Gamadi, T.D., Sheng, J.J., Soliman, M.Y., Menouar, H., Watson, M. C., and Emadibaladehi, H. 2014. An experimental study of cyclic CO_2 injection to improve shale oil recovery. Presented at SPE IOR Symposium. Tulsa, Oklahoma, USA, 12-16 April. SPE-169142-MS. doi:10.2118/169142-MS

Gannaway, G. 2014. NMR investigation of pore structure in gas shale. SPE Annual Technical Conference and Exhibition. Amsterdam, Netherland, 27-29 October. SPE-173474-STU. doi:10.2118/173474-STU

Giesche, H. 2006. Mercury porosimetry: A general (practical) overview. Particle and particle system characterization 23 (1):9-19.

Hirasaki, J. G. and Mohanty, K. K. 2008. Fluid-rock characterization for NMR well logging and spatial core analysis. DE-FC2604NT15515 final report.

Hawthorne, S.B., Gorecki, C.D., Sorensen, J.A., Steadman, E.N., and Harju, J.A. 2013. Hydrocarbon mobilization mechanisms from upper, middle, and lower Bakken reservoir rocks exposed to CO_2. Presented at the SPE Unconventional Resources Conference Canada, Calgary, Alberta, Canada, 5-7 November. SPE-167200-MS. https://doi.org/10.2118/167200-MS.

Hoffman, B.T., and Evans, J.G. 2016. Improved oil recovery IOR pilot projects in the Bakken formation. Presented at the SPE Low Perm Symposium, Denver, Colorado, USA, 5-6 May. SPE-180270-MS. https://doi.org/10.2118/180270-MS.

Hoffman, B.T. 2018. Huff-n-puff gas injection pilot projects in the Eagle Ford. Presented at the SPE Canada Unconventional Resources Conference, Calgary, Alberta, Canada, 13-14 March. SPE-189816-MS. https://doi.org/10.2118/189816-MS.

Hoffman, B.T., and Rutledge, J.M. 2019. Mechanisms for huff-n-puff cyclic gas injection into unconventional reservoirs. Presented at SPE Oklahoma City Oil and Gas Symposium, Oklahoma City, 9-10 April. SPE-195229-MS. https://doi.org/10.2118/195223-MS

Yu, Y., Li, L., and Sheng. 2016. Discuss the roles of soaking time and pressure depletion rate in gas huff-n-puff process in fractured liquid-rich shale reservoirs. Society of Petroleum Engineers. doi:10.2118/181471-MS. Presented Dubai, UAE, 26-28 September

Jacob, Trent. 2019. Shale EOR delivers, so why won't the sector go big. Journal of Petroleum Technology. https://pubs.spe.org/en/jpt/jpt-article-detail/?art=5360 (accessed 20 January 2020)

King, G. E. 2014. Improving recovery factors in liquids-rich resource plays requires new approaches. The American Oil & Gas Reporter, http://www.aogr.com/magazine/editors-choice/improving-recovery-factors-inliquids-rich-resource-plays-requires-new-appr (accessed 30 June 2019).

Li, L. and Sheng, J. J. 2016. Experimental study of core size effect on CH_4 huff-n-puff enhanced oil recovery in liquid-rich shale reservoirs. Journal of Natural Gas Science and Engineering 34: 1392-1402. https://doi.org/10.1016/j.jngse.2016.08.028

Li, L., Sheng, J. J., and Sheng, J.2016. Optimization of Huff-n-Puff Gas Injection to Enhance Oil Recovery in Shale Reservoirs. Society of Petroleum Engineers. Presented SPE Low Perm Sympsium, Denver, Colorado, 5-6 May. doi:10.2118/180219-MS.

McGuire, P. L., Okuno, R., Gould, T. L., and Lake, L.W. 2017. Ethane based enhanced oil recovery: an innovative and profitable enhanced-oil-recovery opportunity for a low-price environment. SPE Reservoir Evaluation & Engineering. SPE-179565-PA. https://doi.org/10.2118/179565-PA

Min, B. 2018. Experimental study of gas injection enhanced oil recovery from shale reservoirs. MS Thesis. University of Oklahoma, Norman, Oklahoma

Morgan, C.D., Chindsey, T.C., McClure, K.P., Bereskin, S.R., and Deo, M.D. 2002. Characterization of oil reservoirs in the lower and middle members of the Green River formation, southwest Uinta Basin, Utah, Presented at AAPG Rocky Mountain Section Meeting, Laramie, Wyoming.

Mukherjee,S. 2020. Measurement and analysis of oil-gas diffusion at reservoir conditions: application to huff-n-puff EOR in unconventional reservoirs. MS Thesis. University of Oklahoma, Norman, Oklahoma

National Energy Board, British Columbia Oil & Gas Commission, Alberta Energy Regulator, British Columbia Ministry of Natural Gas Development. 2013. Energy briefing (accessed 15 April 2020).

Sinha, A. 2017. Surface area study in organic rich shales using nitrogen adsorption. MS Thesis. University of Oklahoma, Norman, Oklahoma

Sondergeld, C. H., and Rai, C. S. 1993. A new concept of quantitative core characterization the leading Edge 12 (7):774-779.

Ramakrishna, R., Merkel, D., and Balliet, R. 2012. Mineralogy, porosity and fluid property determination of oil reservoirs of the green river formation in the Uinta Basin. Presented at the SPWLA 53rd annual logging symposium, Cartagena, Colombia, June 16-20

Rassenfoss, S. 2017. Shale EOR works, but will it make a difference? Journal of Petroleum Technology. https://www.spe.org/en/jpt/jpt-article-detail/?art=3391 (accessed 30 June 2019)

Thomas, W., Helms, L., and Driggers, K. 2016. EOG Resources (EOG) earnings call, May 06, 2016

Yu, Y. 2016. Experimental study of enhanced liquid oil recovery from shale reservoirs by gas injection. PhD dissertation, Texas Tech University, Lubbock, Texas.

Yu, Y., and Sheng, J. J. 2016. Experimental investigation of light oil recovery from fractured shale reservoirs by cyclic water injection. Presented at the SPE Western Regional Meeting, Anchorage, Alaska, USA, 23-26 May. SPE-180378-MS. https://doi.org/10.2118/180378-MS

APPENDIX

Appendix A: List of Acronyms

EOR: Enhanced Oil Recovery

HnP: Huff-n-Puff

MMP: Minimum Miscibility Pressure

HC: Hydrocarbon

OM: Organic Matter

TOC: Total Organic Carbon

S/V: Surface area to Volume ratio

NMR: Nuclear Magnetic Resonance

HAWK: Hydrocarbon Analyzer with Kinetics

FTIR: Fourier Transform Infrared Spectroscopy

MICP: Mercury Injection Capillary Pressure

PSD: Pore Size Distribution

HPP: Helium Pycnometry

SEM: Scanning Electron Microscope

BET: Brunauer Emmett Teller surface area

Appendix B: EOR HnP methodology

1- Crush 50g of rocks into 7-8mm particles and separate using a mechanical sieve.

2- Separate the crushed ~50g into two batches of approximately 25g of 7-8mm particles used for EOR measurements and the other batch for petrophysical measurements, MICP, HAWK/SRA, FTIR, SEM, BET and TOC.

3- Batch 1 of the 25g is used to measure NMR T_2 relaxation and T_1 -T_2 map "as received". The parameters for both relaxation constants are specified in **Table 4**.

Note: For NMR acquisition the samples are place inside a glass vial and then inserted in the NMR spectrometer.

4- Heat both batches (50g) of the sample at 150°F (65°C) for 5-hours to remove any moveable fluid (water or light hydrocarbon) from the sample. We are only interested in fluid production due to the solvent effects and not temperature.

5- Allow the sample to cool for 30 min inside a desiccator. Batch 2 will begin petrophysical measurements mentioned above.

6- After cooling, NMR is run again on Batch 1, and will be considered the new "baseline" as the sample has been heated.

7- Place Batch 1 in the pressure vessel and heat the cell for 2-hours before injection.

8- Inject the solvent at 30 cc/min using the ISCO pump at pressure above MMP (usually 1000 psi above MMP)

9- When the target pressure is reached close the inlet valve using the pressure control on the PC. (The pressure should be maintained for couple minute until the pump flow rate displays 0psi/min before closing the inlet valve). Finally, allow the gas to soak into the rock for 1-hour.

10- Drawdown the pressure to 14 psi by opening the outlet valve for 1-hour.

11- Collect the sample inside a glass vial and allow it to cool off for 30 min in the desiccator before running NMR T_2 along with T_1 -T_2 map for cycle 1.

12- The same methodology is repeated for subsequent cycles until the fluid recovery becomes constant.

Appendix C: NMR sensitivity analysis

Table B1 - Raw data NMR fluid sensitivity analysis

Measured Mass (g)							**Gravimetric volume (ml)**		NMR volume (ml)
m1	m2	m3	m4	After T2	Average	Std	X	Measured	Y
							Blank	0.022397762	
0.0749	0.0746	0.0742	0.0743	0.0714	0.0745	0.0013	0.0993	0.1166	0.0942
0.1521	0.1520	0.1519	0.1519	0.1506	0.1520	0.0006	0.2026	0.2387	0.2163
0.2211	0.2211	0.2219	0.2210	0.2206	0.2213	0.0004	0.2950	0.3110	0.2886
0.3773	0.3772	0.3773	0.3772	0.3768	0.3773	0.0002	0.5030	0.5288	0.5064
0.5611	0.5605	0.5601	0.5606	0.5565	0.5606	0.0017	0.7474	0.7608	0.7384
0.7545	0.7544	0.7542	0.7541	0.7517	0.7543	0.0010	1.0057	1.0404	1.0180
1.5049	1.5044	1.5045	1.5032	1.5003	1.5043	0.0017	2.0057	2.0647	2.0423
2.2541	2.2536	2.2532	2.2520	2.2470	2.2532	0.0026	3.0043	3.0572	3.0348
3.0145	3.0140	3.0137	3.0132	3.0079	3.0139	0.0024	4.0185	4.1015	4.0791
3.7551	3.7541	3.7537	3.7530	3.7510	3.7540	0.0014	5.0053	5.1433	5.1209

Table B2 – Excel LINEST regression between gravimetric and NMR measured volume.

1.020555	-0.0095	Slope	Intercept
0.002812	0.006666	se(slope)	se(intercept)
0.999939	0.014797	r^2	se(y)
131746.2	8	F	df
28.84421	0.001752	ss reg	ss resid